Organizing and Supported by
US Army Research Office

USA - RUSSIAN WORKSHOP

Shock Induced Chemical Processing

N68171-96-M-5711

PROCEEDINGS

St.Petersburg (Russia)
23-24 June, 1996.

Book of Proceedings of the USA-Russian Workshop
"Shock Induced Chemical Processing"
St.Petersberg , June 23 - 24,1996

Book of Proceedings includes review of fundamental aspects of Chemical Physics Processes under Shock Loading

Editors:
S.G.Psakhie
V.A.Skripnyak

Organizing and Supported by US Army Research Office

Organized and Supported by
US ARMY RESEARCH OFFICE

SCOPE OF THE WORKSHOP

- **Defect generation under shock loading**
- **Chemical reaction under shock loading**
- **Synthesis of new materials under shock loading**
- **Computer modeling**

ORGANIZING COMMITTEE

From Russia:

- Likhachev V.A. (St.Petersburg)
- Mescheryakov Yu.I. (St.Petersburg)
- Psakhie S.G. (Tomsk)
- Titov V.M. (Novosibirsk)

From USA:

- Ahmad I. (ARO)
- Crowson A. (ARO)
- Horie Yu. (NCSU)

LOCAL ORGANIZING COMMITTEE

- V.A.Likhachev (St.Petersburg)
- S.G.Psakhie (Tomsk)
- V.A.Skripnyak (Tomsk)
- E.N.Korosteleva (Tomsk)
- V.M.Ktitorov (Arzamas-16)
- V.P.Bulatov (St.Petersburg)
- Yu.I.Mescheryakov (St.Petersburg)
- M.V.Sil'nikov (St.Petersburg)
- S.A.Atroschenko (St.Petersburg)
- N.J.Zhigacheva (St.Petersburg)

CONTENTS

The Workshop: "Shock Induced Chemical Processing"

St.Petersberg , June 23 - 24,1996

LIST OF PARTICIPANTS

The Workshop: "Shock Induced Chemical Processing"

St.Petersberg , June 23 - 24,1996

From USA:

№	Name	Organization / Fax / Phone / E-mail
1	**I. Ahmad**	US Army Research Office, Research Triangle Park PO Box 12211, Research Triangle Park, N.C. 27709 Telephone No.: (919) 549 4202 Fax: (919) 549 4248, 919 549 4310 E-mail: Ahmad@aro.ncren.net
2	**A. Crowson**	Materials Science Division, U.S. Army Research Office,P.O.Box 12211, 4300 S.Miami Blvd., Research Triangle Park, NC 27709-2211 Telephone No.: (919) 549 4261 Fax: (919) 549 4310 E-mail: crowson@aro-emni.army.mil
3	**R. Crowe**	DARPA 1 DSO, Defense Advanced Research Agency Defense Sciences Office, 3701 N. Fairfax Avenue, Arlington, VA 22203 FAX: (703) 696-2201
4	**R.A.Graham**	Sandia National Laboratories, Organization 1153,MS 0345, P.O.Box 5800, Albuquerque, NM 87185-0345 Fax: (505) 844-4045 E-mail: ragraha@sandia.gov
5	**Y. Horie**	North Carolina State Univ., Raleigh, NC 27695 Fax: (919) 515-7908 E-mail: horie@eos.ncsu.edu
6	**J. Illinger**	European Research Office U.S. Army Research, Development & Standardization Group UK, PSC 802 Box 15, FPO AE 09499-1500, (UK) FAX: 44 (171) 724 1433 E-mail: jillinger@army.ehis.navy.mil
7	**P.J. Miller**	Code 474330D, Naval Air. Warfare Center, China Lake, CA 93555 FAX: (619) 939-2597 E-mail: phil_miller@imdgw.chinalake.navy.mil
8	**M.A. Meyers**	Dept. of AMES, R-011, University of California at San Diego, La Jolla, CA 92093 Tel: (619) 534-4719 Fax: (619) 534-7078 E-mail: mameyers@ames.ucsd.edu
9	**V.F. Nesterenko**	Institute of Mechanical Materials, University of California at San Diego, La Jolla, CA 92093 Telephone No.: (619) 534-4719 Fax (619) 534-7078 E-mail: vnestere@imm.ucsd.edu

10	**D. Olson**	Department of Metallurgy and Materials Engineering, Colorado School of Mines, Golden, CO 80401-1887, Fax: (303) 273-3795
11	**N.N. Thadhani**	Georgia Institute of Technology, School of Materials Science and Engineering, Atlanta, GA 30332-0245 Telephone No.: (404) 894-2651, Fax: (404) 853-9140, E-Mail: naresh.thadhani@mse.gatech.edu
12	**D.L. Woody**	Code 474330D, Naval Air. Warfare Center, China Lake, CA 93555 FAX: (619) 939-2597 E-mail: phil_miller@imdgw.chinalake.navy.mil

From Russia:

№	Name	Organization
1	**S.S. Batsanov**	Center for High Dynamic Pressures, Rus. Acad.of Sci., 141570, Mendeleevo, Moscow reg. Telephone No: (095) 535-9330, 535-6380
2	**O.N. Breusov**	Inst. of Chemical Physics(Chernogolovka), Rus. Acad.of Sci., 142432, Chernogolovka, Moscow reg. Fax: (096) 515 3588 E-mail: dremin@icph.sherna.msk.su
3	**O.B. Drennov**	Russian Federal Nuclear Center, (VNIIEP) 607190, Arzamas-16, Nijnij Novgorod region
4	**A.K. Divakov**	Inst. of the Mechanical Engineering Problems, Rus. Acad.of Sci. 199178, St.Petersburg, V.O., Bolshoi, 61
5	**V.A. Ermolaev**	Inst. of the Mechanical Engineering Problems, Rus. Acad.of Sci. 199178, St.Petersburg, V.O., Bolshoi, 61
6	**A.V. Fisenko**	Inst. of Chemical Physics(Chernogolovka), Rus. Acad.of Sci., 142432, Chernogolovka, Moscow reg Fax: (096) 515 3588
7	**V.M. Fyodorov**	Inst. of Strutural Macrokinetics, Rus. Acad.of Sci., 142432, Chernogolovka, Moscow reg Phone: (096) 517 1851, Fax: (095) 201 7357 E-Mail: gordop@isman1.unicon.msk.su
8	**V.M. Fomin**	Inst. of Theoretical and Applied Mechanics, Rus. Acad.of Sci., 630090, pr. Academician Lavrentyev, Novosibirsk Phone: (383-2) 353 533
9	**Yu. A. Gordopolov**	Inst. of Strutural Macrokinetics, Rus. Acad.of Sci., 142432, Chernogolovka, Moscow reg Phone: (096) 517 1851, Fax: (095) 201 7357 E-Mail: gordop@isman1.unicon.msk.su
10	**Yu. A. Ivchenko**	Inst. of Strutural Macrokinetics, Rus. Acad.of Sci., 142432, Chernogolovka, Moscow reg Phone: (096) 517 1851, Fax: (095) 201 7357 E-Mail: gordop@isman1.unicon.msk.su
11	**S.P. Kiselev**	Inst. of Theoretical and Applied Mechanics, Rus. Acad.of Sci., 630090, pr. Academician Lavrentyev, Novosibirsk

12	**A.V.Kolesnikov**	Inst. of Chemical Physics(Chernogolovka), Rus. Acad.of Sci., 142432, Chernogolovka, Moscow reg Fax: (096) 515 3588 E-mail: dremin@icph.sherna.msk.su
13	**S.Yu. Korostelev**	Russian Materials Science Center 634021, pr.Academicheskii, 2/1,Tomsk Telephone No.: (382-2) 258 881 Fax: (382-2) 259 576 E-mail: sergeyk@monster.tomsk.su
14	**V.M Kuznetsov**	Institute of Strength Physics and Materias Sciences 634021, pr.Academicheskii, 2/1,Tomsk Telephone No.: (382-2) 259 481 Fax: (382-2) 259 576
15	**Y.I. Mescheryakov**	Inst. of the Mechanical Engineering Problems, Rus. Acad.of Sci. 199178, St.Petersburg, V.O., Bolshoi, 61 Phone: (812) 217-81-83, (812) 224-58-84 Fax: (812)217-86-14 E-mail: myi@tribol.ipme.ru
16	**A.L.Mikhailov**	Russian Federal Nuclear Center, (VNIIEP) 607190, Arzamas-16, Nijnij Novgorod region
17	**V.V. Mohova**	Russian Federal Nuclear Center, (VNIIEP) 607190, Arzamas-16, Nijnij Novgorod region
18	**A.A.Metrevely**	Inst. of Chemical Physics(Chernogolovka), Rus. Acad.of Sci., 142432, Chernogolovka, Moscow reg
19	**S.S.Nabatov**	Inst. of Chemical Physics(Chernogolovka), Rus. Acad.of Sci., 142432, Chernogolovka, Moscow reg Fax: (096) 515 3588 E-mail: dremin@icph.sherna.msk.su
20	**Yu.A. Petrov**	Inst. of the Mechanical Engineering Problems, Rus. Acad.of Sci. 199178, St.Petersburg, V.O., Bolshoi, 61 Phone: (812) 217-81-83, (812) 224-58-84 Fax: (812)217-86-14 E-mail: myi@tribol.ipme.ru
21	**S. G.Psakhie**	Russian Materials Science Center 634021, pr.Academicheskii, 2/1,Tomsk Telephone No.: (382-2) 258 881 Fax: (382-2) 259 576 E-mail: psakhie@monster.tomsk.su
22	**M.V. Silnikov**	Special Materials Inc., St. Petersburg
23	**G.V.Simakov**	Russian Federal Nuclear Center, (VNIIEP) 607190, Arzamas-16, Nijnij Novgorod region
24	**V.A. Skripnyak**	Tomsk State University, 634050, pr. Lenina 36,Tomsk Telephone No.: (382-2) 410 703 Fax: (382-2) 226 162 E-mail: skrp@ftf.tsu.tomsk.su
25	**E.V.Shilko**	Inst. of Strength Physics and Materials Sci., Rus. Acad.of Sci., 634021, pr.Academicheskii, 2/1,Tomsk Telephone No.: (382-2) 258 881 Fax: (382-2) 259 576 E-mail: shilko@monster.tomsk.su

CHEMICAL SYNTHESIS UNDER HIGH PRESSURE SHOCK COMPRESSION LOADING : MATERIALS, MEASUREMENT AND MODELING.

R.A.Graham
(Sandia National Laboratories, Albuquerque ,The Tome Group , Tome, New Mexico, USA)

It is now widely recognized that synthesis of compounds, alloys and amorphous materials can be readily accomplished with the application of high pressure stress pulses produced by intimate contact with detonation waves from high explosives or high velocity impact. Nevertheless, after 30 years of research, it is apparent that there is no consensus as to the appropriate fundamental descriptions of the shock-induced chemical synthesis processes. Indeed, fundamentally different and contradictory paradigms are invoked by various investigators. The basic choices for scientific definition of the processes are paradigms based on either mechanical- and thermodynamic-equilibrium or nonequilibrium mechanochemical processes. The present paper summarizes the status of shock-induced chemical synthesis science and indicates directions required to develop realistic scientific models of powder mixtures in the highly porous (about 50%) state.

Based on the newly available nanosecond, time-resolved stress and stress-rate measurement capabilities as well as combined PVDF-VISAR techniques, there is now specific quantitative date which to develop scientific models of the shock-compression processes resulting in chemical synthesis. The data on titanium-silicon, aluminum-hematite, and inert mixtures provide rich detail of the details of the mechanochemical processes. It will be necessary for fully qualified models to incorporate coordinated studies of materials science, nanosecond time-resolved wave profile measurements and mechanochemical models which are based on qualitative and quantitative data on a range of materials in various porosities and morphologies. It appears that the field of shock-induced solid state chemistry is a watershed from an early exploratory phase to a more quantitative scientific phase from which detailed models can be developed.

DYNAMIC-STATIC COMPRESSION OF INORGANIC MATERIALS

S.S. Batsanov
(Center for High Dynamic Pressures, Mendeleevo, RUSSIA)

Introduction

40 yeas ago Yu.N.Rabinin [1] for the first time had preserved and studied the shocked chemical compound and by this opened a new chapter in science, namely the shock induced chemistry.

Development of this field permitted to carry out constructions of the different recovery ampoules, to realize the physical-chemical transformations, to obtain the new phases and materials. Results of these investigations are reviewed in books [2-5].

In the shock recovery experiments the temperature may be varied from a few degrees to several thousand degrees and the pressure may be a few kbar or a few Mbar. However, high temperature generated by the residual heat lasts much longer than high pressure and leads to the annealing of metastable phases, thus strongly devaluating the advantage of shock chemistry.

The many methods of countering the negative influence of the temperature factor reduce to cooling the experimental devices before, during or after shock compression. As well as trivial cooling of the recovery ampoules by cryogenic liquid prior to explosion or the use of explosion in water of liquid nitrogen, other common approaches are adding water to the initial powder, pressing it in a copper matrix, applying a thin layer between massive metal plates, or else the detonation of a mixed charge, where temperature reduction accompanies scattering of the detonation products.

Another way of reducing the annealing effects of a heat is to extend the duration of the dynamic pressure by increasing the charge or the density of the surrounding media (water, ground, metal shells). However, these techniques extend the duration of the pressure by only 1-2 orders of magnitude and thus have no significant influence on the temperature parameters of the unloading body and hence on its structure and properties.

In our laboratory was carry out a novel approach to this task - the method of dynamic-static compression (DSC).

Principle of the DSC-method

If a strong recovery ampoule contains, besides a sample to be compressed a condensed substance (for example, water) able to evaporate under action of the residual temperature, then after an impact loading such an ampoule becomes an autoclave, the dynamic pressure being replaced by a static one [6].

However, opening of such an ampoule (still containing high pressure) presents a very complicated technical problem due to its brisance. Therefore we proposed [7] to use a solid working body undergoing during unloading a polymorphous transformation or melting with an increase of volume by 10-20%, which is not enough to provide a big brisant effect (Fig.1). Recently, it has been concluded that a high residual pressure may be produced in the absence of phase transformations in the working body,

simply as a result of the difference in compressibility of the ampoule shell and its contents [8] (Fig.2).

Obviously a magnitude of the residual pressure is determined by strength and rigidity of the ampoule shell. Partially one can obtain the static pressure about 15 to 20 kbar in the strong cylindrical ampoule.

Special case is using the explosive substance, for example RDX, as a working body. If to add some percents of high explosives to a powder to be shock compressed, then after an explosion of the outside charge we can obtain as a result of the inner detonation a solid foam. RDX can be added as a homogenic mixture or in form threads, spirals, plats. In these cases one can obtain solid foams with canals and gaps of the special form.

As long time one can keep the residual pressure? If the working body is a solid the static pressure may be conserved during few months. In cases of liquid and gas working bodies very difficulty to keep the residual pressure under high temperature, but after cooling the recovery ampoule to the room temperature the static pressure reduces usually to few kbars due to a condensation some gases or solidification some liquid.

Thermodynamic parameters of DSC-ampoules

DSC-method was realized in the cylindrical and plane recovery ampoules. Cylindrical ampoules with a spherical end are used from the very beginning of experiments, to eliminate stress concentrators. The ratio of the diameter (50 mm) to the height (70 mm) is 0.7, which is such that the strength if the cylinder approximate the characteristics of a sphere. The ampoules are exploded on a lathe with a steel tube with an aperture for cutting, preventing the loss of parts of the ampoule on thinning of the shell. The ampoule breaks, as a rule, when the wall thickness reaches 1-3 mm; the fracture thickness is a good measure of the residual pressure.

Increasing the static pressure in DSC-ampoule above the level of 15 kbar is a special problem, which is may be approached by several ways. A first method is to produce a two-chamber ampoule in which a static pressure P=15 kbar acts between the inner and outer shells and the total pressure ~ 30 kbar acts on the investigated material (Fig.3). The second approach is to use a working body that contains several components with increasing phase-transition pressure or compressibility which are either pressed into a homogeneous mixture or else are placed individually in concentric layers within the ampoule so that are successively included in the creation of the static pressure in the course of dynamic unloading and, remaining inert, apply in the additional shell. Both approaches were investigated in our laboratory, however we think that the maximal perspective has the magnetic method.

It is known that the metal shell under the magnetic field of 10^6 ersted may be compressed for several tens microsecond to pressure ca.50 kbar. The source of magnetic field may be the battery of condensators or the magneto-cumulative generator. The simultaneous action of shock waves and a magnetic field prolongates the dynamic pressure till several tens or even hundred microsecond. We carried out the simulation of this process and began to prepare the physical experiment.

Studying shock-wave parameters in the recovery ampoules is the very complicate task and now this work is in progress. The preliminary results are presented on Fig.4. As one can see the shock-wave velocity approaches the detonation velocity only at the very bottom of the DSC-ampoule. The sample to be compressed we put just at this place.
To clarify the picture of shock-wave propagation in such ampoules we carried out the experiments where the initial powder of the working body was intercalated with several sheets of steel or copper foil perpendicular to the ampoule axis. The diameter of the hole punched in such a foil during shock compression is known to correlate with the Mach stream dimensions [9].

In DSC-experiment a hole in the foil appeared for the first time at a distance from the top of the ampoule equal to its inner diameter. Down from this level the hole diameter increases and then decreases (Fig.5), indicating the instability of shock waves' interaction in the axial part of the ampoule.

Taking in consideration the formation of holes in the axial part we carried out measurement of shock pressures by a manganin gauge in the form of a ring (diameter 10 mm) which show that P=190 kbar at a distance of 5 mm from the ampoule axis was used an explosive with D=7.6 km/s.

The residual temperature in DSC-ampoules was measured calorimetrically. The ampoules were plunged into a water calorimetr in 45-100 s after an explosion, then after cooling the same ampoules were heated in an electric furnace to 400^0C and placed in an explosition chamber (in reproduce the cooling conditions), where a cooling curves were recommended. By this procedure, the residual temperature for zero delay after explosition was determined by an extrapolation to an accuracy of 5-7 % . Calorimetric experiments were conducted for the actual ampoules, for steel dummies, and for ampoules with weakly reinforced bottom that were blown away (with the filler) in the course of explosition. This permits to determine the shell temperature and to calculate the filler temperature: T_{res} =900°C for D= 7.2 and 1200 °C for D=7.8 km/s. If a hole of 3-mm-diameter is made in the ampoule bottom, the compressed material escapes from the ampoule (into the volume of a coaxial cylinder of the same cross section in the course of unloading. The residual temperature of this ampoule is measured by comparison with temperature of the closed ampoule to estimate T_{res} of the axial region (the Mach stream), which was found to be 1500-2000 °C.

In our laboratory were constructed and used the plane recovery ampoules for DSC-method. Thermodynamic parameters in these ampoules may be calculated with a good accuracy.

Results of DSC of inorganic materials

The described method was used for the investigation of the BN phase transition in the plane and cylindrical ampoules.

The plan experiment was realized by using the gas gun (Fig.6) [10]. The thickness of sample is equal1 mm, one of projectile is equal 5 mm, the weight of

projectile is equal 150 g. Time of impact is ca. 2.5 micro-second. Conditions and results of ballistic experiments are given in Table:

Velocity of projectile, m/s	Pressure, kbar		Yield of w-BN, %
	Shock	Residual	
673	156	0	15-20
678	158	0	15-20
685	160	10	80-90

As one can see, the residual pressure increases the yield of the dense phase of BN few times.

Using the cylindrical ampoule and a melt of trotyl/hexogen (40/60) permitted to realize the complete phase transition h-BN in w-BN and form a strong monolithic sample of specified dimensions [11]. The material produced has a microhardness of 5000-7000 Vickers units in the axial region (in the form of an especially hard spot extending over up to 15% of the internal diameter of the ampoule), which falls to 1000-1500 units at the periphery of the cylindrical sample; Fig.7. The sample density is 3.35 g/cm^3 , and the pressure of crushing is 110 kg/mm^2 . X-ray data show that the sample hardness varies antibatically with variation in the regions of coherent scattering and the domain size is ca. 100 Å for the hardest part of sample.

DSC of diamond powder also leads to the formation of a hard briquette with a microhardness of up section. Approximately the same in samples obtained by the DSC of würtzitlike and cubic form BN powder. A microhardness all these materials are ca. 5000-6000 Vickers units in the axial region, densities ca. 3.3 g/cm^3 . DSC-method was used with a success for compacting of SiC, B_4C, B, and TiB_2 powder.

DSC the mixtures of powders of SiO_2, GeO_2, SnO_2 and 10-35% RDX lead to a formation of solid foams of these materials . X-ray analysis showed, that the SiO_2 -foam has the quartz structure, GeO_2 -tetragonal structure, and SnO_2 is cassiterite. The density of the SiO_2 - foam varies from 0.6 to 1.4 g/cm^3 , densities of the GeO_2 and SnO_2 -foams are 2.6 and 2.9 g/cm^3 respectively.

An estimation of temperatures in these experiments leads to magnitude 1200 to 1500 ^0C. This temperature is enough for the contact melting and bonding of particles and a formation of solid foams.

An attempt to form the foams from Mo, Si and $MoSi_2$ by the same conditions was unsuccessfully. The reaction consists in the high temperatures of melting of these materials. When we used for DSC the mixture of composition Mo+ 10% RDX, the foam was syntheses very easy. Probably the additional temperature from the exothermic reaction of the $MoSi_2$

formation was enough for melting of a product and bonding particles. This fact shows that the chemical reaction is undergoing during the shock compression.
We carried out also DSC- experiments with mixtures of the SiO_2 powder and small additions of the different metals (Cu, Ni, Pt) and oxides (Eu_2O_3, TiO_2) powders, which may be catalysts. Taking into consideration that by DSC-method we can obtain porous and additions of different forms and concentrations in the any solid foams, this method may have a practical applications.

References

1. Yu.N.Riabinin Sov.Phys.-Tech. Phys. 1 , 2575 (1956)
2. R.A.Graham, Solids Under High-Pressure Shock Compression, Springer-Verlag, New York, 1993
3. Y.Horie, A.B.Sawaoka, Shock Compression Chemistry of Materials, KTK Sci.Publ., Japan, 1993
4. S.S.Batsanov, Effects of Explosion on Materials, Springer-Verlag, New York,1994
5. M.A.Meyers, Dynamic Behavior of Materials, J.Wiley, New York, 1994
6. S.S.Batsanov, Russ.Chem.Rev. 55, 297 (1986)
7. S.S.Batsanov, L.G.Bolkhovitinov, A.I.Martynov, Sov.Tech.Phys.Letters 16, 64 (1990)
8. V.A.Tumanov, V.N.Isaev, S.S.Batsanov, Comb.Expl.Shock Waves 29, N5 (1993)
9. S.S.Batsanov, G.S.Doronin, V.P.Stupnikov, J.Eng.Phys. 13, 307 (1967)
10. B.I.Abashkin, D.L.Gur'ev, I.N.Ermilov, et.al., Comb.Expl.Shock Waves (in press)
11. S.S.Batsanov, S.V.Vasilevsky, D.L.Gur'ev, et al., Sov.J.Chem.Phys. 10, 425 (1992)

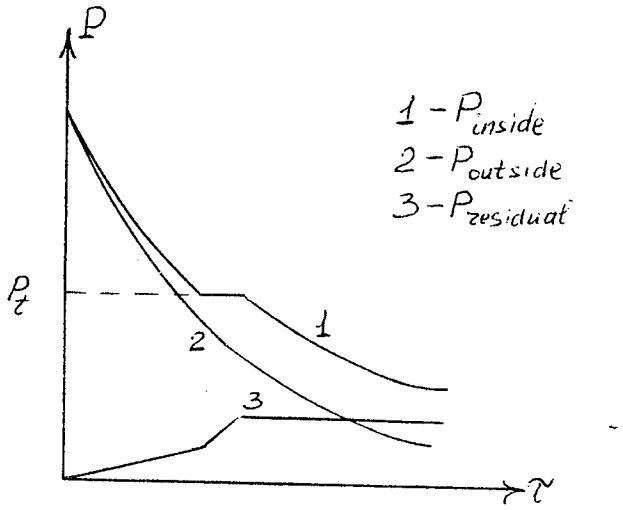

Fig.1 Unloading curves of a recovery ampoule and a working body with a phase transition

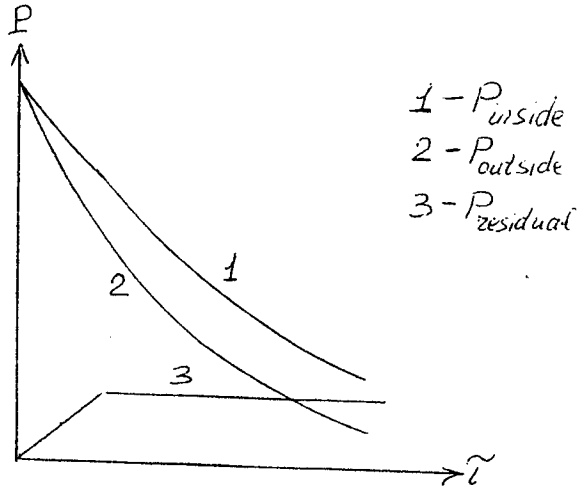

Fig.2 Unloading curves of a recovery ampoule and a inert softer working body

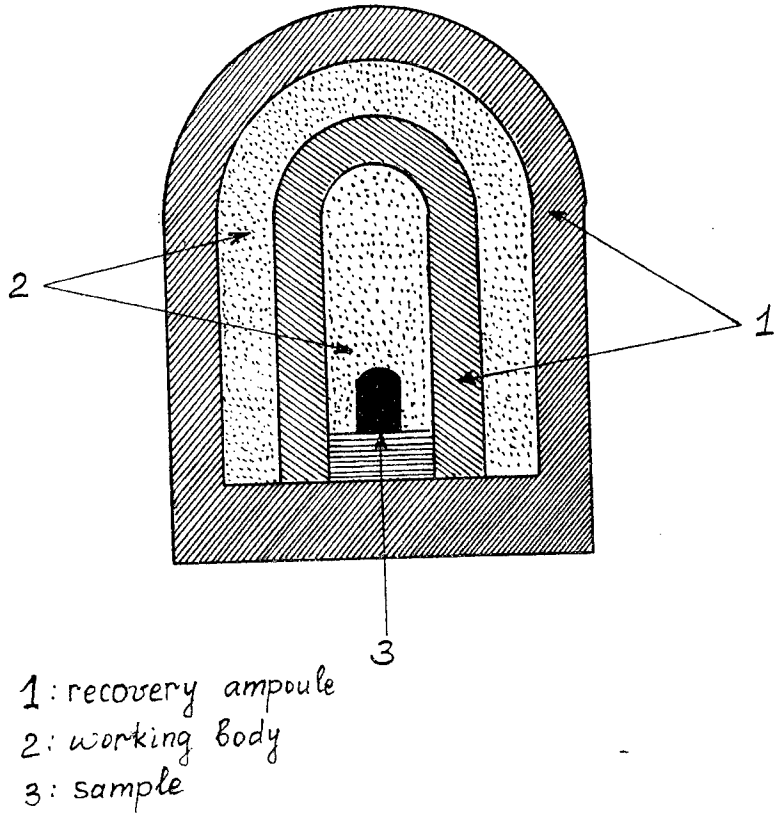

Fig.3 Two-chamber recovery ampoule for DSC

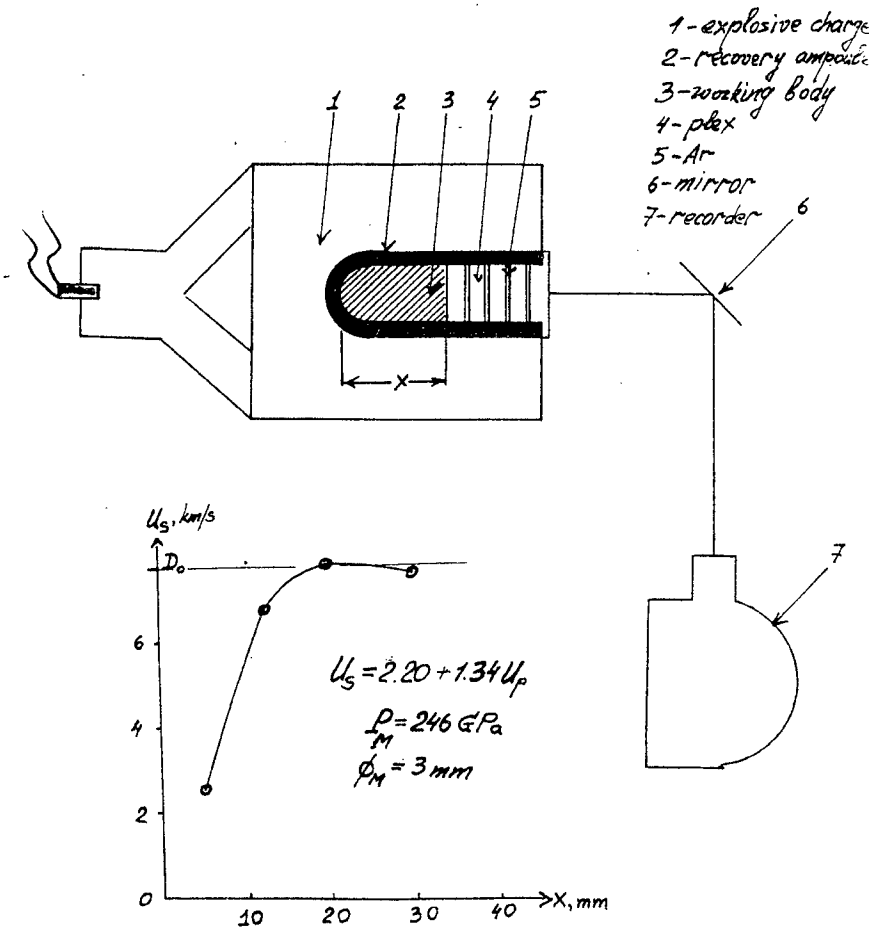

Fig.4 Schema and results of measurements of the shock velocity in the recovery cylindrical ampoule

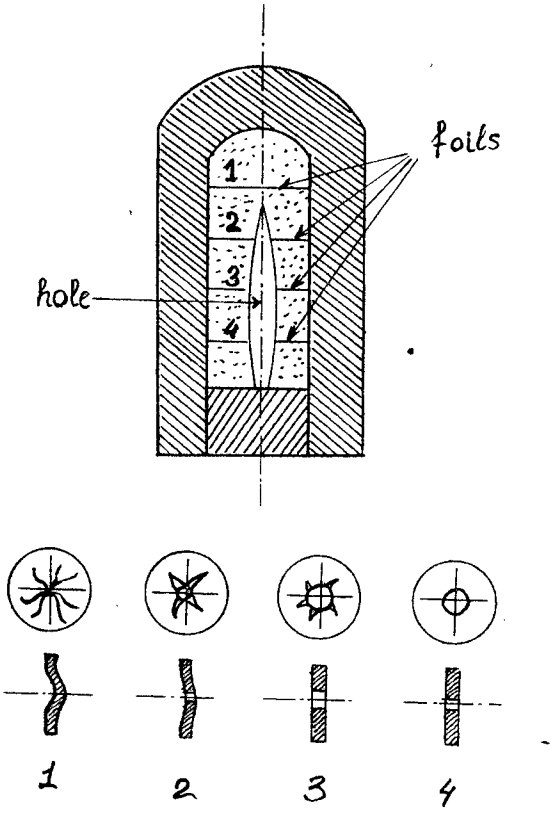

Fig. Estimation by the foil method of cross sections of the Mach stream

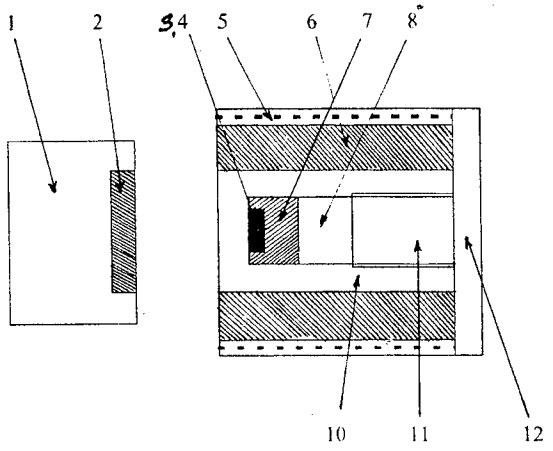

1: shabot, 2: projectile, 3,4: capsule + sample, 5: heating device, 6: support ring, 7: working body, 8: hermetic plug, 10: recovery ampoule, 11: bolt, 12: spall plate

Fig.6 Schema of ballistic experiments with the plane DSC-ampoule

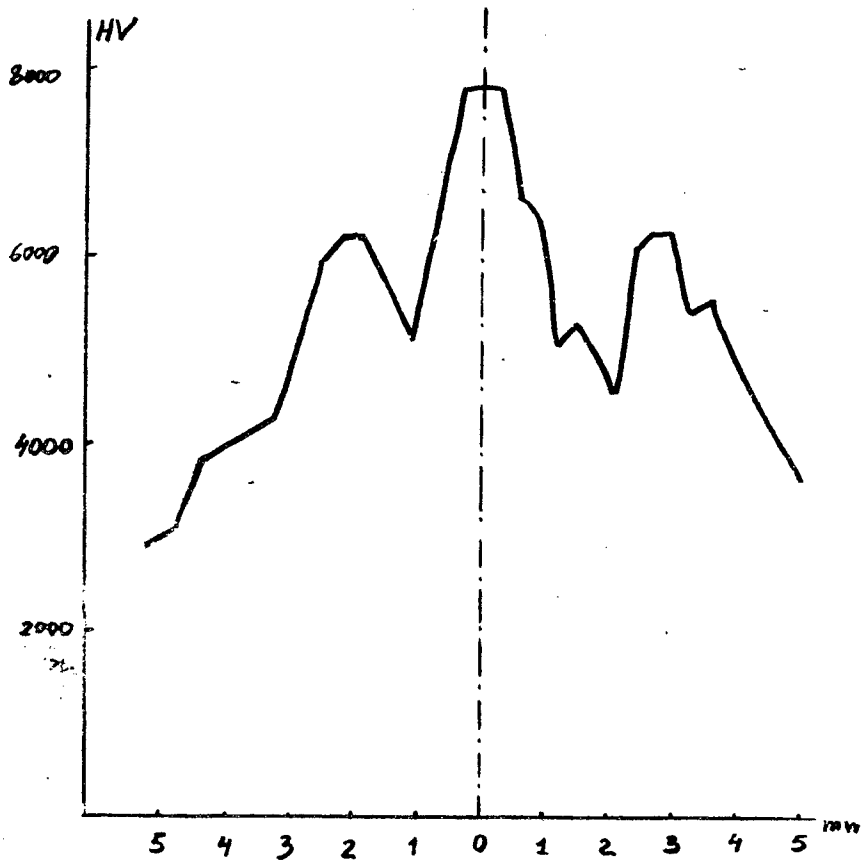

Fig.7 Distribution of tme microhardness along the cross section of the w-BN sample

COMPUTER AIDED STUDY OF REACTION-ASSISTED POWER MIXTURE SHOCK COMPACTION AT MESO-SCALE. NEW COMPUTATIONAL TECHNIQUE.

S.G.Psakhie, E.V.Shilko , A.Yu.Smolin, A.I.Dmitriev, S.Yu.Korostelev
(Institute of Strength Physics and Materials Sci., Rus. Acad.of Sci.,Tomsk, Russia)

1. MCA method general formalism

The method of Movable Cellular Automata (MCA) [1-3] is developed on the base of rigid body dynamics. At the same time it includes all the advantages of conventional cellular automata approach. This has become possible due to introduction of the new definition: - ***"the state of pair of automata"*** ("relation" of interacting pair of automata) in addition to the conventional one of ***"the state of a separate automaton"***. Note that introduction of this definition allowed to go from the net concept to the concept of neighbors, that is of principal importance. As a result of this the automata have ability to change their neighbors by switching *the states ("relations") of the pairs of automata.*

Thus, within the new method of Movable Cellular Automata the automata are allowed to move, owing all the advantages of classical cellular automata approach.

Within the framework of the Movable Cellular Automata method the simulated material is considered as an ensemble of discrete elements (cellular automata), interacting by certain rules, relations and laws. Such automata, in turn, combine the elements of heterogeneous media, in particular: separate grains of polycrystal, separate particles of powder mixture, etc. Certainly, the size of the automata are defined by conditions of specific problem. It is very important to select the size of automata correctly for adequate description of the material.

Mechanical state of the simulated system is characterized by the following parameters: position-vectors of the elements $\{\vec{R}^i\}$; translation velocities of the elements $\{\vec{V}^i\}$; rotation angles of the elements $\{\vec{\theta}^i\}$; rotation velocities of the elements $\{\vec{\omega}^i\}$. Every automaton is characterized by the size parameter d^i, mass m^i and inertia moment tensor $\hat{J}^i$. Mechanical behavior of the ensemble of the automata is defined by "relations" of interacting pairs and the forces of inter-element interaction. The type of relations defines the type of forces interacting between automata. In the simplest case the relations among the pair of interacting automata may be divided in the two types: ***linked*** (the pair of the automata, among which there are any chemical bonds) and ***unlinked*** (there is no any chemical bonds among the automata of the pair). Note that the ***unlinked*** pairs of automata may be divided in its turn in the two types: ***contacted*** (the pairs of interacting automata) and ***uncontacted*** (there is no any interaction among the automata of the pair), when: $h^{ij} = r^{ij} - r_o^{ij} \geq 0$

Formation of initial structure is performed by setting up certain relations to each pair of neighboring elements. The change of relations among the cellular automata is defined by the value of their overlapping h^{ij}, calculated as $h^{ij} = r^{ij} - r_o^{ij}$, where r^{ij} is the

distance between the centers of the neighboring elements, and r_o^{ij} is defined as $r_o^{ij} = (d^i + d^j)/2$, where d^j is the size parameter of the automaton. The pair of ***linked*** automata remains to be ***linked*** while: $h^{ij} \le h^{ij}_{max}$. The pair of ***unlinked*** elements remains to be ***unlinked*** while: $h^{ij} \ge h^{ij}_{min}$. If the two elements were initially ***unlinked***, they become to be ***linked***, when: $h^{ij} < h^{ij}_{min}$. And vice versa - if the two elements were initially ***linked***, they become to be ***unlinked***, when their overlapping parameter $h^{ij} > h^{ij}_{max}$. It must be noted that, if mutual rotation of the elements are taken into account, then it is necessary to introduce the criterion of transition of the pair from the ***linked*** to ***unlinked*** relations due to their relative rotation. In this case, if $\Delta r^{ij}_{cp} \ge \Delta r^{ij}_{max}$, then the pair been ***linked*** becomes ***unlinked***. Here Δr^{ij}_{cp} is the distance between the contact points of the two interacting automata, calculated from the moment, when they become ***linked***.

The pair approach is used for description of the inter-automata mechanical interaction. $\vec{F}^{ij}$ is the force acting from j-th automaton to i-th one. In general case $\vec{F}^{ij}$ can be represented as: $\vec{F}^{ij} = \left(\vec{p}^{ij} + \vec{f}^{ij}\right)$, where $\vec{p}^{ij}$ is central type of interaction, and $\vec{f}^{ij}$ is a tangential type.

The central force of pair interaction may be divided into two components: elasto-plastic component (depending on degree of deformation) and viscous component (damping). The elasto-plastic component reflects the property of the material to resist the deformation and is defined by degree of deformation of the automaton $\varepsilon^i = \dfrac{q^i - d^i/2}{d^i/2}$, where q^i is the distance from center of automaton to contact point of this automaton with its neighbor. In general case the following regions may be resolved when calculating the force resisting to deformation (Fig. 1):

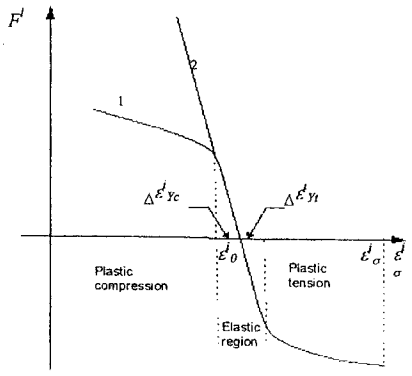

Fig. 1. Force resisting to deformation.

1. The region of elastic interaction $[\varepsilon^i_0 - \Delta\varepsilon^i_{Yc} : \varepsilon^i_0 + \Delta\varepsilon^i_{Yt}]$, where $\Delta\varepsilon^i_{Yc}$ is the limit of elasticity of the material under compression (*c – compression*), and $\Delta\varepsilon^i_{Yt}$ is that one under tension (*t – tension*).
2. The region of plastic flow under tension $[\varepsilon^i_0 + \Delta\varepsilon^i_{Yt} : \varepsilon^i_\sigma]$, where ε^i_σ is the strength limit of the material under tension.
3. The region of plastic flow under compression $[\varepsilon^i_0 - \Delta\varepsilon^i_{Yc} : \varepsilon^i_L]$, where ε^i_L is the ultimate compression deformation. This parameter is defined by the strength of the material under compression and its compressibility. The curve corresponding to central force is labeled 1.

In the region of elastic interaction the force of resistance in the simplest case may be calculated following the linear dependence:

$$F^i_{(E)}(\varepsilon^i) = -E^i(\varepsilon^i - \varepsilon^i_0)S^{ij}, \tag{2}$$

where S^{ij} is the contact area of the automata i-th and j-th ones, E^i is the modulus, defining the materials response to shape-changing under deformation.

In the simplest case the value of E^i may be defined by such a way. Consider uniaxial tension (compression) of a parallelepiped shape specimen along X-axis. Assume that it is deformed uniformly. Then following X-component of stress-tensor will be:

$$\sigma_x = 2G\left(\frac{\Delta X}{X} + \frac{1}{3}\frac{\Delta V}{V}\right) + K\frac{\Delta V}{V}, \tag{3}$$

where ΔV is the volume change under deformation, G is the shear modulus, K is the bulk modulus. Since deformations are uniform $\Delta Y = \Delta Z = -\sigma\Delta X$, and then $\Delta V \approx V(1 - 2\sigma)\Delta X/X$, where σ– is Poisson ratio. So the stress corresponding to resistance to shape change will be

$$\tau_x = 2G\left(1 - \frac{1-2\sigma}{3}\right)\frac{\Delta X}{X},$$

And we can define our modulus as $E^i = 2G^i\left(1 - \frac{1-2\sigma^i}{3}\right)$.

In the regions of plastic flow in the simplest linear case the resistant force may be calculated as:

$$F^i_{(Pl)}(\varepsilon^i) = -[E^i\Delta\varepsilon^i_{Yt} + E^i_{II}(\varepsilon^i - \varepsilon^i_0 - \Delta\varepsilon^i_{Yt})]S^{ij},$$

where E^i_{II} is the coefficient, taking effectively into account the hardening of the material of i-th automaton under plastic flow.

The viscous component describes the dissipate properties of the material and is defined by the velocity of relative movement of the elements $\vec{V}^{ij}_n$: $\vec{p}^{ij}_n = -\eta^{ij}_n \vec{V}^{ij}_n$, where η^{ij}_n is the coefficient of the force of normal damping. $\vec{V}^{ij}_n$ is the normal component of the relative velocity of j-th automaton in the coordinate system centered at i-th automaton.

The tangential force of pair interaction may be divided into three components: elasto-plastic component (depending on degree of shear deformation), viscous component and dry friction force (only for ***unlinked*** and ***contacted*** pairs of automata).

Within this model the force of resistance to shear deformation is applied to the ***linked*** automata only. The angle of shear deformation γ^i of i-th automaton under its interaction with j-th automaton is defined by relative translation movement of i-th and j-th automata and rotations of j-th and i-th automata. Increment of shear deformation angle γ^i is defined as follows. The total tangential displacement of i-th and j-th automata relative to their contact point in one time step Δt will be

$$\Delta\vec{l}^{ij} = (\vec{\omega}^{ij} r^{ij} - \vec{\omega}^i q^i - \vec{\omega}^j q^j) \times \vec{n}^{ij} \Delta t ,$$

where $\vec{\omega}^{ij} = \vec{n}^{ij} \times (\vec{V}^j - \vec{V}^i)/r^{ij}$. This displacement is considered as sum of increments of shear deformation angles

$$\Delta l^{ij} = q^i \tan(\Delta\gamma^i) + q^j \tan(\Delta\gamma^j) ,$$

therewith the following equation is required: $f^{ij}(\gamma^i) = -f^{ji}(\gamma^j)$. To oppose rotation of the automata as gears ($\vec{\omega}^{ij} = 0$, $\vec{\omega}^i q^i = -\vec{\omega}^j q^j$) the couple forces is applied to each automaton. This forces are proportional to $\theta^i - \theta^j$.

The expression for calculation the viscous friction force may be written as: $\vec{f}_v^{\,ij} = -\eta^{ij} \vec{V}_S^{\,ij}$, where η_v^{ij} is the viscous friction coefficient, $\vec{V}_S^{\,ij}$ is the tangential component of the relative velocity of j-th automaton in the coordinate system centered at i-th automaton.

Dry friction force $\vec{f}_{dr}^{\,ij}(p^{ij})$ if $\vec{V}_S^{\,ij} = 0$ is varied from zero to its maximum value $\mu^{ij} p^{ij}$. This force is equal to tangential component of resultant force of reaction F^{ij}, defining by all the forces acting on the automata. Here p^{ij} is vertical component of the force F^{ij}. If the value of the tangential component of the force F^{ij} exceeds the value of $\mu^{ij} p^{ij}$, then $\vec{V}_S^{\,ij} \neq 0$ and the dry friction force reaches its maximum value.

Resistance of the automata to the change of its volume is taken into account by analogy to the "embedded atom" method. Volume dependent force $\vec{F}_P^{\,i}$, acting of i-th automaton due to environment pressure, may be calculated as:

$$\vec{F}_P^{\,i} = \sum_j P^j S^{ij} \vec{n}^{ij} ,$$

where the index j ($j = 1...N^i$) numbers the automata being ***linked*** or ***contact*** with the i-th one; P^j is the pressure of j -th neighboring automaton; S^{ij} is the contact area of i -th and j -th automata; $\vec{n}^{ij}$ is the unit vector normal to the contact area and directed to the j-th. The pressure P^j of j -th automaton is defined by change of the volume of automaton, and the volume change may be calculated from changes of the distances from center of j -th automaton to contact points of this automaton with its neighbors. In Fig. 1 the curve corresponding to volume-dependence force is labeled 2.

Since in MCA method the size of an automaton is introduced directly, then for complete description of the system evolution it is necessary to add the equations for the moments to the motion equations for the mass centers. Then the motion equations will be:

$$\begin{cases} m^i \dfrac{d^2\vec{R}^i}{dt^2} = \vec{F}_p{}^i + \sum\limits_j \vec{F}^{ij} \\ \hat{J}^i \dfrac{d^2\vec{\theta}^i}{dt^2} = \sum\limits_j \vec{K}^{ij} \end{cases},$$

where $\vec{F}^{ij} = \left(\vec{p}^{ij} + \vec{f}^{ij}\right)$, $\vec{K}^{ij} = q^i\left(\vec{n}^{ij} \times \vec{F}^{ij}\right)$, q^{ij} is the distance to contact point of i-th automaton with j-th one. The unit vector $\vec{n}^{ij}$ is defined as $\vec{n}^{ij} = (\vec{R}^j - \vec{R}^i)/r^{ij}$, where r^{ij} is the distance between the centers of the automata.

Using boundary conditions of different types (hard, elastic, visco-elastic, etc.) it is possible to imitate different properties of surrounding medium, containing the simulated system. It is possible to model different modes of mechanical loading (tension, compression, shear strain, etc.) by setting up additional conditions at the boundaries.

2. Chemical reaction modeling

Model of virtual crystal. In the simplest case the cellular automaton may be of the material of the same type (an initial compound of the mixture or the product of reaction). Lets call the state of this element the "simple state" for it is totally defined by characteristics of the only one compound. In general case a cellular automaton can be considered as the mixture of several different substances and it's complicated state will be defined by the properties of the all compounds and their interactions. To describe the properties of such a combined cellular automaton we follow the model of virtual crystal. In this model all the specific characteristics of an element as well as parameters of it's interaction with the neighbors are defined by averaging over the all atoms of the compounds making up the element:

$$\bar{b} = \left(\sum_{i=1}^{N} b_i n_i\right) \Big/ n,$$

where b_i and n_i are some certain unit characteristics and quantity of i-th compound correspondingly, n is the total number of atoms, N is the number of all possible compounds.

In this approach some certain components of the material composing an element are able to realize independently phase transformations, de-solution into initial components (in the case of chemical compounds) and chemical reactions among themselves. In parallel account of these possibilities, phase transformations will have the highest priority, and chemical reactions will be considered as the last possibility.

Thus, movable cellular automaton may change its state both because of inner transformations and under chemical reactions with its neighbors.

Mechanism of shock-induced solid phase reactions. In general case the mechanism of a solid phase reaction in a shock wave is presented as follows. Only the pairs of automata (of reagents A and B) in the states "linked" or "contact" are taken into account. High compression of the interacting elements takes place under shock wave propagation, that corresponds to input of elastic energy into material. The processes of abnormal high rate mass transfer and mixing the reagents are possible in heterogeneous media on different scale levels (from atomic to micron) under similar conditions.

The mechanisms of mass transfer are different and connected not only with intensive plastic deformation, but also with the grinding of the material and further mixing of the fragments. Beside this, under these conditions an intensive mass transfer may take place on the atomic level because a portion of the atoms (especially in micro-damage zones, "hot-spots", etc.) may have the energy considerably higher than the diffusion activation threshold. This mixture containing the atoms and molecules of the reagents with high kinetic energies is reacting by generation of the products.

In the case of exothermic reactions there is characteristic time (the time of transition to thermal equilibrium). During this time the released energy is transformed into the energy of mechanical compression of neighboring regions and into the thermal energy of atomic oscillations. The formation of the reaction product is completed when in the whole automata volume the processes of mixing, reacting in the mixture and redistribution of the released energy are finished.

Reaction between the pair of elements. It is possible to divide the process of the reaction of a pair of the automata into 3 main sub-processes, ongoing in parallel:

1. Mixing the reagents and formation stoichiometric mixture.

To estimate the mixing velocity the following equation may be used:

$$\upsilon_{mix} = \alpha_a \upsilon_a + \alpha_{ba} \upsilon_b,$$

where $\upsilon_{a(b)} = \sqrt{2E^{el}_{a(b)} - E^{b}_{o\,a(b)}/\mu_{a(b)}}$ is the upper limit of penetration velocity of A(B) component, $\alpha_{a(b)}$ is some effective coefficient, $E^{el}_{a(b)}$ is the elastic energy of compression of A(B) element per 1 mole, $E^{b}_{o\,a(b)}$ is the binding energy of the atom of A(B) component, $\mu_{a(b)}$ is the molar mass.

2. Forming the product of the mixture.

To estimate the time of chemical reaction between interacting elements A and B Arrhenius dependence for constant of the rate of chemical reaction may be used:

$$\overline{K}^{react} = \overline{A} e^{-(\overline{E}-\overline{E}_{el})/RT}$$

where $\overline{A}$ is the frequency factor, $\overline{E}$ is the threshold energy of the reaction, $\overline{E}_{el}$ shows the decrease of the activation threshold due to input of non-heat energy, T is the temperature.

3. Re-distribution of the released energy.

The energy of the system (automaton) released due to the reaction is re-distributed (including its transformation into mechanical energy of interaction with the neighboring automata) during some certain time of relaxation t_{relax}. The value of t_{relax} is of the same order that the time of transition to thermal equilibrium state.

3. Simulation of shock compression of powder mixture

To demonstrate the abilities of the MCA method to simulate shock compression of powder mixture consider the Ni–Al powder mixture. Powder mixture is simulated as an assembly of randomly packed circle particles with certain variance and appointed porosity. Al and Ni powder particles are randomly distributed in the mixture. Each particle consists of close packed elements of the same sort. In this task the mass ratio of Ni and Al particles corresponds to stoichiometric ratio of the reaction (0.01 and 0.007 respectively). Size of a separated element was equal to 0.001 sm.

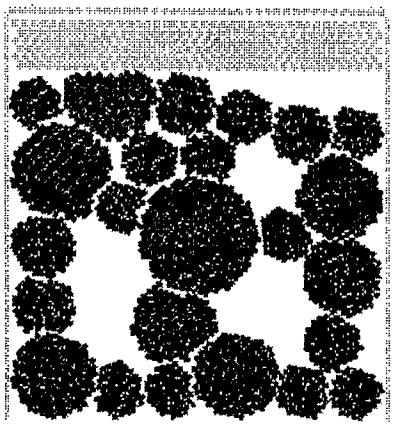

Fig. 2. Initial structure of the sample.

The mixture is placed in the hard box simulated by elements with fixed coordinates (Fig. 2). Special layer imitates plastic material of the top of the mixture. Shock loading is simulated by setting up constant velocity to elements combining a movable piston. The value of loading velocity was amounted to 1 km/sec. Further it can be seen some results of simulation of shock loading of Ni-Al powder mixture. Fig. 3 shows evolution of the structure of powder mixture under loading. One can see fracture of Ni particles and filling of the voids between Ni particles by the Al. Also some reaction at the interface between of Ni and Al is seen. Fig. 4 and 5 show velocity fields and trajectories of elements of the simulated system, respectively, at some time steps during loading process.

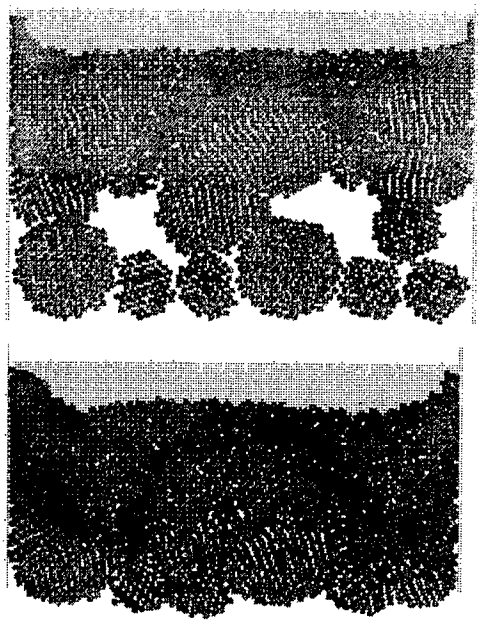

a)

b)

Fig. 3. a)-b) Structure of powder mixture at different stages of loading.

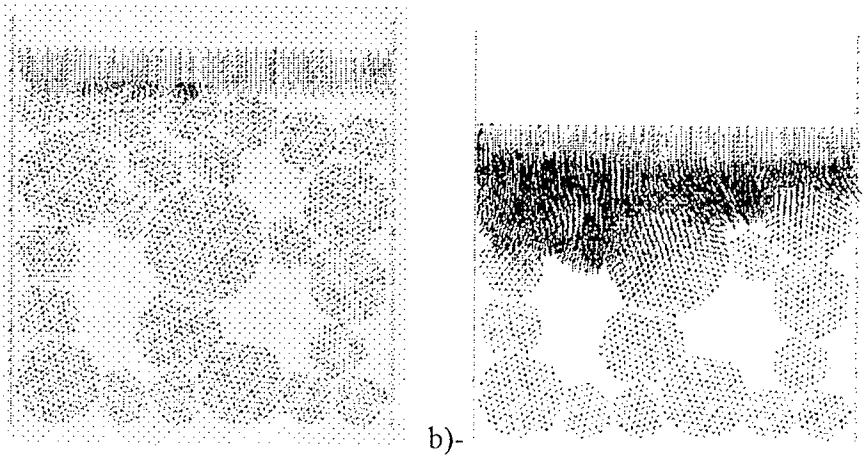

a) b)-

Fig. 4. a)-b) Velocity fields of powder mixture at different stages of loading.

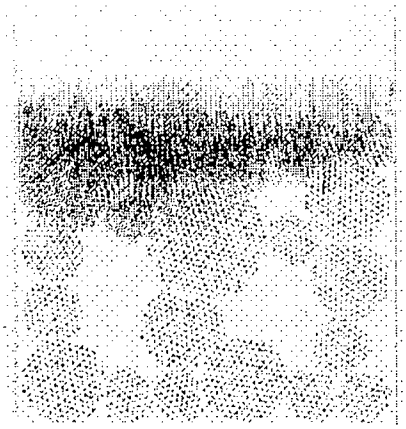

Fig. 5. Trajectories of elements in some period of calculation.

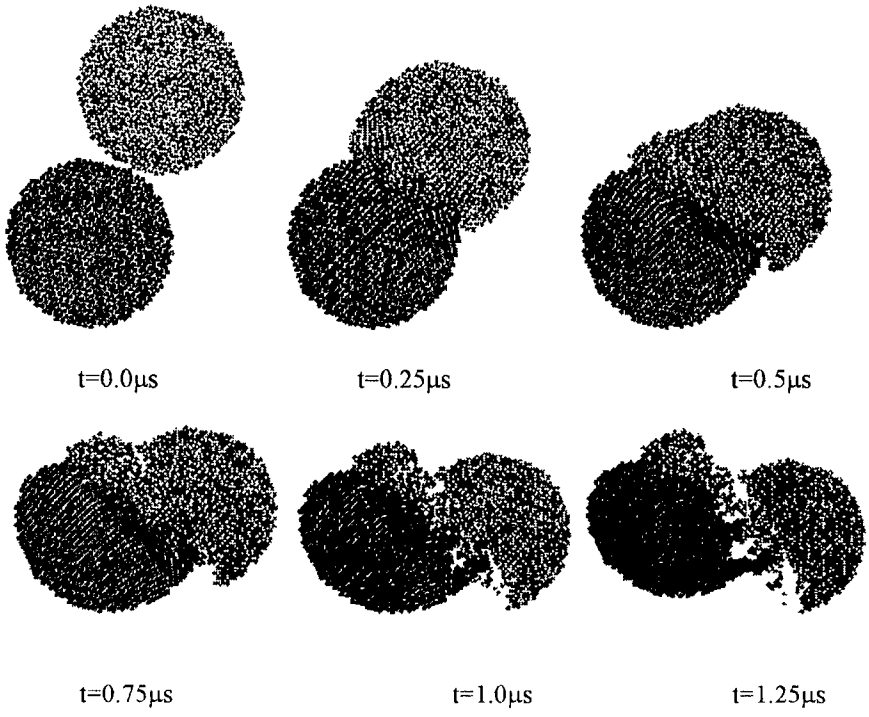

Fig. 6. Collision of aluminum and nickel particles. Structures at different time moments.

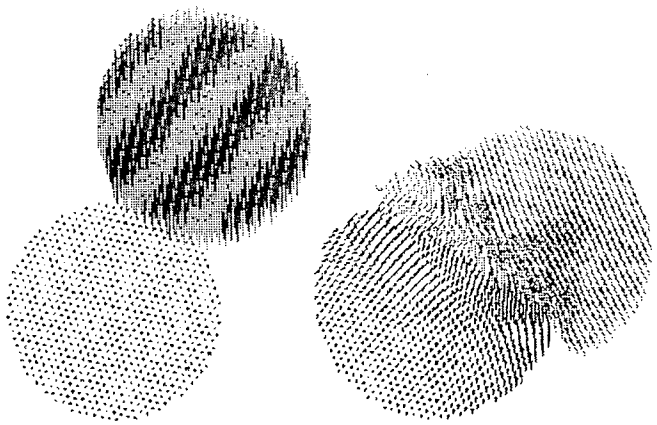

Fig. 7. Collision of aluminum and nickel particles. Velocities of automata.

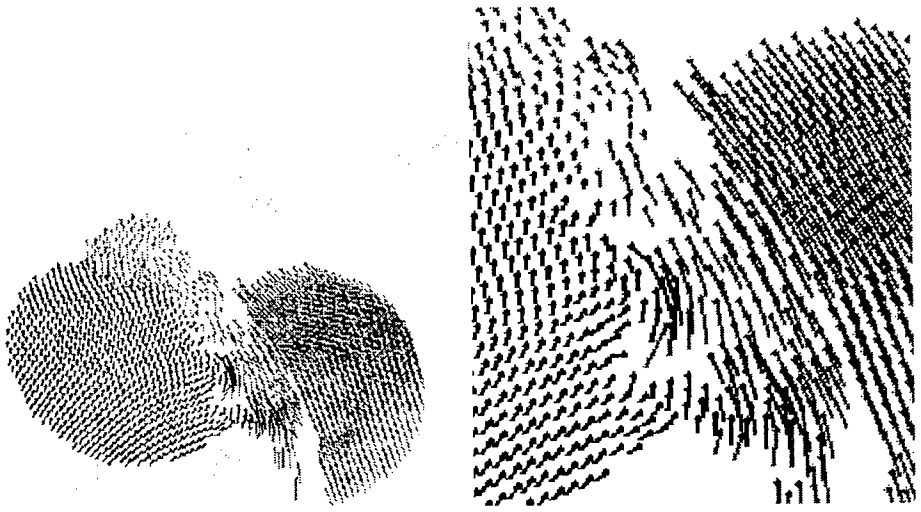

Fig. 8. Collision of aluminum and nickel particles. Velocities of automata at the interface (t=1.25μs).

4. Modeling of particle collision

Let consider the problem of interaction of two particles. Initially aluminum (upper) particle moves with velocity of 800 m/s and nickel one does not move. The size of

particles is 300 μm, size of automata is 0.3 μm. Figs. 6 and 7 show the results of simulation at different stages of the process.

In Fig. 6 one can see the process of mixture of automata of different particles at the inter-particle interface. It is very important that MCA method allows to investigate the process of interaction at meso-scale level. In Fig. 7 one can see that the velocity of aluminum automata moving to the crack in nickel particle is higher than automata velocities at the interface. In Fig. 8 one can detail distribution of automata velocities at the inter-automata interface. It is important that there is intensive shear deformation at the interface.

5. Hot spot formation under high rate shear deformation

The simulation of the Ni-Al powder mixture showed that an intensive mechanical mixing of the components, caused by penetration effects, takes place under shock compression of powder mixture. This leads to localized initiation of chemical reaction. To investigate the mechanisms of that mixing on atomic level special modeling was carried out by molecular dynamics method. The simulation showed that a great number of "hot spots" may be formed under considered conditions. The problem of hot spots is very important for studying the solid-phase chemical reactions. It is necessary to say that the hot spots at certain critical size may initiate chemical reactions in the material.

The hot spot is an ensemble of atoms, the average kinetic energy of which exceeds to a great extent over the average kinetic energy of the sample. According to the Maxwell-Boltzman distribution of velocities of atoms, there are always some groups of atoms, the energy of which are higher than the average one. However these groups can not be considered as a hot spot, since they have such an energy for a short time (comparable to a single atomic oscillation). It also should be noted, that in the perfect crystals the hot spots never appear, even though the sample is subjected to heating or high energy loading. Hot spots are not observed in the material with structural defects, if it has been relaxed and in equilibrium.

The mechanism of formation of hot spots was studied in the work [4] based on molecular dynamics method. As a rule, the hot spots appear in the regions with high density of defects due to interaction with different perturbation. In the present work the interaction of solitary waves, appearing under shear loading, with vacancy clusters was investigated. At first the initial coordinates and velocities of atoms of a simulating system are determined. Then the equations of motions are calculated on the base of known interatomic potentials and forces. Three-dimensional crystallite of Al, containing 2 vacancy clusters of 4 vacancies for each was simulated. The calculations were carried out using the unique software "Monster MD" [5]. This software allows: 1) to simulate the behavior of materials with different kind of structural defects under external loading; 2) to draw fields of distribution of atom velocities, stresses, internal energies, local temperatures, radial distribution functions for different time moments, and etc. The method of molecular dynamic is the base of this software. The structure of software can be

easily changed (other methods of numerical integration, boundary conditions, external loading, interatomic effective potential, structure of sample, an other metal or alloy and so on can be used).

Three-dimensional crystallite of aluminum, including near 9000 atoms, was modeled at the temperature near to 0K. Coordinate axes were directed as: OZ – along $< 1\,1\,1 >$, OY – along $< 2\,\bar{1}\,\bar{1} >$, OX – along $< 0\,1\,\bar{1} >$ directions. Periodic boundary conditions were used in OY and OZ directions. On the two side surfaces normal to OX direction the boundary condition were: $V_z = V_x = 0;\quad V_y^r = 0;\quad V_y^l = const;$ (where V^l is the component of the velocities on the left side surface of the sample; V^r is the component of the velocities on the right side surface of the sample). The interatomic pair interaction potential was calculated on the base of pseudopotential theory, either as in work [5].

To initiating the solitary waves, for the first time it was discovered in [6,7], a shear loading was applied on the sample for 40 time steps (time step $\Delta t=2.42*10^{-15}$ sec). Then propagation and interaction of solitary waves with the defects of structure were studied.

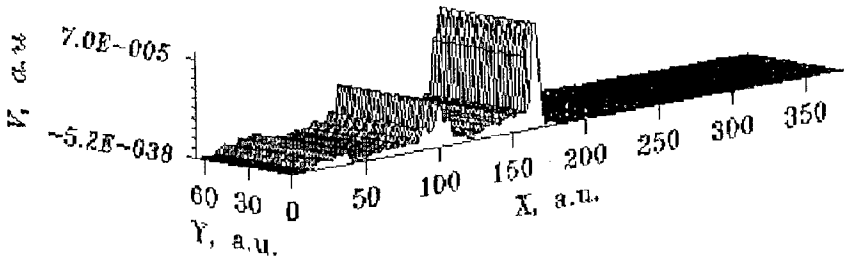

Fig. 9. XY- projections of atomic velocities in perfect crystallite under shear loading with the rate of 200 m/sec at the 900-th time step.

On the first stage of studies the mechanical shear loading of an ideal crystallite was simulated. The results of simulation are shown in Fig. 9. At first the waves have only X-component of velocities, they are compression-extension waves and propagate with the speed close to the sound velocity for this material. These waves may be considered as a certain analogue of elastic forerunners. Then the waves propagating with much less speeds (near 3700m/sec) are observed. They are characterized by considerably greater amplitude and have X, Y and Z components of velocities. The calculations showed that, when changing the shearing rate, the propagating speeds of the solitary waves remain constant, but the amplitudes of the waves herewith are changed. Particularities of propagation and interactions of such waves were studied in [6,7]. It was shown that they may be formed in heterogeneous materials even at low mechanical loading, in particular, as a result of creation of "shear bands", microdamages, at jump-type growing of cracks and etc.

On the second stage of studies the interaction of perturbations. caused by shear loading, with vacancy clusters were simulated.

For this purpose the shear loading with different rates of 200m/sec. 50m/sec and 30m/sec were applied to the left side surface of the sample. The results of such simulation are shown in Fig. 10. It should be noted that the hot spot arises in the defect region. The parameters of hot spot such as the starting time of heating, the local temperature, the duration of hot spot life were discovered to depend extremely on the value of shear loading rates. The region containing vacancy clusters will be heated to higher temperature, the heating of this region will start at much earlier time and duration of the hot spots life will be decreased by increasing the amplitude of solitary wave (increasing of shear loading). It follows to note that the size of hot spot will not be changed under reducing the shear loading from 200m/sec to 30 m/sec. This proves that the nature of arising the hot spot is connected with elastic energy release which accumulated in the region of the defect.

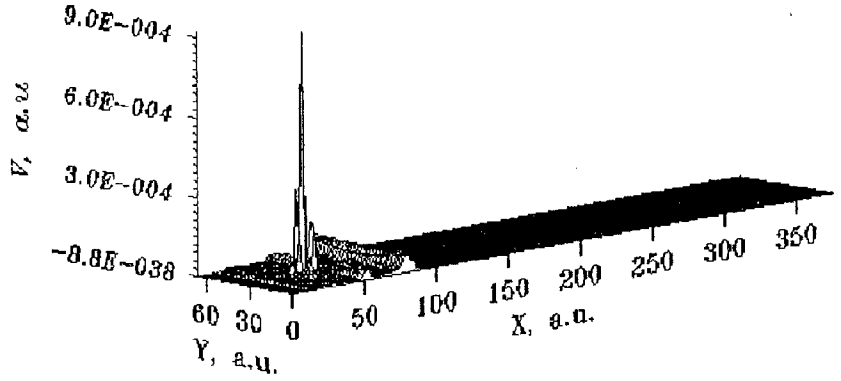

Fig. 10. XY- projections of atomic velocities in the sample with a vacancy cluster under shear loading with the rate of 200 m/sec at the time 400-th steps .

The creation and development of the hot spots are accompanied with essential structural relaxation in the region of their locations. Moreover the most displacements are observed towards OZ axis perpendicular to the direction of shear loading and the solitary waves propagation. During the process of structural re-arrangement the velocities of separate atoms may reach very high values (1000 m/sec).

Thus, the energy of the hot spot is defined by the avalanche process caused by decreasing of potential energy under the local structural re-arrangement initiated by mechanical loading. The obtained results allow, in particular, to explain some effects of mechanical activation of solid-phase chemical reaction of the materials components [8-10] and to better understand the response of the materials under shear loading.

Profile of potential relief was shown to be changed. Conditions for low temperature thermo-nuclear synthesis were shown to be reached in such systems.

References

1. S.G.Psakhie, Y.Horie, S.Yu.Korostelev, A.Yu.Smolin, A.I.Dmitriev, E.V.Shilko, S.V.Alekseev. Method of Movable Cellular Automata as a Tool for Simulation Within the Framework of Mesomechanics // Russian Physics Journal, 1995.- V.38.- P. 1157 - 1168.

2. S.G.Psakhie, S.Yu. Korostelev, E.V. Shilko, A.I.Dmitriev, A.Yu. Smolin, S.V. Alekseev. New approach to modeling on meso- and macro-level shock compaction of reaction-assisted powder mixtures // Proc. of the International WorkShop Materials Instability under Mechanical Loading.- St.Petersburg.- Russia, 1996.- P.30.

3. S.G.Psakhie, Y.Horie, S.Yu.Korostelev, A.Yu.Smolin, A.I.Dmitriev, E.V.Shilko, S.V.Alekseev Movable Cellular Automata Method as a New Technique to Simulate Powder Metallurgy Materials // Proc. of the Int. Conf. Deformation and Fracture in Structural PM Materials. Stara Lesna, Slovakia, 1996.

4. D.H.Tsai: J.Chem.Phys., 1991, **95**, 7497.

5. S.G.Psakhie, S.Yu.Korostelev, S.I.Negreskul, K.P.Zolnikov, Z.Wang, S.Li: Phys.Stat.Sol., 1993, **B176**, K41.

6. S.G.Psakhie: Proc. of International Conf. of Metallurgical and Materials Applications of Shock Wave and High Rate Phenomena, "Explomet", El Paso, Texas, USA, 325, 1995.

7. S.G.Psakhie, K.P. Zolnikov, S.Yu. Korostelev: Pisma v JETF, 1995, **21**, 1. (in Russian)

8. N.S.Enikolopjan, V.B.Voleva, A.A.Hzardgan et al: DAN USSR, 1987, **292**, 1165. (in Russian)

9. V.V.Boldyrev: Izv.AN USSR, ser. chem:, 1990, 2228. (in Russian)

10. V.V.Boldyrev: Experimental methods in mechanochemistry of solid nonorganic substances, Nauka, Novosibirsk, 1983. (in Russian)

THREE PEARLS OF SHOCK COMPRESSION INORGANIC CHEMISTRY.

Yu.Horie
(North Carolina State University, Raleigh, USA)

There are many problems in shock compression chemistry of inorganic materials that cry out for solution. This paper is concerned with three of the most outstanding issues: strong chemical initiation, growth, self-sustainability.

A review will be made of recovery experiments and real-time measurements to infer or delineate controlling material responses that initiate strong chemical reactions at the shock front. It will be proposed that analogous to crack propagation, chemical initiation is primarily controlled by local mechanisms and can not be described by global conditions such as input energy. An approach based on local differential particle velocity will be discussed and an elementary initiation model will be evaluated using such mixtures as Sn/S and Al/Ni.

Chemical kinetics at present cannot be discussed quantitatively due largely to lack of measurements. However, we shall present model calculations of pressure measurements to suggest (1) that global kinetics has a characteristics time constant on the order of 1 μm or less and (2) that the amount of reaction at the shock front is limited. We surmise that this limit is a result of the fact that the initiation takes place in spatially localized regions of reactant materials. Thus, the extent of fast reaction is also controlled by the same mechanisms that initiate the reaction.

Self-sustained reaction (condensed phase detonation) is of interest because it provides unequivocal proof of strong, ultra-fast chemical reaction at the shock front. we shall discuss a model calculation of self- sustained shock-induced chemical reaction in a Ni/Al mixture, based on the idea of layered composite material to induce and to support the chemical reaction.

MATHEMATICAL MODELLING OF SHOCK WAVE PROCESSES IN CHEMICALLY REACTING INORGANIC POWDERS.

V. M. Fomin, S.P.Kisclev, A.P.Alhimov, O.B.Kovalenko
(Institute of Theoretical and Applied Mechanics Rus. Acad. of Sci., Novosibirsk, Russia)

The behavior of the mixture of non-organic chemically reacting powders in shock waves is discussed. The influence of strength properties of the materials and inhomogenity of deformation of the powders on the process of chemical reactions and formation amorphous alloys at the surface of the powder particles is analyzed. The structure of the shock wave and dilatation wave is studied in powder mixture. The method of cool gas-dynamic spraying is considered for obtaining composite materials. The paper presents the results of mathematical modeling of propagation of SHS stationary wave in Ni-Al powder mixture.

X-DIFFRACTION INVESTIGATION CONCERNING STRUCTURES OF BE,AL,SI,FE, LIF,SIO2,KCL UNDER DYNAMIC PRESSURES FROM 2GPA TO 20 GPA.

V.V.Mokhova, L.A.Egorov, A.I.Barenboim, V.V.Dorokhin
(Russian Federal Nuclear Center (VNIIEP), Arzamas-16)

High velocities of deformation during effect of shock waves on solids cause fast-going structural changes with generation of metastable intermediate phases and states. To investigate these processes it is necessary to employ structural - sensitive methods of solid physics.

Currently, the only direct method to study behaviour of solid crystal substance structures under dynamic compression is method to record X-rays diffraction pictures of crystal structures under shock compression.

The paper presents results of X-rays diffraction measurements concerning structural parameters of shock compressed substances at pressures higher than Hugoniot elastic limit (Be, Al, LiF, Fe+3%Si), lower than Hugoniot elastic limit (Si, SiO2, LiF) and under pressure of phase transformation begining (KCl).

Recorded states of shock-compressed substance structures demonstrate indentity of structural deformations at pressures higher and lower than Hugoniot elastic limit as well as at pressures above the phase transformation point, which can be characterized as single-axial deformations.

HIGH-SPEED CHEMICAL REACTIONS AT SHOCK LOADING OF CONDENSED SYSTEMS

V.A. Skripnyak, E.G. Skripnyak, E.V. Shilko*
Tomsk State University, Tomsk, Russia,
*Institute of Strength Physics and Materials Science SB Russian Academy of Sciences, Tomsk, Russia

Introduction

In the case of chemical processes in solids we deal with a new class of phenomena, which are different in principle from the chemical processes in reacting liquids and gases. The scientific interest to chemical processes and mechanisms of reactions ongoing in solids is stimulated by 3 reasons:

1. Possible difference in reaction products of the same initial components [1-3].
2. The realization of chemical reactions in the solid phases, which cannot be realized in the liquid phases [1].
3. Difference in the stages of chemical reactions in solids and liquids. Solid phase chemical process goes for a single stage, while the reactions in liquid phases can proceed in several stages with formation of metastable intermediate products [1-3].

Solid phase chemical reactions can be used for production of new chemical products and materials and to release the energy with high rates that lead to explosion.

It is well known, that at usual conditions the chemical processes in solid-phase systems proceed more slower, than in liquid and gas phases. It is stipulated by slow speed of diffusion, ensuring the mass transfer of components in solid phase. At present, several methods are used to accelerate the chemical reactions in solid phases [1- 13].

The methods of solid-phase chemical reactions acceleration are connected with mechanical loading of powder mixtures. The solid components are processed into fine powders with the grain size of about 10-100 μm. High speed solid-phase chemical reactions of decomposition or sintering may be realized in powder mixture under quasi-static mechanical loading. This loading is a combination of high hydrostatic pressure and intensive plastic shearing. At laboratory conditions high-speed solid-phase reactions are obtained under loading in circuit rotated - Bridgmen anvil and under mechanical extrusions of mixture through a head of cold extruder. The time of the reactions is 10^{-3}-10^{-5} sec [1-4]. The characteristic time of the shock-assisted chemical reaction is of about 10^{-6}- 10^{-7} sec in such powder mixtures as Sn-S, Mo-S [3]. Thus, in the both cases the high rate chemical reactions take place. The Arrhenious effective factor of diffusivity will have the value of about 10 decimal orders higher, than at usual conditions.

High rate chemical reaction can be produced under liquid-phase sintering and by technology of self-propagating high-temperature synthesis (SHS) [5-7].

The time of liquid-phase sintering of previously compacted powder mixtures of inorganic materials is of about tens minutes.

The speed of combustion front propagation is 4-10 mm/sec in the mixtures (Mo-S , Ti-C, Ti-Si etc.). The appropriate characteristic time of the chemical transitions in SHS front is about 1-10 sec. Direct observation over the SHS process in a thin layer of mixture showed, that the reaction goes at formation of thin layers of liquid phase [5]. The rough estimation of the particle heating time in the reacting mixtures gives 10^{-3} sec. The diameter of the grains is less then 0.5 mm and maximum temperature corresponds to the melting point. Therefore, the reactions at SHS are not caused by thermal activation due to the heat transfer from the heated layers. It is possible to solve this paradox, if to assume, that the formation of the melting zone is stipulated by the energy release in the zone during the process of exothermic chemical reaction. This process is self accelerated.

The most effective, but not enough studied method of acceleration of practically important classes of solid-phase reactions (decomposition, restoration and synthesis) is a shock-wave loading of powder mixtures.

The experimental study of solid-phase chemical reactions under shock loading are being carried out for more than 30 years already. In Russia the basis of this direction was founded by G.A.Adadurov, S. S.Batsanov, A.N.Dremin, Yu.A.Gordopolov, A.G.Merzhanov and others. The overview of this works was done in [3].

Up to now, the studying of solid phase chemical processes under shock loading are performed by experimental methods. At the same time the grate interest is exhibited to research the solid-phases chemical processing by mathematical modeling. At present there is no united approach to describe all kinds of high-speed solid-phases chemical reactions. Therefore, it is of great importance to define both the application fields of the existing approaches to investigation of high-speed chemical processes and necessity of development of new approaches.

The main question is : which of already developed mathematical models and methods are applicable to research of high-speed chemical processes and mechano-chemical phenomena. In this paper we shall discuss the mathematical models of chemical processing only under shock loading.

Models of mechano-chemical processing under shock loading

Experimental studies showed that the phenomena of high rate solid phase chemical reactions are strongly differed from chemical processes in mixture of liquids and gases [1-14]. The solid-phase chemical processes are defined mostly by the mechanical factors (stress, intensity of plastic deformation, uniformity of a stress-strain condition) and less by thermodynamic factors (such as temperature). That is caused by the difference between mechanisms of mass transfer at chemical processes in solids and diffusion mechanisms in gases and liquids.

The basis for modeling mechano-chemical processes in gas and liquid mixtures are the continuum mechanics and Arrhenious chemical kinetics [3].

As a rule, a model of mechano-chemical processes includes three groups of equations [8-10]. The first group consists of equations of mechanical conservation laws and laws of phenomenological thermodynamics. The second group includes the equations of states for multiphase medium. Kinetic equations of chemical processes are united in the third group.

The continuum models of mechano-chemical processes in powder mixtures under shock loading can include the same groups of equations [8-10]. However, the specific forms of the equations may be different.

There are some difficulties at the development of the models of solid state mechano-chemical processing. Some of this difficulties are connected with adequate describing of:

- the mechanical behavior of porous powder mixtures under loading;
- the energy release at the phase transformation under loading;
- the change of the solid phases concentrations at chemical reactions under loading.

Mechanical behavior of powder mixture under shock loading is described by the approach of multiphase media mechanics [10]. The solid phase chemical reaction is known to be initiated under application of hydrostatic pressure and shearing.

One of the problems of this approach is the necessity of construction of state equation for the mixture, the phase structure of which is varied at chemical transformation. It should be taken into account, that the initial mixture have pores, which are collapsed under shock loading.

Plastic deformations are more non-uniform on meso-level of porous powder mixture, than in continuous solids under shock loading. Therefore the chemical reactions are initiated in local micro-volumes.

Distribution of particle velocity in front of shock waves was observed in metals and alloys [13]. Dispersion of particle velocity behind the front of the shock wave is not decreased in materials with essentially heterogeneous structure (for example in steel and high-strength alloys). This can be explained by the fact, that the shear stress relaxation keeps going behind the front of the shock wave, but with the less speed. The most probable mechanisms, ensuring the shear stress relaxation behind the front is the rotational mechanisms of plastic flow.

Metallographical studies of shock-loaded metals and alloys proved the reality of such mechanisms [14 -15].

Two-level micro-dynamic model can be offered for analysis of mechano-chemical phenomena. This approach was developed for studying the connection between micro-localization of plastic deformations and particle velocity dispersion in front of plane shock waves in alloys and metals [16].

In the framework of this approach the mechanical behavior of powder mixture are considered on two connected structural levels. At macro-level the effective mechanical parameters are used. This parameters are averaged over representative volume of the mixture.

The material point of the medium on meso-scopic level is considered as heterogeneous media.

System of conservation equations on macro-level includes:

$$\frac{\dot{\rho}}{\rho} = -div\ \vec{u} \quad , \quad \rho\dot{\vec{u}} = div\,\sigma \ , \quad \rho\dot{E} = -\sigma(\dot{\rho}/\rho) + \rho\dot{Q} \quad , \qquad (1)$$

where ρ_0, ρ - initial and current average mass density, $\vec{u}$ - particle velocity, σ - stress tensor , E - specific internal energy, $\dot{Q}$ - rate of energy

The mechanical parameter of state, mechanical and release in chemical reaction.thermodynamic properties have a distributions on meso-level.

The initially two component powder mixture can be considered as 4 phases mixture after initiation of chemical reaction. In the simplest case, there are 2 initial solid phases, 1 solid phase of reaction product and 1 gas phase in pores.

The equation system of phase mixture includes

$$\sum_{j=1,4} C_j = 1 \ , \quad \rho_j C_j = \rho \quad , \ j = 1,4 \qquad (2)$$

where C_j - concentration of j - phase, ρ_j - mass density of j phase in representative volume.

Density of gas phase can be supposed to be equal to zero. Volume concentrations of initial solid phases C_1, C_2 and volume concentration of the product of chemical reaction C_3 are connected with stoichiometric relation

$$K_1 \rho_1 C_1 + K_2 \rho_2 C_2 = K_3 \rho_3 C_3 \ , \qquad (3)$$

where K_j - stoichiometric coefficients.

The specific internal energy can be calculated for representative volume

$$\rho E = \rho_j E_j \ .$$

(4)

The local thermodynamic equilibrium is assumed within representative volume. Thus,

$$\rho_j \dot{E}_j = -P_j(\dot{\rho}_j/\rho_j) + S^j_{mn}\dot{\varepsilon}_{mn} \ , \ j = 1,2 \ ,$$

$$\rho_j \dot{E}_j = -P_j(\dot{\rho}_j/\rho_j) + S^j_{mn}\dot{\varepsilon}_{mn} + \rho_j \dot{Q}_j \ , \ j = 3,$$

(5)

where S^j_{mn} , ε^j_{mn} - components of stress tensor deviator and strain tensor in j-th component, $\dot{Q}_j$ - rate of specific energy release .

The internal energy of representative volume ρE equal sum of internal energy of solid phases $\rho_j E_j$ under adiabatic loading in front of shock waves.

The value of S_{mn} can be supposed equal to zero in hydrodynamic approach.

It is known, that chemical reactions of sintering are initiated in powder mixture under shock pressure of 15- 20 GPa [3, 4] .

The Mie-Gruneisen equation of state of solid phase can be used [3, 17]:

$$P_j = P_j(\rho_j, E_j) \ , \ j = 1,3 \ .$$

(6)

The pressures P_j are assumed to be equal to each other in solid phases:

$$P_1 = P_2 = P_3 \qquad (7)$$

The models of damaged media are popular for calculation of mechanical behavior of porous materials under dynamic loading [8-10] .

The effective pressure P can be calculated on macro-level within the framework of the model of damaged media [10].

$$P = P_j \ (1 - F (C_4)) \quad ,$$

(9)

where $F (C_4)$ - phenomenological function.

For metal powder mixtures it can be approximately linear $F(C_4) \approx C_4/C_4^*$, C_4^* is the constant.

The decreasing of volume concentration of gas phase in the pores of the mixture are usually described by evolutionary or kinetics equations [8-10]. The main problem is to use the most adequate kinetics equation for the mixture. The simple kinetic equation can be used:

$$\dot{C}_4 = \left[P - P_0^*(1-F(C_4))\right] / \tau_4 \, P_0^* , \quad P > P_0^*(1-F(C_4)), \quad C_4 > 0 ,$$

$$\dot{C}_4 = 0 , \qquad P \le P_0^*(1-F(C_4)), \quad C_4 = 0 ,$$

(10)

where τ_4 - characteristic time of the pores collapse, P_0^* - constant of mixture.

It is established, that the solid-phase chemical transformations can be realized both in self-consistent front of chemical reactions and in front of shock waves. In the first case the speed of the reaction front can be less than the speed of the shock wave [11] . Thus, the mechanisms of chemical transformation can be different in the different solid phase mixtures under shock loading. It should be supposed that intensity and speed of energy release at solid-phase chemical transformations play the important role in realization of this mechanisms.

The energy release under chemical transformations ought to be included in the equation of energy conservation law (1). The rate of specific energy release must be also allowed in (5) for chemical transformation of components at meso-level.

The method for calculation of specific energy release was offered by S.S. Batsanov for two-component mixtures [3,13,18]. This method may be recommended for calculation. If the specific energy release Q is known, then the rate of specific energy release can be calculated as

$$\dot{Q}_3 = Q \dot{C}_3 \qquad (11)$$

The problem comes up, when the mixture has three or more reactants. The system of equations (1)-(11) is not closed. The equation of chemical transformation ($\dot{C}_3 = \Psi (P_j , E_j , \ldots)$) ought to be add to (1)-(11).

The change of the phase concentrations at chemical processing is described

by kinetics equation of chemical reaction. There is no universal kinetics equation for high rate solid phase chemical reactions. Two questions have to be solved for developing kinetic equations of high rate chemical reaction :

a). What are the conditions of loading which initiate high rate solid phase chemical reaction ?

b). How the solid phase chemical transformation evolves under loading ?

Initiation of high rate solid phase chemical reactions

It is necessary to introduce the description of distribution of mechanical parameters into evolutionary equation. It may be constructed with the usage of the result of modeling the chemical processes in the mixture by molecular dynamics method. Criteria of initiation and the end of the chemical transformations can be constructed, using parameters of phase deformation on meso-level. The kinetic or evolutionary equations have to be designed in terms of phase concentrations and mechanical parameters (both averaged and phase ones).

The plastic deformation is the most important factor, that controls of the initiation and the process of chemical reaction. Collapse of the pores in mixture is caused by plastic deformation of grains of the mixture. Thus, the effective bulk plastic deformation of macroscopic medium is defined by decreasing volume concentration of pores C_4. The following approximation can be used:

$$d\,\varepsilon_{kk}^{P} = \left(\frac{1}{3}\right)\left(\frac{d\,C_4}{C_4^0}\right), \quad (12)$$

where C_4^0 is the initial volume concentration of pores .

As it was mentioned above, two kind of chemical processes are realized in powder mixture under shock loading. The processes of the first kind are shock-initiated and the second ones are shock-assisted [3].

Short time of solid phase chemical reaction initiation requires super high speeds of mass transfer on atomic or molecular structural level. The opportunity to realize such mechanisms was proved in [4]. At the same time, high-speed of solid-phase chemical processes in front of shock waves were found to be caused by mass transfer at the distances of about some μm. However, this mechanism does not explain chemical transformations in powder particles of the mixture at the depth up to 100μm. Thus, after initiation of reaction the new mechanisms of high-speed mass mixing can occur.

Direct and indirect estimation of temperature in front of shock-initiated chemical reactions shows that the high-speed solid-phase chemical reactions are not thermally activated [11-13]. For example, thin polyethylene film in a mixture was not melted after the passage of the front of exothermic solid-phase chemical reaction through the mixture [12]. At propagation of the shock-initiated solid-phase reaction of decomposition of bicromat ammonia the introduced thin films of low-melting metals

(Sn and Pb) remained not melted. while the film made of Wood alloy was completely melted. The speed of the chemical reaction front was equal to1.3 km / sec, that is less then the speed of the shock wave propagation in bicromat ammonia.

The model of solid-phase chemical reaction initiation has to include the three conditions:

1). The concentration of reactant in mixture ought to be more than 0.

$$C_j > 0, \quad j = 1,2, \qquad (13)$$

where C_j is the volume concentration of chemical components.

2). The second condition can be formulated in two forms, either for pressure or for internal energy. The applied pressure has to be higher than come critical value P^*, which depends on the mixture porosity, average grain size and distribution of grain size.

$$P > P^*. \qquad (14)$$

Specific internal energy of each reactant E_j ought to be higher than critical value E_j^*.

$$E_j > E_j^* \quad , j = 1,2 . \qquad (15)$$

The specific internal energy of components E_j are different under adiabatic loading in the shock waves.

3). The third condition is connected with the specific mechanisms of high rate solid phase chemical reactions. The effective plastic deformation of the medium ought to be increased.

$$\begin{aligned} d\,\varepsilon_i^P &> 0, \\ d\,\varepsilon_{kk}^P &> 0, \end{aligned} \qquad (16)$$

where $d\,\varepsilon_i^P = \sqrt{\left(\frac{2}{3}\right)\left[d\,\varepsilon_{kl}^P\, d\,\varepsilon_{kl}^P - \left(d\,\varepsilon_{kk}^P\right)^2 / 3 \right]}$ is the increment of intensity of effective plastic deformation, $d\,\varepsilon_{kk}^P$ - the increment of the bulk effective plastic deformation (12).

The energy release under exothermic chemical reaction leads to the rise of non-uniformity of temperature and stress fields and initiates the rotational modes of deformation on different scale levels. Within this framework the two following experimental phenomena can be explained: 1) the dependence of critical of pressure of initiation of solid-phase reaction on the size of powder particles and 2) the decrease of the critical pressure at introduction of inert powder inclusions into the mixture [2].

Kinetic equations of chemical reactions

The rate of solid-phase reactions under shock-wave loading is not constant. Last year experiments carried out in the Institute of Chemical Physics (Moscow) showed, that the chemical reactions can be initiated in the very front also. Shock front structure was studied in reacting two-component mixtures Sn-S, Mg-S, Ni-Al by pyrometric method [3]. The time of solid-phase reactions is about 50-200 nano-sec for these mixtures [3, 18].

Application of Arrhenious kinetic equation in computer modeling of solid-phase chemical processes needs to define the effective kinetic coefficients in:

$$\frac{d\,C_1}{d\,t} = F\ (\ \{C_1\},\{k\}\ ), \qquad (17)$$

where t- the time, F - a function. C_1 - the specific volume of component 1 , k - the parameter connected with the speed of chemical reaction.

Specific volume of reaction product C_3 can to calculate by (2)-(3), (17). The kinetic equation (17) can be written in linear form in the simple case:

$$\frac{dC_1}{d\,t} = -k\,C_1 . \qquad (18)$$

The value of k is not constant in the phase mixture on meso-level. It is the complex characteristics of the loading process and the average size of powder particles:

$$k = k\{E, U, T\}, \qquad (19)$$

where E - an activation energy, U - the work of stresses, T - the temperature in the energy units.

The equation (19) can be used in the form:

$$k = \nu_0 \exp\left[-(E+U)/T\right], \qquad (20)$$

where $\nu_0 \approx 10^{13}\ c^{-1}$.

The characteristic time of exothermic synthesis reaction in solid-phase systems Sn-S , Al -Fe_2O_3 etc., measured by pyrometric measurements of intensity of radiation on the border of the reacting mixture, is of about 0.1-0.5 10^{-6} sec [3]. Thus, the rate of solid phase chemical reaction in powder mixture under shock loading can be of 3-8 decimal orders higher than the rate of similar reaction in a liquid phase. The estimation based on the speed of front propagation of shock-initiated solid-phase chemical reaction gave the same values [11].

The calculation results of plane shock-wave loading of stoichiometric Ti-Al powder mixture with application (1)-(11) , (12) -(16) and (18) are shown in Fig.1 and Fig.2 . Profiles of the shock wave front are shown corresponding to the time moment 0.4 μsec after the impact.

The initiation of chemical reaction is not realized in front of the shock wave in Fig.1. The condition of formation of two-wave structure of shock front is defined by the kinetics of pore collapse (9)-(10). If the chemical reaction is initiated in front of the shock wave, the front structure is transformed. Shock-assisted chemical reaction leads to acceleration of shock wave front propagation and some rise of the pressure. Results of calculation of shock wave structure in that case are shown in Fig.2. Non-uniformity of distributions of internal energies and strains of solid phases are risen on meso-level of mixture after beginning of chemical reaction. The chemical conversion is not full in stoichiometric mixture (Al ,Ti → Ti Al) after shock wave loading with amplitudes of 13 GPa. The specific volume of TiAl slowly grows with the distance from the impact surface. The chemical reaction is finished when specific volume of pores comes to zero.

Conclusion

The multi-level model of solids can be used for modeling chemical processing of solids under shock loading. Multi-phase mechanical models of reacting gases or liquid mixtures are rough-casts for the solids. The distributions of mechanical parameters on meso-level of solid mixture includes the information about possibility of the initiation and the process of chemical reactions.

References

1. Enikolopian N.S. Super high rate chemical reaction in solids // (Sov.) Journal Physical Cemistry 1989, N 9, pp. 2289-2298.
2. Enikolopian N.S. Explosive chemical reactions of metals, oxides and soles // (Sov.) Journal Physical Cemistry.1987. V. 1591, N10, pp. 912-915.
3. Batsanov S.S. Effects of explosion on materials / Springer Verlag, N.-Y. Inc. 1994. 194 p.
4. Horie Y. Mass mixing and nucleation and growth of chemical reactions in shock compression of powder mixtures // Metallurgical and Materials Applications of Shock Wave and High Strain Rate Phenomena/ Ed. By L.E. Murr, K.P. Staudhammer, M.A. Meyers . Elsev. Sci. B.V. 1995, pp. 603-614.
5. Alexandrov V.V., Korchagin M.A., Bolgyrev V.V. Michanizms and macrokinetics of interaction of the components in powder mixtures / (Sov.) Physical Cemistry. Vol. 1192, N 8 , pp. 879-881.
6. Vadchenko S.G., Merzganov A.G., Mukas'yan A.S., Sychev A.E. Influence of one axial loading on macrokinetics of combustion of nongas systems // DAN RAS. Cemistry. 1994. V.337. N.5, pp. 618-621.
7. Gordopolov Yu.A. , Trofimov V.S., Merzganov A.G. About the possibility of non-gas detonation of condensed systems // DAN RAS. Cemistry. 1995. Vol. 341.N.3, pp. 327-329.
8. Gryadunov A.N., Shteinberg A.S., Dobler E.A., Gorel'skii V.A., Zelepugin S.A. Ignition and development of chemical reaction of Ti and carbon under shock loading // Int. Journal SPHTS. 1994. Vol.3. N.3, pp. 252-266.
9. Arinshtein A.E. Kinetics of chemical reactions of anizotropic // (Sov.) Chemical Physics. 1993. Vol. 12. N. 1, pp. 73-81.
10. Ahmadeev N.H., Bolotnova R.H. Modeling of reaction of sintesis in powder mixture of Sn - S under shock loading // (Sov.) Chemical Physics. 1996. Vol. 15. N. 6, pp. 102-112.
11. Enikolopian N.S., Alexandrov A.I. , Gasparyan E.E. and other The transition of chemical energy to mechanical without thermolization // DAN RAS. Physical Cemistry. 1991. Vol. 319. N.6, pp. 1384-1387.
12. Enikolopian N.S., Hzardjan A.A., Gasparian E.E. and other Kinetics of explosive chemical reactions in solids // (Sov.) Physical Cemistry. 1987, pp. 1151-1154.
13. Batsasnov S.S. // Physics of Combustions and Explosives 1996. Vol. 32. N.1, pp. 115-129.

14.Nesterenko V.F. . Meyers M.A., H.C. Chen, J.C. LaSalvia // J. Appl. Phys. Lett. 1994, Vol. 65 , N 12, pp. 3069-3071.
15. Mescheryakov Yu.I. , Atroshenko S.A. /Metallurgical and Materials Applications of Shock-Wave and High -Strain -Rate Phenomena / Ed. by L.E.Murr, K.P. Staudhammer, M.A. Meyers . Elsevier Sci. Publ. V. 1995, pp. 443-450.
16. Skripnyak V.A., Potekaev A.I. Obout localization of plastic flow in front of shock waves // (Rus.) Izvestiya Vuzov. Fizika. 1995, N 4 , pp. 125-127 .
17. Gust W.H. High impact deformation of metall cylinders at elevated temperatures // J.Appl. Phys. 1982, Vol. 53, N. 5, pp. 3566-3575.
18. Shteinberg A.S., Knyazik V.A., Fortov V.E. About possibility of non-gas detonation in condensed systems // DAN RAS. Chemistry. 1994, vol. 336, N. 1, pp. 71-74.

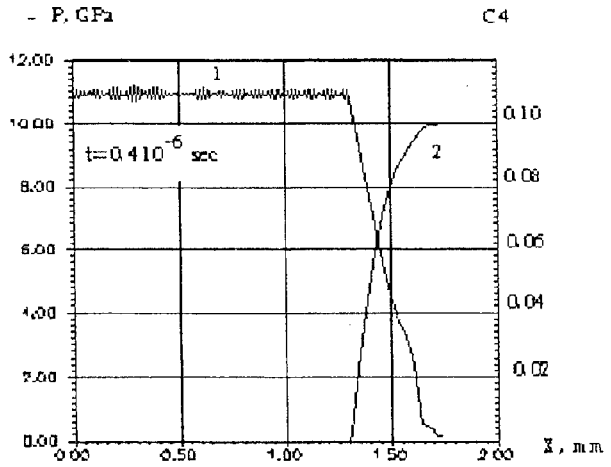

Fig.1. Structure of the shock wave front in stoiheometric Ti-Al mixture with initial specific volume of pores 0.1. Time after impact corresponds to 0.4 10^{-6} sec. The chemical reaction was not initiated. 1 - pressure P, 2 -specific volume of pores (C_4).

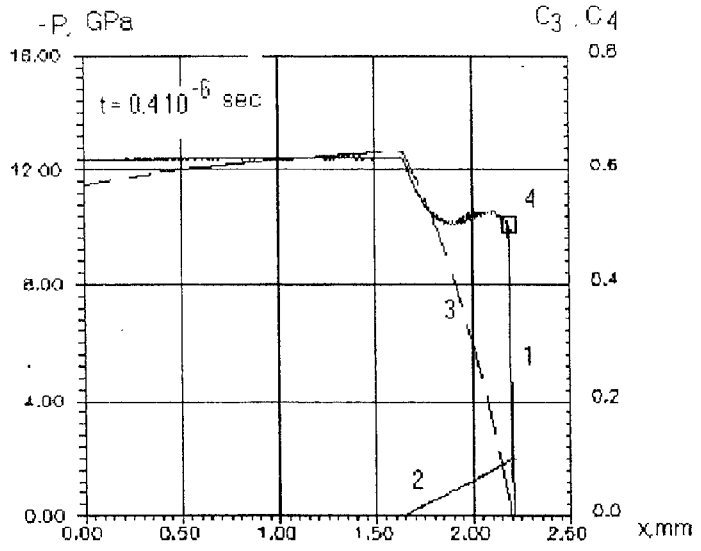

Fig.2. Structure of the shock wave front in stoiheometric Ti-Al mixture with initial specific volume of pores equal to 0.1. Time after impact corresponds to 0.4 10^{-6} sec. The chemical reaction was not initiated. 1 - pressure P , 2 - specific volume of pores (C_4), 3 - specific volume of TiAl (C_3), which are created in the shock wave front , 4 - point of chemical reaction initiation.

INTERFEROMETRIC MEASUREMENT OF THE PARTICLE VELOCITY DISPERSION IN DYNAMICALLY LOADED SOLIDS

Yu.I. Mescheryakov
Institute of the Mechanical Engineering Problem
Russian Academy of Sciences, Saint-Petersburg

1. Introduction.

Mechanics of deformed solid is traditionally based on the concept of mean stresses and mean strains. However, the processes of strain localization cannot be understood and described without introducing an intermediate scale level of deformation - the so-called mesoscopical level [1]. To date there are several scientific schools in Russia which developed and advocate mesomechanical approach to the strain localization problems [2,3].

As for dynamic plasticity, the only possibility to watch a behavior of elementary carriers of deformation (ECD) at the mesolevel is to introduce into consideration particle velocity distribution function (VDF). In practice, however, its determination seems to be very difficult if possible at all. Therefore the measuring of statistical moments of VDF becomes of great importance. In the shock-wave experiments as a rule only the first statistical moment of VDF is measured, namely the time profile of average particle velocity. In case of uniaxial strain loading this profile is registered, for example, with capacity or interferometric gauges. In [4,5] the technique for determination of the second statistical moment of VDF, particle velocity dispersion $< V(t)>$, has recently been developed. For different materials it has experimentally been shown that particle velocity dispersion does not remain to be constant along the average velocity profile V (t) but currently changes. For example, for the steady plastic fronts maximum value of dispersion occurs at the middle of front. As for the unsteady plastic fronts the behavior of dispersion is not so definite. It may often increase along the plastic front up to pulse plateau.

Microstructure analysis of specimens after shock loading shows that there exists a certain correlation between particle velocity dispersion at the mesolevel and strain localization processes. It was found that kind of kinematical mechanism at the mesolevel (translational, i.e. shear banding, or rotational) depends on the value of the velocity dispersion during the shock wave passage.

The objective of this paper is to show that kind of kinematical mechanism depends not only on the longitudinal component of velocity dispersion but on the transverse component of dispersion as well.

2. Mesolevel and statistical approach.

Technique for determination of mean particle velocity in a shock loaded material (the first statistical moment of VDF) is based on the interferometric measuring Doppler frequency shift of laser radiation when the latter drops on the free surface of shock loaded target. In case of the so-called velocity interferometer mean particle velocity V (t) relates to fringe number N(t) with a well-known relation. [6]:

$$\bar{V}(t) = \frac{\lambda}{2\tau} N(t) \qquad (1)$$

where τ is the interferometer delay time. When the particle velocities at the free surface of target are equal to each other, so that the scattering of particle velocities are absent, interference signal amplitude is constant and fringe frequency changes in accordance with changing the free surface velocity. If however, within laser beam spot at the free surface of target there exists a scattering of the particle velocity, amplitude of interference signal decreases due to widening of laser radiation spectrum after reflecting from the target [4,5].

Until now, when speaking about particle velocity dispersion under conditions of dynamic deformation we did not give concrete expression for their kind and space scale. It is not hard to estimate their typical scale by using the principle of interference. Measuring the particle velocity dispersion is based on concept that different particles at the free surface of target within laser beam spot give different Doppler frequency shifts. Effective interaction of separate particle and laser radiation is possible only if dimensions of particles are more greater as compared to laser radiation wave length λ_O (approximately ten times). On the other hand, uniform widening of radiation spectrum is possible only in case if within laser beam spot D_{SP} at the free surface of target there is sufficient quantity of similar particles (at least about hundred). From here the following estimate for dimension of particle can be accepted:

$\lambda_O << d_P << D_{SP}$

As a rule, being focused on the free surface laser beam has a transverse dimension about 100 μm and laser radiation length equals ≈ μm from where the value of particle approximately equals d_P = 10μm. That dimension in accordance with generally accepted in physics of plasticity classification belongs to the so-called mesoscopical scale level.

Note that the expression which relates interference contrast I and particle velocity dispersion $< V(t)>^2$, [5]

$$I = \exp\left[-\frac{\left(V-\bar{V}\right)^2}{\left\langle \Delta V\right\rangle^2}\right]; \qquad (3)$$

It has been obtained under assumption that VDF is equilibrium, i.e. has a symmetrical maxwellian form. This is true only for the steady plastic fronts. In general case of unsteady fronts in [8- 9] alternative technique for determination of the particle velocity distribution width. has been developed. It is grounded on the phenomenon of the so-called "fluctuative decay" of waves in a structure nonuniform media. Consider this approach in details.

In accordance with classification suggested by G.E. Duvall [7], there exist three kinds of wave decay: i). geometrical decay, ii) hydrodynamical decay, iii) maxwellian decay. The first kind of decay relates to space geometry of shock wave. For the spherical wave decay is proportional to $1/r^2$, for the cylindrical wave decay is proportional to 1/r and for the plane wave decay does not depends on propagation distance.

Hydrodynamical kind of decay relates to the circumstance that back front of compressive pulse propagates with the higher velocity than the first front since the former moves in a compressed material. For the short three-angle pulses this results in "cutting" upper part of pulse. Lastly the so-called "maxwellian" decay is stipulated by dissipative processes in a medium.

Beside the enumerated kinds of wave decay, which can exist in uniform medium, in nonuniform medium an additional kind of wave decay appears, which results from the nonuniform character of the particles motion - the so-called "fluctuative " decay. Its nature can be understood from the statistical consideration of the wave propagation process in a structure-nonuniform media.

Aforepresented estimate shows that space scale of structure nonuniformity attributes to mesoscopical level. Investigations in physics of plasticity which were carried out during the last ten year have shown that one of the most typical features of mesolevel is the space and charge heterogenization of dislocation structure on the distances of the order of free run of dislocations. Simplified scheme of heterogenization of dislocation ensemble is presented in Fig.1. It is seen that majority of dislocations from the mesovolumes V is subdivided in sign and gathered into narrow layers ΔV in vicinity of the mesovolume boundaries. These ranges have abundant dislocation density $\Delta\rho$.This means that these layers can be considered as superdislocatins having some summary Burgers vector B. Ensemble of similar particles are known to have a strong long-range interaction, which in turn superimposes the specific features on their statistical behavior. In other words, mesovolume with polarized dislocation structure can be represented as a quasiparticle with effective charge and therefore has a more higher radius of interaction as compared to initial quasineutral state in which $\Delta\rho$ and accordingly Δq are small. This permits for description of mesoscopical plasticity to use the statistical approach based on application of Fokker-Plank equation for mesoparticle velocity distribution function:

$$\frac{\partial f}{\partial t}+V\frac{\partial f}{\partial x}+\frac{F}{m}\frac{\partial f}{\partial V}=-\frac{\partial}{\partial V}\left(D_1 f\right)+\frac{1}{2}\frac{\partial^2}{\partial V^2}\left(D_2 f\right) \qquad (4)$$

Here m is the mesoparticle mass, F is the external force.

Diffusion coefficients D_1 and D_2 characterize change of VDF due to random interactions of mesoparticles with each other. The first diffusion coefficient $D_1=\frac{\partial(\Delta V)}{\partial t}$, or dynamic friction coefficient, characterizes the change of mean flow velocity due to mutual interaction of mesoparticles. Here <Δv> is averaged on the particle ensemble change of mean velocity owing to interaction of particles with each other. Thus, the value $D_1=\frac{\partial(\Delta V)}{\partial t}$ has a sense of deceleration and being multiplied by mesoparticle mass defines the value of fluctuative friction force directed opposite to the driving force. As a matter of fact, this value defines the fourth kind of decay which

can be classified as a "fluctuative decay". It disappears when partical velocity dispersion becomes negligible.

The second diffusion coefficient in the Fokker-Plank equation $D_2 = \frac{\partial(\Delta V \, \Delta V)}{\partial t}$ defines averaged on the mesoparticles ensemble the rate of change of particle velocity dispersion. As it has been shown in [8], in case of long-range mutual interaction of particles between diffusion coefficients there exists the following relation:

$$D_1 = D_1^{pol} + \frac{\partial}{\partial V}(D_2) = D_1^{pol} + \frac{1}{V}\frac{\partial D_2}{\partial t} \; ; \qquad (5)$$

where D_1^{pol} is the invariable part of friction coefficient related to polarization of particle ensemble. It follows from equation (5) that fluctuative decay depends on the rate of changing the second diffusion coefficient. This conclusion is of great importance for understanding the nature of fluctuative decay. In a sense it means that change of the mesoparticle velocity dispersion , for example due to nucleation of shear bands, results in fluctuative braking of mesoparticles, i.e. decreasing the pulse amplitude.

In Fig.2 two different free surface average velocity profiles obtained for two kinds of aluminum alloys are presented to compare different features of material depending on the dispersion behavior. Both profiles has been obtained under the same impactor velocity of 160 m/s. Under symmetrical shock loading when impactor and target have identical acoustic impedance there is following relation between impactor velocity, particle velocity and free surface velocity: $V_{imp} = 2V_p = V_{fs}$.

It is clearly seen from Fig.2 that while in aluminum AMg-6 maximum pulse amplitude corresponds to impactor velocity in aluminum alloy V-95 free surface velocity at the plateau of pulse achieves only 110 m/s, so that decrease of the mean particle velocity equals approximately to 50 m/s. This decreasing occurred owing to of catastrophic nucleation of shear bands under free surface velocity of 110 m/s . Thus, abrupt increasing a mesoparticle dispersion results in fluctuative decay of average velocity pulse.

Note, further, that at the back front of compressive pulse a number of interference fringes is again restored. This means that fluctuative decay at that part of pulse is absent. From the point of view of microstructure kinetics this means that random mutual motion of mesoparticles relative each other is stopped since a development of shear bands results in relaxation of internal microstresses. Thus, fluctuative decay proves to be reversible process. At the first pulse front the energy related to motion of mesoparticle with mean velocity pumps into energy of their chaotic motion. During the pulse plateau relaxation of internal stresses leads to decreasing dispersion. This, in turn, results in disappearing the fluctuative decay. Schematically the process of changing a mean velocity can be represented in form of changing the shape of particle velocity distribution function as it is shown in Fig.3. Under free

surface velocity of 110 m/s a desymmetrization of the VDF happens whereas to the end of pulse plateau VDF again restores to symmetrical shape.

It should be noticed that total reversibility of transition from symmetrical VDF to nonsymmetrical one and *vice versa* is possible only for the elastic interactions of mesoparticles. In the case of unelastic interaction the energy loss at the expense of unelastic dissipative processes takes place. For example, development of shear bands is exclusively dissipative process resulting in local heating of material. It should be remembered, however, that all what related to dissipative losses is already taken into account in a "maxwellian" decay. Fluctuative decay is the pumping of energy from the mesoparticle motion with mean velocity into chaotic motion and vice versa, while "maxwellian" decay is non-reversible energy scattering. In a certain sense, fluctuative decay can be considered as a latent energy box from which under specific conditions the energy of chaotic motion suddenly transforms into energy of directed motion of particles, which can often result in fracture of material. The same reason can lie in a unexpected onset of earthquake.

3. Kinematics of straining at the mesolevel.

In this connection the question arises how the particle velocity distribution function and/or its statistical moments are related to the kind of kinematical mechanism of dynamic straining. One possibility to analyze this coupling seems to use the continual theory of dislocation keeping in mind that instead of dislocation it is implied the mesoparticle having a summary Burgers vector equaled to dislocation charge of mesoparticle. Complete equation system can written as follows, [9]:

$$M\frac{\partial V_k}{\partial t} = \frac{\partial \sigma_{ik}}{\partial X_i}, \quad \sigma_{ik} = \lambda_{ikl} W_{lm} \qquad (6)$$

$$\frac{\partial V_k}{\partial X_i} = \frac{\partial W_{ik}}{\partial t} - J_{ik} \qquad (7)$$

Here $V_k = \frac{\partial U_k}{\partial t}$ is the mesoparticle velocity, W_{ik} are components of elastic distortion, U is the total displacement (elastic plus plastic) and J_{ik} are the components of mesoparticle flow tensor. Kinematics of plastic straining can be inferred from the continuity equation (7). By using this equation it may be written:

$$\frac{\partial V_k}{\partial X_i} - \frac{\partial V_i}{\partial X_k} = \frac{\partial W_{ik}}{\partial t} - \frac{\partial W_{ki}}{\partial t} + \left(J_{ik} - J_{ki}\right) \qquad (8)$$

Since we are interested only in kinematics of plastic straining elastic rotations will be neglected. Then the rate of plastic rotation is determined by difference of antisymmetrical components of flow tensor:

$$\dot{\omega} = \left(\frac{\partial V_k}{\partial X_i} - \frac{\partial V_i}{\partial X_k}\right) = J_{ik} - J_{ki} \qquad (9)$$

In accordance with definition of flow tensor via particle velocity distribution function [10]:

$$J_{ik} = e_{ikl}\int V_l f_{kj}\, d\vec{V} \qquad (10)$$

its components for the concrete rotation along coordinate X_3 are:

$$J_{12} = \int \left(V_3 f_{22} - V_2 f_{32}\right) d\vec{V};$$

$$J_{21} = \int \left(V_1 f_{31} - V_3 f_{11}\right) d\vec{V}; \qquad (11)$$

$$J_{12} - J_{21} = \int V_3\left(f_{22} + f_{11}\right) d\vec{V} - \int V_1\left(f_{32} + f_{31}\right) d\vec{V}$$

Here f are the components of tensor mesoparticle velocity distribution function, [10] :

$$f = \begin{pmatrix} f_{11} & f_{12} & f_{13} \\ f_{21} & f_{22} & f_{23} \\ f_{31} & f_{32} & f_{33} \end{pmatrix} \quad ; \qquad f_{ii} \text{ are the screw components}$$

f_{ik} are the edge components.

It is seen from Eq.(11) that: i) rotational motion of medium in plane $X_1 X_2$ is provided by motion of screw components of VDF along axis X_3, ii) rotational motion achieves maximum value when motion of edge components at plane $X_1 X_2$ is suppressed, iii) when the densities of screw and edge components of VDF are identical, difference between antisymmetrical components of flow tensor equal to zero:

$$J_{12} - J_{21} = 0,$$

which means that rotational motion of medium is absent and there is only translational motion.

Let $V_3 = V_{II}$ is the component of mesoparticle velocity along the wave propagation and $V_1 = V_2 = V_\perp$ are the components in transverse direction. If the densities of screw and edge dislocations are identical one obtains:

$$J_{12} - J_{21} = 2\int \left(V_{II} - V_\perp\right) f(V)\, d\vec{V} \qquad (12)$$

Let

$$V_{II} = V_{II}^0 + \Delta V_{II} \qquad \textit{and} \qquad V_\perp = V_\perp^0 + \Delta V_\perp$$

Suppose then that longitudinal and transverse mean mesoparticle velocities are equal to each other. Here ΔV_{II} and $\Delta V_\perp$ are the total mesoparticle velocity decrease in longitudinal and transverse direction due to fluctuative decay mechanism. They relate to the first diffusion coefficient D as follows:

$$\Delta V_\parallel = \int D_\parallel^{II}\, dt \qquad \Delta V_\perp = \int D_\perp^{\perp}\, dt \qquad (13)$$

By using Eq. (5) one obtains:

$$\Delta V_{II} = \frac{D_2^{II}}{V_{II}}; \qquad \Delta V_{\perp} = \frac{D_2^{II}}{V} \tag{14}$$

where D_2 is the second diffusion coefficient of the Fokker-Plank equation. Thus, the rotation rate can be expressed in the following form:

$$\varpi = \int f(V)\left(\frac{D_2^{II}}{V_{II}} - \frac{D_2^{\perp}}{V_{\perp}}\right) d\vec{V} \tag{15}$$

It is seen that intensity of rotation motion depends on the difference between variation coefficient in longitudinal and transverse directions. For the constant mesoparticle density this equation can be-written in the form:

$$\varpi = \rho B\left(\delta_{\text{II}} - \delta_{\perp}\right) \tag{16}$$

where

$$\delta = \frac{\langle \Delta V \Delta V \rangle}{V}$$

is the variation coefficient.

It can be concluded experimental technique to be used must provide the simultaneous measuring of both longitudinal and transverse dispersion at the single action of dynamic straining.

References

1. V.I. Vladimirov, V.N.Ivanov, N.D.Priemski Mesoscopical level of plastic deformation. Fizika prochnosti i plastichnosti . Leningrad, Nauka 1986 pp.69-80
2. Physical mesomechanics and computer-aided desigh of materials.
In two volumes Editor Academician V.E. Panin Novosibirsk, Nauka. 1995
3. V.V.Pybin. Large plastic strains and fracture of metals. Metallurgiya, 1986, 224 p.
4. J.R.Asay and L.M.Barker. Interferometric measurement of shock induced internal particle velocity and spatial variation of particle velocity. J. Appl. Phys. v.48, pp.2545-2550,(1974).
5. Yu.I.Mescheryakov, A.K.Divakov. Maltiscale kinetics and strain-rate dependence of materials. DYMAT-journal 1994, vol.1 pp. 271-287.
6. L.M.Barker. Fine structure of compressive and release wave shapes in aluminum measured by velocity interferometer technique. Symposium on High Dynamic Pressure. Paris. 1967. pp 369-382.
7. G.E.Duvall. Proceeding of Iris University. 1972.
8. J.Hubbard. The friction and diffusion coefficients of the Fokker-Plank equation in a plasma. Proceedings of the Royal Society, Series A, Mathematical and Physical Sciences, No 1300, 1961, v.260, pp.114-126
9. A.M.osevich. Dynamic theory of dislocation. Russian physical annals, 1964, v.83, pp.579-592
10. Yu.I.Meschervakov, E.I.Prockuratova. Kinetic theory of continuously distributed dislocations. Int.J. Sol. Strs, 1995, v.32, N 12,pp.1711-1726

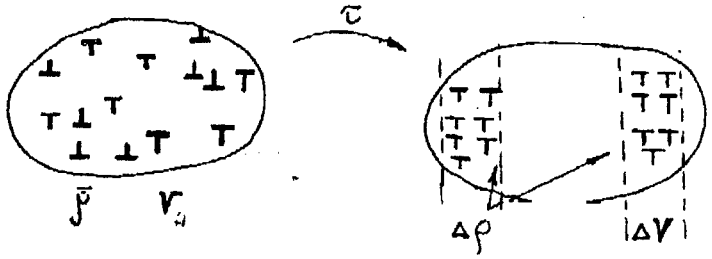

Fig. 1. Simplified scheme for heterogenization of dislocation ensemble. ΔV is the mesovolume

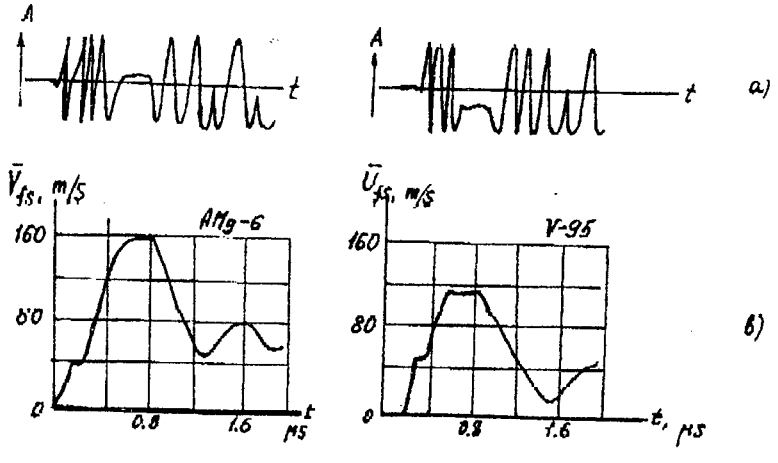

Fig.2. Interference signals (a) and mean free surface velocity profiles (b) for two kind of aluminum

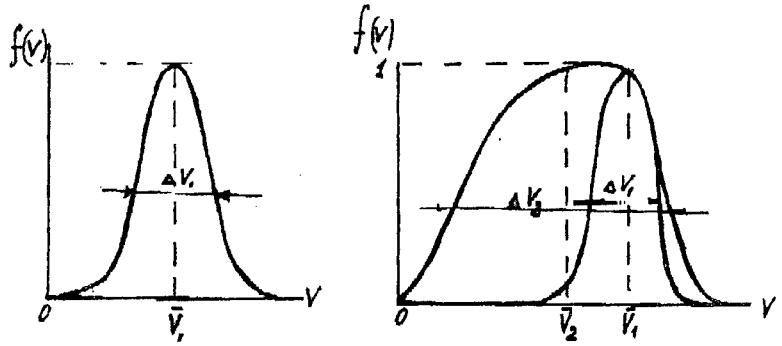

Fig.3. Symmetrical (a) and nonsymmetrical mesoparticle velocity distribution functions

Electrical response of (Sn+S) reactive heterogeneous system on shock wave effect

S.S. Nabatov

(Institute of Chemical Physics (Chernogolovka). Rus. Acad. of Sci., Chernogolovka. Russia)

Introduction

Investigations of electrophysical phenomena in inorganic materials understanding of the mechanism of shock induced transformations in heterogeneous systems. Electrical methods attract attention and have promising perspectives because they can be used in dynamic experiments, restricted by microsecond time interval [1], as well as in recovery experiments with an unlimited registration time [2,3].

In the present report a new method of investigation of the (A+B->AB) type reactions at shock compression is described. In this case A is metal component, B - dielectric component, and AB semiconductor compound. The method idea, first formulated in [4], is based on the well known fact that emf generated at shock compression of metals (1-10 mV) is much lower than that for semiconductors (100-1000 mV).the experimental realization of the idea consists in the registration of the electrical response of shock compressed mixture to the effect of shock have reflected from electrode of the experimental device. It is supposed that the shock compressed mixture will generate sufficiently large signal under the effect of reflected stock wave if semiconductor compound is appeared behind the front of the first shock wave.

The method has been proved with the system Sn+S->SnS in the pressure range 10-30 GPa (first compression). It has been found out that the electrical signals registered at the mixture compression by the reflected wave correspond to semiconductor state of the sample when the pressure of the first shock wave exceeds 15Gpa. Preliminary conclusion has been made that the signals can be explained be the formation of the semiconductor compound SnS behind shock wave front.

Experiment and results

Shock wave experiments were carried out with the use of monolithic samples made from elemental powder mixture corresponding to the stoichiometry of the SnS compound. The size of tin particles was about 100 micrometers. The scheme of the experimental arrangement is illustrated in Fig.1. The sample with a sickness of 1-2 mm and 10 mm in diameter is sandwiched between the aluminum driver plate and the thick copper electrode. The sample and electrode are placed inside teflon ring. The mixture is subjected to a plane shock wave compression with the help of the high explosive charge (60 mm in diameter) which is in contact with driver plate.

The pressure of the first shock wave P1 and the pressure of the wave reflected from the electrode P2 were calculated on the base of the standard shock impedance matching method using the known pressure in the driver plate and the Hugoniots of Cu, Al and the system Sn+S. The Hugoniot of the system Sn+S is [5]
D=2.13+1.62*U, km/s; po=4.74 g/cc, where D is shock velocity, U - particle velocity and po - initial density.
The voltage V of the electrical signal was recorded by a fast digital oscilloscope with the input resistance Re=75 Ohm. Since the sample resistance is small compared to Re the voltage V is equal to the emf generated by the shock wave when it propagates between the electrodes.

As it has been reported in [6] SnS sample generates at shock compression signals of characteristic voltage 200-300 mV. The response form is shown qualitatively in Fig.2, where t1 - time of shock wave entrance into a sample t2 - time of shock wave arrival at the second electrode. The system Sn+S does not reveal semiconductor properties at P1 about 10 GPa. However at more higher pressures the reactive mixture really behaves as a semiconductor substance. This fact is illustrated by experimental oscillograms presented in Fig.3. The upper record (Fig. 3a) was obtained at P1=21.0 GPa. The first shock wave generates weak positive signal on the level about 20 mV. At the moment of the first wave reflection from the electrode (t2) the negative impulse with the amplitude more than 250 mV arises. During the reflected wave propagation through the mixture the response changes its polarity. Oscillogram obtained at P1=25.5 GPa and P2=39.6 GPa (Fig. 3b) is qualitatively similar to previous one with the exeption of the short positive impulse at the beginning of the record. It is important to note that this impulse arises before the shock wave reflection from the electrode.

Discussion

Within the scope of the qualitative model of the method it is impossible to evaluate the extent of the chemical transformation. But there are indirect evidences showing that the mixture does not react completely behind the shock front. The above mentioned short impulse at the beginning of the oscillogram in Fig. 3b is an example of such evidence. The rise of the impulse before reflection of the first wave from the electrode can be explained be the following way. Due to partial chemical interaction the contacts between tin particles were destroyed and the mixture acquired semiconductor properties behind the front of the first shock wave. Thus the compressed part of the mixture can respond as a semiconductor element on a thermal effect. The thermal affect can be caused by a full completion of the reaction in some localized region («hot spot») of the compressed mixture. To our mind there is analogy between the sharp signal in Fig. 3b and signals that have been observed during registration of the reaction Sn+S-> SnS in recovery experiments [3]. The experimental arrangement for electrical measurements in recovery experiments is illustrated schematically in Fig. 4. The sample under investigation is in

contact with the semiconductor element generating thermo emf signal due to temperature difference between its sides. The thermo emf signal obtained in the experiment with the system Sn+S is shown in Fig. 5. The pressure in this experiment was 16 GPa (multiple compression). One can see short impulses caused by hot spots bounding with semiconductor (SnS) element surface But this case chemical reaction takes place in millisecond time interval.

It is believed that the method developed will find wide applications in the field of shock wave chemistry.

REFERENSES

1. Yakushev Electrical measurements in dynamic experiment.
   Fizika Goreniya i Vzryva, 1978, v.14, № 2, pp. 3-19.
2. Nabatov, A.N. Dremin, S.O. Shubitidze, V.V. Yakushev.
   Use of electroconductivity measurement method for physic-chemical
   transformation investigation in recovery capsules.
   Fizika Goreniya i Vzryva, 1986, v. 22, № 6, pp. 130-134.
3. Nabatov, S.O. Shubitidze, V.V. Yakushev.
   Use of termo-emf phenomenon in semiconductors for investigation
   of exothermic processes in recovery device.
   Fizika Goreniya i Vzryva, 1990, v. 26, № 6, pp. 114-116.
4. Nabatov, A.V. Lebedev.
   Use of electrical response of semiconductor compound for chemical
   transformation registration behind shock front.
   Khimicheskaya Fizika, 1994, v. 13, № 12, pp. 175-176.
5. Batsanov, M.F. Gogulya, M.A. Brazhnicov,
   Simakov, I.I. Moksimov.
   Behavior of the reactive system Sn+S in shock waves.
   Fizika Goreniya i Vzryva, 1994, v. 30, № 3, pp. 107-112.
6. Nabatov, A.V. Lebedev.
   Thermoelectrical signals at shock compression of semiconductor sample
   in plane recovery capsule. Khimicheskaya Fizika, 1993, v. 12, № 2, pp. 167-169

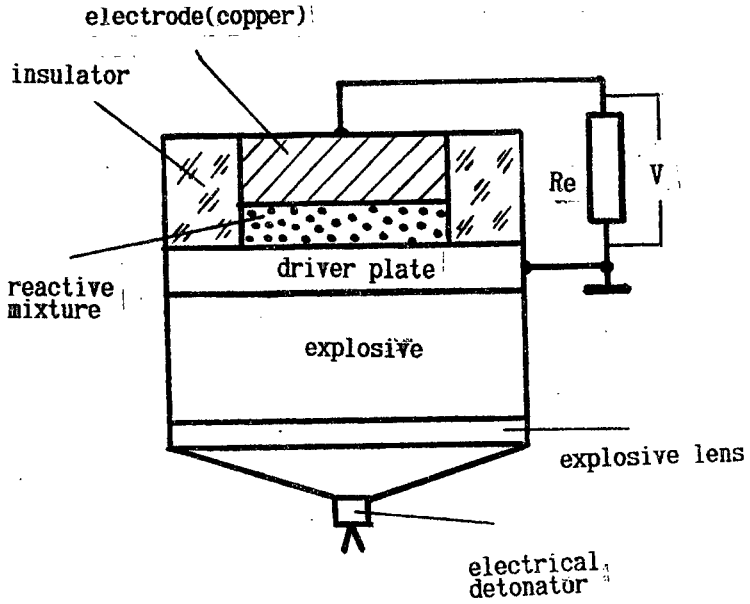

Fig.1. Experimental arrangement

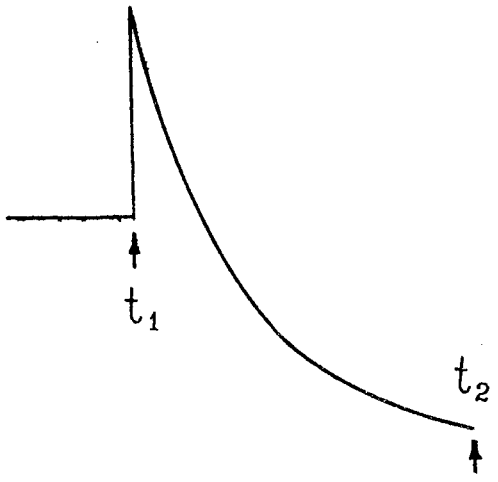

TYPICAL SIGNAL FORM

Fig.2. Qualitative shape of signal generated by the CdS sample

Electrical response of the system Sn+S

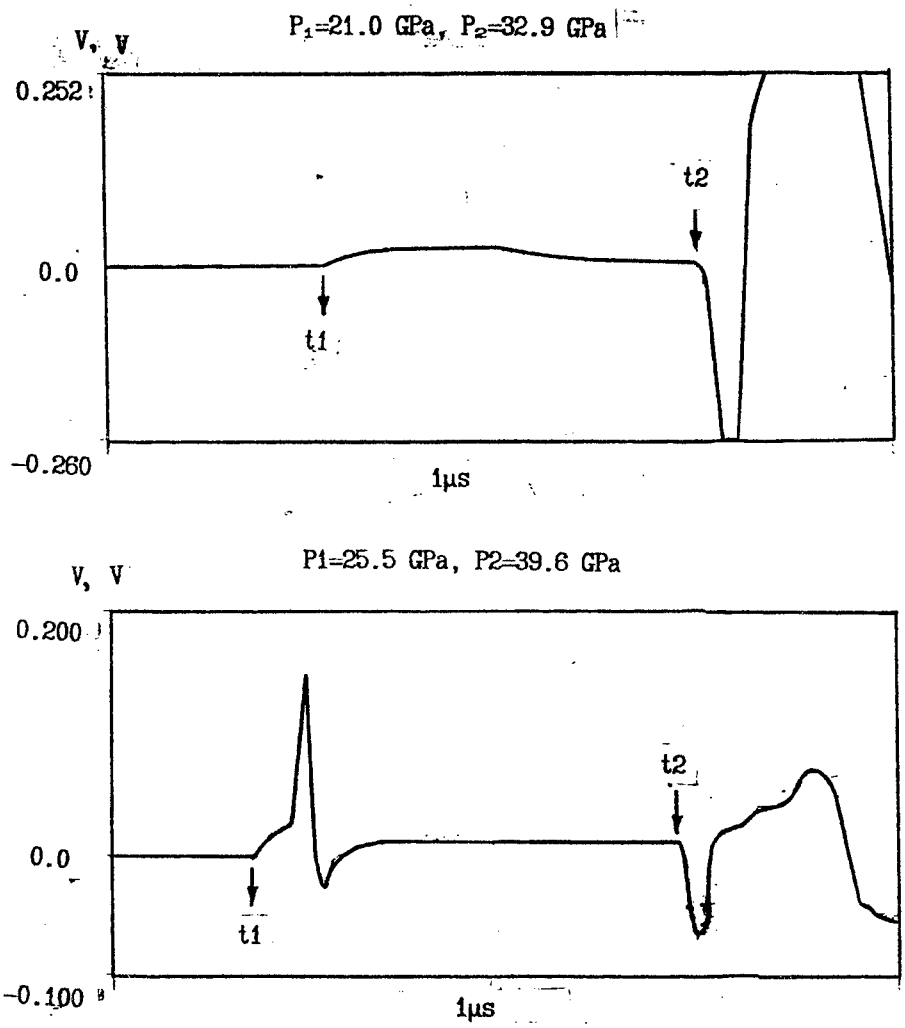

Fig.3. Experimental oscillograms. t1 – time of shock wave entrance into the sample; t2– time of shock wave arrival at the electrode.

Exothermic reactions registration in recovery experiments

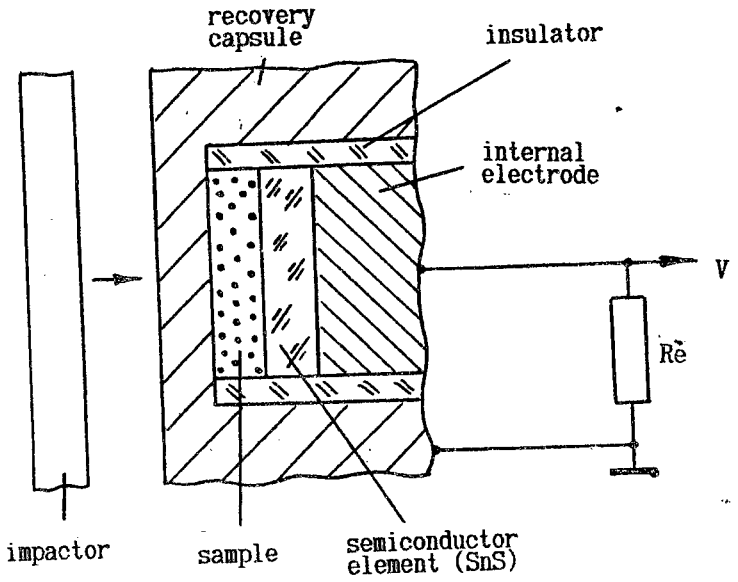

Fig.4. Arrangement for registration exothermic prosses in recovery experiments

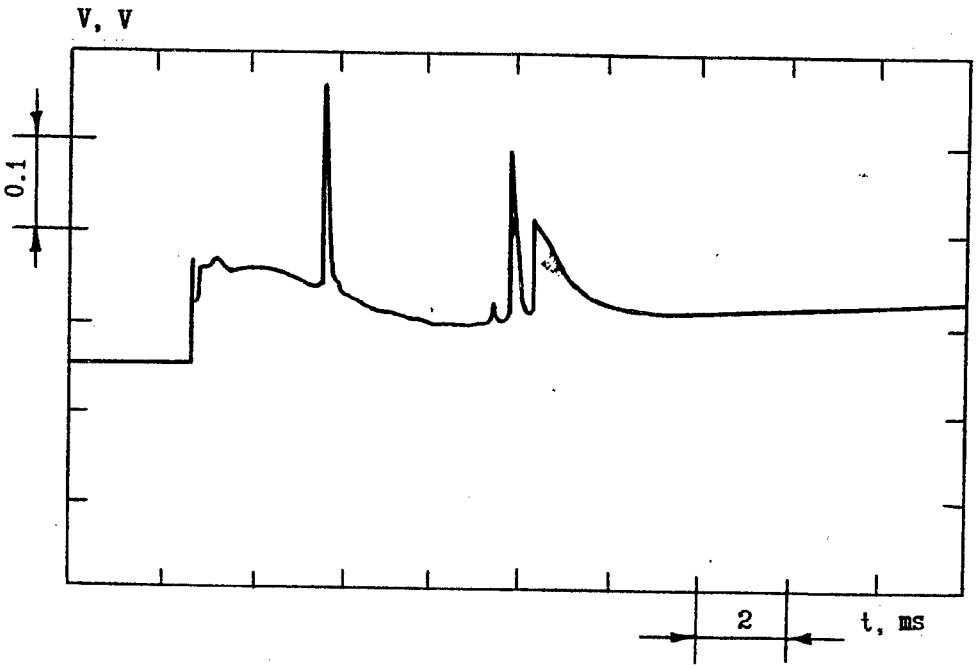

Fig.5. Experimental oscillogram of the thermoelectrical signal

IMPACT INDUCED SOLID STATE METAL/METAL REACTIONS*

Diana L. Woody and Jeffery J. Davis
Naval Air Warfare Center Weapons Division
Chine Lake, California 93555-6001

ABSTRACT

This paper discusses experimental results from an effort conducted to discern the basic mechanism of reactions in porous metal/metal compositions under rapid plastic flow conditions. Small-scale impact tests were performed on various intermetallic mixtures: 3CuO + 2Al, Fe_2O_3 + 2Al, Ni + Al, and 5Ti + 3Si. The addition of polytetrafluoroethylene (Teflon) to the metal/metal mixture has been demonstrated to affect the extent of the reactions. Real-time emissivity of the reacting materials was used to discern the exothermic reactions occurring under rapid flow conditions.

INTRODUCTION

Metal/metal and metal/metal oxide materials have exhibited the ability to generate highly exothermic reactions capable of occurring in the same time frame as detonations in conventional energetic materials.[1,2] Until recently, these materials were assumed to initiate exclusively under shock conditions. However, work done by Woody and Davis[3,4,5] with materials under mechanical impact conditions as well as by Nestereenko and Meyers [6,7] with materials under explosive compaction conditions, has demonstrated the role that rapid plastic flow can play in the reactions of these mixtures. Horie has modeled their shock reaction based upon a critical plastic flow.[8]

Small-scale experiments have been performed to observe the effect of rapid plastic flow produced by impact reactions on porous metal/metal compositions.[3] This paper explores the effect of the addition of polytetrafluoroethylene (Teflon) to several metal/metal and metal/metal oxide mixtures including 3CuO + 2Al, Fe_2O_3 + 2Al, Ni + Al, and 5Ti + 3Si. Reactions such as those found in high-temperature, self-propagation synthesis (SHS) have been observed under impact conditions. Shear due to impact-induced plastic flow plays an important role in the rapid energy release of these types of materials. The plastic flow induced reaction process is comparable to shock assisted reactions and SHS. A two-color infrared detector was used for real-time emission measurements of the reacting materials.

- Approved for public release; distribution is unlimited.

EXPERIMENT

A drop weight impact machine was used to induce a plastic flow in the test samples. The impact machine used for these experiments consisted of an anvil, an accelerated guided drop weight, a base, and a release triggering device. The impact

machine is described fully in another publication [4] Elastic shock cords were used to accelerate the drop weight to obtain impact velocities of 13 m/s. At these velocities, the plastic floe has been measured to be approximately 60 m/s. The impact of the drop weight on the anvil as planar to within 2 mrad. The samples used for the tests weighed 0.2 g and were in loose powder from prior to impact. Because the samples were loose powders, their initial porosity was not measured. The light emanating from the impacted sample came from its surface.

Teflon was mixed with the metal mixtures described above by the mortar and pestle method. The specifics of the materials are listed in Table I.

TABLE I. Characteristics of Materials Used in This Study.

Material	Manufacturer	Material Data
Titanium (Ti)	CERAC, Inc.	325 mesh, 99.5% purity, 20μm or less
Silicon (Si)	CERAC, Inc.	325 mesh, 99.5% purity, 10μm or less
Aluminum (Al)	CERAC, Inc.	325 mesh, 99.97% purity, 5 - 15 μm
Teflon	DuPont	7A, 35 μm, 60% crystallinity
Iron Oxide (Fe_2O_3)	CERAC, Inc.	325 mesh, 99.97% purity, ≥15 μm
Copper Oxide (CuO)	CERAC, Inc.	325 mesh, 99.97% purity
Nickel (Ni)	CERAC, Inc.	325 mesh, 99.5% purity, 10 - 20 μm
Garnet Paper	Norton, Inc.	180A Garnet A511

The two-color infrared detector consisted of a HgCdTe element juxtaposed to an InSb element. Each element measured 0.101 by 0.101 cm with am active area of 0.010 cm^2. The elements were housed in a liquid-nitrogen-cooled Dewar and kept at an operating temperature of 77 K. The InSb element's spectral response was from 2 to 5 μm. The HgCdTe element was capable of detecting wavelengths from 5 to12 μm. The signal from each infrared detector element was transmitted as a voltage through an initial voltage amplifier and the transferred to a LeCroy digital oscilloscope.

RESULTS AND DISCUSSION

The reaction of the materials to impact was quantitatively defined from the infrared detector's signals. The extent of the reaction was quantified from the area under the infrared emission curve. The most extensive reactions in these experiments were defined as the largest peak emissions and the shortest time-to-peak emission registered by the two-color infrared detector. The peak emission and time-to-peak emission for some of the experiments are given in Table II.

TABLE II. Results Obtained with the Infrared Detectors for Some of the Compositions Tested.

Material and Composition	Radiation From InSb Detector, mV	Radiation From HgCdTe Detector, mV	Time-to-Peak Emission, μs
5Ti + 3Si	29	1.41	2950
(99%) 5Ti + 3Si (1%) Teflon (35 μm)	16	6.4	2950
(90%) 5Ti + 3Si (10%) Teflon (35 μm)	3547	55	56
(80%) 5Ti + 3Si (20%) Teflon (35 μm)	3664	68.9	56
(80%) Ti (20%) Teflon (35 μm)	2890	64.5	31.5
3CuO + 2Al	3250	164.1	16.25
(90%) 3CuO + 2Al (10%) Teflon	3090	163.8	27
(75%) 3CuO + 2Al (25%) Teflon	3000	158.1	44
(50%) 3CuO + 2Al (50%) Teflon	62.5	10.2	750
Fe_2O_3 + 2Al	22.7	3.9	2300
(99%) Fe_2O_3 + 4Al (1%) Teflon	3280	94.5	3075
(90%) Fe_2O_3 + 4Al (10%) Teflon	3500	154.7	36
Ni + Al	34.8	10.9	1340
(90%) Ni +Al (10%) Teflon	63.3	7.7	810
(50%) Ni +Al (50%) Teflon	62.5	10.2	750

Note: Percentages are by mass.

Qualitative signs of reactions consisted of such parameters as a visible light emission, an audible signal, and characteristics of the recovered simple's surface. The most exothermic samples exhibited a visible flash and sustained burning after impact up to 1 to 3 seconds in duration; charring was also found on the recovered sample. It was observed that the burning duration could be varied by changing the percentages of Teflon added to the mixtures. The results obtained with the infrared detectors are given in Table II.

5Ti + 3Si

As shown in Table II. impact of the 5Ti + 3Si mixture generated a small emission. as recorded by the infrared detectors. The small emission coupled with the longer time-to-peak emission indicated a heating of the impacted metals due to dynamic compaction rather than a chemical reaction. X-ray diffraction of the recovered samples reinforced our conclusion that reaction did not take place in that system. The addition of Teflon to 5Ti + 3Si considerably increased the peak emissions recorded by the infrared detectors and reduced the tine-to-peak emission by tow orders of magnitude (from milliseconds to microseconds). A detailed study has been performed on the effect that varying the percentage by weight of Teflon added to various 5Ti + 3Si mixture has upon the exothermic reactions observed.[9]

3CuO + 2Al

An extensive exothermic reaction was observed for the neat 3CuO + 2Al mixture. The reaction was characterized by a large infrared emission from the two detector elements, a visible flash, and sustained burning. The spectrometer registered strong emission lines for the neat mixture. The 3CuO + 2Al mixture was the only material in our study that reaction without the addition of Teflon. The addition of polymers to the metal/metal mixtures has been demonstrated to affect the extent of the reactions. As can be seen in Table II, increasing the percentage by weight of Teflon added to the 3CuO + 2Al mixture progressively decreased the peak emission and increased the reaction time registered by the infrared detectors. It was also shown that varying the percentages of the materials in the composites could determine whether a material is more likely to produce a sustained burning reaction. Studies were also performed in which the mixture containing 90% (3CuO + 2Al) and 10% Teflon was pressed into pellets to measure the effect of porosity on reaction initiation. The porosity of the material was a significant factor in determining the extent of reaction and exothermic output of these metal/metal/polymeric mixtures. The current study demonstrated that, when the mixture of 90% (3CuO + 2Al) + 10% Teflon was pressed into pellets, the % TMD had a significant effect on the reactivity of the material. The observable exothermic sensitivity decreased when the metal/metal/polymeric mixtures was pressed into a pellet. These data are detailed in another publication.[10]

Fe_2O_3 + 4Al

As show in Table II, the Fe_2O_3 + 4Al mixture generated a relatively small emission upon impact. These results were similar to those obtained upon impact of the 5Ti + 3Si mixture. The addition of Teflon to the Fe_2O_3 + 4Al mixture considerably increased the peak emissions upon impact. Increasing the percentages of Teflon added to the Fe_2O_3 + 4Al mixture gad a significant effect on the extent of the exothermic reaction and the signature of the infrared emission curve. The time-to-peak emission was decreased two orders of magnitude (from milliseconds to microseconds) for the mixture containing 10% Teflon.

Ni + Al

Table II shows that, although the addition of Teflon to the Ni + Al mixture increased the infrared emission recorded by the detectors and decreased the reaction time, the overall increase in exothermic release was not as substantial as that observed during the impact of the 5Ti + 3Si/Teflon and Fe_2O_3 + 4Al/Teflon mixtures. The qualitative signs of the reaction mentioned in the preceding paragraphs of this paper were not present these impact conditions.

CONCLUSIONS

The results of these experiments show that the variation in the amount of Teflon added to the metal/metal and metal/metal oxide mixtures can significantly alter the extent, initial time of reaction, and the duration of the exothermic reaction upon rapid shear conditions. The addition of Teflon also influences the likelihood of a material to produce a sustained burning reaction. The 5Ti + 3Si, and Fe_2O_3 + 4Al mixture exhibited relatively similar responses to the addition of varying percentages of Teflon. Under the impact conditions discussed in this paper, the highly exothermic reaction of 2Al + 3CuO did occur under plastic flow conditions without the addition of Teflon. However, when Teflon was added to the 3CuO + 2Al mixture, the exothermic reactions decreased in intensity. Overall, the most exothermic reactions were observed for the most porous mixtures. This gives an indication that shear due to rapid plastic deformation plays an important role in the initiation of the metal/polymeric mixtures under impact conditions.

ACKNOWLEDGMENTS

The authors gratefully acknowledge the Office of Naval Research (6.1 Independent Research program, Judah Goldwasser, cognizant technology area manager) for sponsoting and supporting the work reported.

REFERENCES

1. N. N. Thadhani, *Journal of Applied Physics* 76, p. 2129 (1994).
2. R. A. Graham, *Solids Under High-Pressure Shock Compression,* Springer-Verlag, 1993.
3. J. J. Davis and D. L. Woody, «Reactions in Neat Porous Metal/Metal and Metal/Metal Oxide Compounds under Shear Induces Plastic Flow Conditions», in *Metallurgical and Material Applications of Shock-wave and High-Strain-Rate Phenomena,* Eds. L. E. Murr, K. P. Staudhammer, M. A. Meyers, Elsevier, Amsterdam (1995) Chapter 78 pp. 661-668.
4. D. L. Woody, J. J. Davis, and J. S. Deiter, «Plastic Flow Generated Solid State Metal/Metal Reactions», in *Shock in Shock Compression of Compression of Condensed Matter - 1995,* Eds. S. C. Schmidt and W. C. Tao, AIP Press (1996) pp. 717 - 720.

5. L. Woody, J. J. Davis, and P. J. Miller. «Impact Induced Solid State Metal/Metal Reactions», *Proceedings of JANNAF Hazards Meeting*, San Diego, CA, August 1994.
6. F. Nestereenko, M. A. Meyers, H. C. Chen, and J. C. LaSalvia. *Applied Physics Lett.* 65 (24), December 1994.
7. F. Nestereenko, M. A. Meyers, H. C. Chen, and J. C. LaSalvia. *Metallurgical and Materials Transactions A,* Vol. 26A, 1995.
8. Y.Horie, «Kinetic Modeling of Shock Chemistry», in *Metallurgical and Material Applications of Shock-wave and High-Strain-Rate Phenomena,* Eds. L. E. Murr, K. P. Staudhammer, M. A. Meyers, Elsevier, Amsterdam (1995).
9. L. Woody, J. J. Davis, *Journal of Aplied Physics*, in progress.
10. D. L. Woody, J. J. Davis, «The Effect of Particle Size and Porosity on Metal/Metal Exothermic Reactions Induced by Low Velocity Impact», 14th US Army Symposium on Solid Mechanics, October 1996

Overview : BOUNDARY INSTABILITIES AND PHASE TRANSFORMATIONS SOLID MEDIA UNDER SHOCK LOADING

A.L.Mikhailov, O.B. Drennov, V.N. German, A.I. Lebedev, V.A. Raevski
(Russian Federal Nuclear Center (VNIIEP), Arzamas-16, Russia)

The phenomena of instabilities typical of boundaries dividing heterogeneous (stratified) liquids or gases under conditions of high-velocity flows are well-known: Kelvin-Helmgoltz instability (slip instability), Rayleigh-Taylor (gravitational) instability, Richtmyer-Meshkov instability (i.e. instability of Rayleigh-Taylor type under pulse effect). Phenomena of such a kind are less studied, if we deal with solid media, for example, metals, when strength and viscous-elastic characteristics of media have determining influence on instability.

The paper presents review of fulfilled experiments to investigate developments of three instability types mentioned above on boundaries dividing heterogeneous metals under effect of shock waves with high intensities (up to 50-100 GPa).

The paper analyses relation between instability development and the strength as well as phase transformations in media under investigation. The paper illustrates some methods to stabilize growth of disturbances. Experimental methods and diagnostics are described.

Attention is played in particular to investigation of phase transformations under shock loads observed in the similar experimental set-up.

MECHANISTIC PROCESS INFLUENCING SOLID -STATE SHOCK CHEMISTRY AND SHOCK SYNTHESIS OF MATERIALS.

N.N.Thadhani

(Scool of materials Science and Engineering, Georgia Institute of Technology, Atlanta, Georgia USA)

Shock chemistry and its implementation in synthesis of materials requires the development of a fundamental understanding of the complex mechanistic processes occurring during shock compression of powders. This understanding can be obtained by combined analysis of time-resolved measurements and characterization of microstructure of materials obtained from shock recovery experiments. In this presentation, we will describe our recent research work performed using nanosecond-resolution time- resolved pressure measurements and detailed characterization of the microstructure of recovered materials in several intermetallic-forming (e.g., Ti-Si and Ti-Al) and ceramic-forming (Ti-C and Ti-B) , highly reactive, powder mixtures.

Results of experiments performed at and below the threshold conditions for occurrence of reactions in the systems will be shown that the results of these experiments clearly demonstrate the unique effects of the shock-compression response of powders, which are in turn influenced by not only the shock loading conditions, but also the morphological characteristics (size and shape) of individual powder particles, the volumetric distribution of the reactant powders in a mixture, and the dissimilarities in the mechanical properties of the reactants. For example in the case of Ti-si system, powders of 10-25 μm particle size are able to plastically deform and flow (as revealed by post-mortem microstructural characterization), resulting in an intimately mixed, highly-activated, dense-packed configuration, which readily undergoes chemical reaction in the high- pressure shock state. Evidence of shock- induced chemical reaction in these powders is obtained by increases in wave sped measured using time- resolved pressure measurements. In contrast, powders of coarse particle sizes undergo fracture, and the fragments particles remain entrapped without mixing with each other, thereby remaining in an unreacted state. Powders of very fine particle sizes also show limited mixing and inability to mix and react due to effects of agglomeration of particles, as observed by post-mortem microstructural characterization, and as evidenced by time- resolved measurements. Observations of similar effects on reaction propensity will also be presented for the Ti-Al; Ti-B, and Ti-C powder mixtures. In general, it will be shown that in these various powder mixtures, the propensity for reaction can be explained on the basis of the ability of individual reactant particles to undergo deformation and flow, or fracture and dispersion. Thus, conditions which inhibit the deformation (or Fracture) and subsequent mixing of reactants exhibit a reduced propensity for reaction, irrespective of the heat of reaction of the system.

For applications relevant to synthesis of materials, it will be shown that the mechanochemical characteristics also provide a means of control for " shock-induced" reactions (occurring in the shock state) or "shock-assisted" reactions (occurring during post-thermal treatments due to shock- activation effects). Thus, products with tailored stoichiometry and microstructure can be synthesized, using either" shock-assisted" processes.

INVESTIGATION OF PHASE FORMATION UNDER THE EFFECT OF SHOCK WAVE IN THE V-HF SYSTEM.

A.V.Kolesnikov

(Institute of Chemical Physics(Chernogolovka), Rus. Acad.of Sci.,Chernogolovka, Russia)

Phase diagram of the V-Hf system has been investigated in detail at equilibrium conditions. The existence only of V2Hf intermetalide as well as solid solutions on the base of initial components have been established.

The use of explosions as a preparative method permits to hope for receiving of new compounds, which can be of interest in the chemistry of metallic superconductors and metastable states.

Explosion experiments have been performed with the use of cylindrical recovery capsules, subsequent X-ray phase analysis of the recovered specimens being carried out.

As the result of the investigations two new compounds of V2Hf3 and VHf3 compositions has been found out in the V-Hf system besides V2Hf known before. The compound V2Hf3 has sufficiently wide region of homogeneity (50-70 At. % Hf).

V2Hf3 rentgenographical data permit to consider its structure as the disordered variant of the intermetallic structure of Fd3m space group. The disordered structure has been identified on the base of cubic sell with the parameters: a=4,591 Angstrem, z=1, X-ray density 10,5 g/cm3, Fm3m space group.

The compound VHf3 has been identified on the base of hexagonal primitive sell with the parameters: a=4,999 Angstrem, c=8,151 Angstrem, X-ray density 11,04 g/cm3, z=2, Pb3mmc space group.

Thus the use of the techniques of shock wave synthesis leads to an essential extension of preparative methods. In particular, in the case of the V-Hf system it resulted in the synthesis of two new metastable compounds. The necesary condition of shock wave synthesis is the formation of melt.

CHEMICAL REACTIONS IN CONDITIONS OF INTENSIVE, CONTROLLED HIGH-STRAIN RATE SHEAR DEFORMATION

M.A. Meyers ,V.F. Nesterenko, J. LaSalvia and H.B. Chen
(University of California, San Diego ,La Jolla, USA).

The controlled high-strain-rate shear bands, having thicknesses of 5-20 microns, were generated in heterogeneous reactive porous materials (Nb+Si, Ti+Si) using axially symmetric experimental configurations, based on the radial collapse of a thick-walled cylinder ("Thick-Walled Cylinder" method). The experimental method generated overall strains up to 100 and strain rates of approximately = 10000000 sec-1 inside shear bands. Changes in particle morphology, melting, and regions of partial reaction were observed only inside shear bands for Nb+Si system. At the same conditions of high-strain rate deformation, for Ti-Si system the reaction being initiated inside shear bands propagated through the whole sample. The threshold conditions were established for global chemical reaction in the volume of Ti-Si mixture.

SHOCK INDUCED CHEMICAL REACTIONS IN TI-C AND TI-B POWDER MIXTURES

V.M.Fyodorov, Yu.A.Ivchenko, Yu.A.Gordopolov
(Institute of Structural Macrokinetics, Rus. Acad.of Sci., Chernogolovka, Russia)

The experiments of shock-wave loading of exothermic mixtures Ti-C and Ti-B of stoichiometric composition prove that at relatively low pressures (about 1GPa) initiation of the chemical reaction occurs with complete transformation of initial mixtures into products TiC and TiB2. Increase of pressure or elongation of time results first in cessation of the chemical reaction initiation. However, at 10-20GPa partial transformation of initial components into products TiC and TiB2 takes place, and at higher pressures complete transformation is observed. Such behavior of the mixtures under study can be explained by the change of mechanisms of chemical transformation due to the change of shock-wave conditions.

The experiments prove that chemical transformation in the system Ti-C at pressures above 11 GPa occurs in the shock wave front (at least, partially).

The results obtained can be used in further investigations of mechanisms and kinetics of chemical transformations in Ti-C and Ti-B systems upon shock-wave loading.

Special report

SOFTWARE BASED ON MOVABLE CELLULAR AUTOMATA METHOD ORIENTED TO SIMULATE RESPONSE OF MATERIALS AND STRUCTURES UNDER HIGH RATE LOADING

S.G.Psakhie, A.Yu.Smolin, A.I.Dmitriev,
E.V.Shilko, S.Yu.Korostelev, S.V.Alekseev

Institute of Strength Physics and Materials Science, Russian Academy of Science, Tomsk, Russia.

1. Main features of the software

The **MCA-Compaction** software is basically developed for simulation of powder compacting processes including chemical reactions under the contract of Sandia National Laboratories, USA, Contract No AM 2957B. The main code of **MCA-Compaction** is written in "C" programming language for OS UNIX System V and is an implementation of **MCA Method** [1]. The software also includes the utility **MCA-Analyzer** to overview the obtained results in on-line regime as well as during the run of **MCA-Compaction**. **MCA-Analyzer** is written in "C++" programming language using the X11 graphic interface. The **MCA-Compaction** software was tested on SUN and DEC workstations and also in CRAY Y-MP supercomputer.

To run **MCA-Compaction** the user have to prepare some necessary data. Namely one have to describe the materials characteristics, the sample and the parameters of the task. Materials characteristics describe mechanical, physical properties and parameters of phase and chemical transformations and are stored in **materials_db.dat** file. The information about the samples, including chemical compounds, size and geometry of the sample, the size of the automata etc., is specified in ***.smp** files. The parameters of interaction among automata depending on their types is specified in ***.pai** file. And such parameters as the time of calculations, time step of integration, type of the task (total, chemical or mechanical calculations only), loading conditions (velocity or force value on boundaries and initial ones) etc., are specified in ***.tsk** files.

MCA-Analyzer is developed for **X11 Window System** and utilizes standard **Xlib** library. This program has main window with the menu and allows to display in separate windows the following characteristics:

- structure of the simulated sample (automata are presented as circles),
- rotation angles of the automata,
- temperatures of the automata,
- velocity field of the automata,
- trajectories of automata between two any time moments,
- net structure of the interacted pairs of the automata,
- scale for displayed results (in this window user may change the scales).

Every separate window has the buttons for changing the time step and storing the results in GIF format.

Beside it user has an opportunity to set a number of "gages" in the sample. In this case **MCA-Compaction** will write specified parameters of "gage" automata to text file **task.dat**. And then user can view the plots of result parameters versus time or other parameter by standard visualization software.

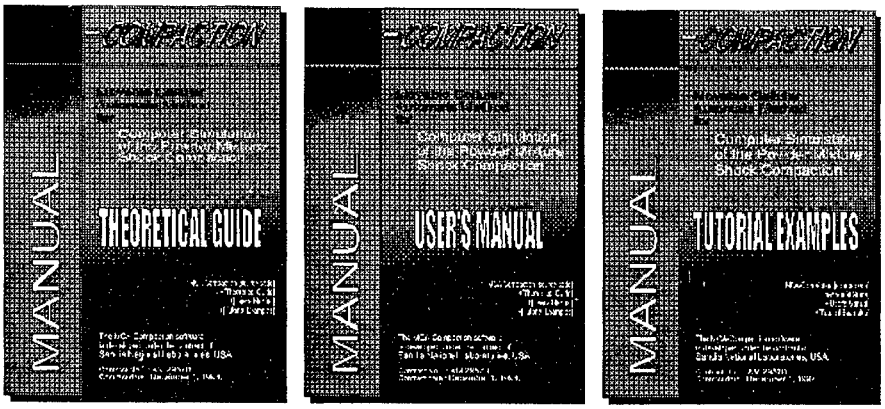

2. Demonstration of Possibilities

To demonstrate the main possibilities of **MCA-Compaction** software the result of simulations of two problems are shown. The first one is tension of a sample. The size of the sample is 0.29x0.53 mm. The loading of constant rate of 50 m/s is applied to the top of the sample. In Fig. 1 the structures of the sample are shown for different time moments In Fig. 1,a the initial structure is presented, in Fig. 1,b one can see the

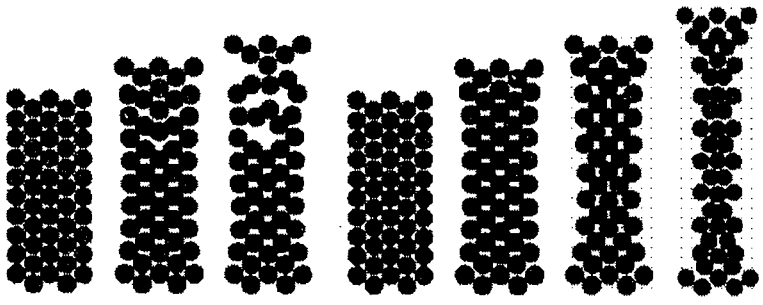

a b c d e f g

Fig. 1. Results of modeling of sample fracture under tension: a,b,c – the case of ordinary material; d,e,f,g – the case where automata of the sample are allowed to rotate without breaking their bond.

beginning of fracture and in Fig. 1,c the sample is broken. In the frame of the **MCA Method** we can vary parameters of the interaction among automata and allow them to rotate relatively each other without breaking linkage (bond). The results of simulation of tension the sample consisting of automata with these properties are presented in Fig. 1,d,e,f,g.

The second demonstration is bending of the sample under tangential pulse. The size of the sample is the same as previous one. The initial velocity of pulse applied to the top of the sample is 170 m/s. The velocities of automata of the sample at different time moments are presented in Fig. 2. One can see that plasticity of the material cause dissipation of initial pulse and at the end the shape of the sample is changed.

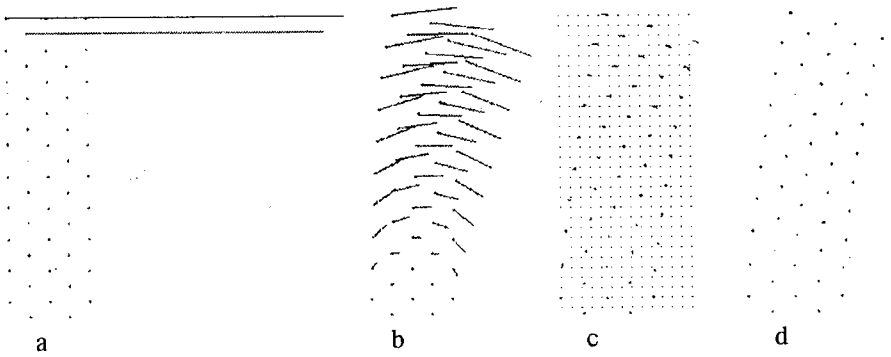

Fig. 2. Results of modeling of the sample bending under tangential pulse loading.

3. Shock Chemistry

At first we consider the problem of interaction of two particles. Initially aluminum (upper) particle moves with velocity of 800 m/s and nickel one does not move. The size of particles is 300 μm, size of automata is 0.3 μm. Figs. 3 and 4 show the results of simulation at different stages of the process.

In Fig. 3,d,e,f one can see the process of mixture of automata of different particles at the inter-particle interface. It is very important that **MCA-Compaction** allows to investigate the process of interaction at meso-scale level. In Fig. 4 one can see that the velocity of aluminum automata moving to the crack in nickel particle is higher than automata velocities at the interface.

The following example demonstrates modeling of shock compaction of powder mixture. The results of modeling are shown in Figs. 5 and 6. In the structure windows smaller particles are aluminum ones and bigger – nickel particles, light gray automata compose the flyer.

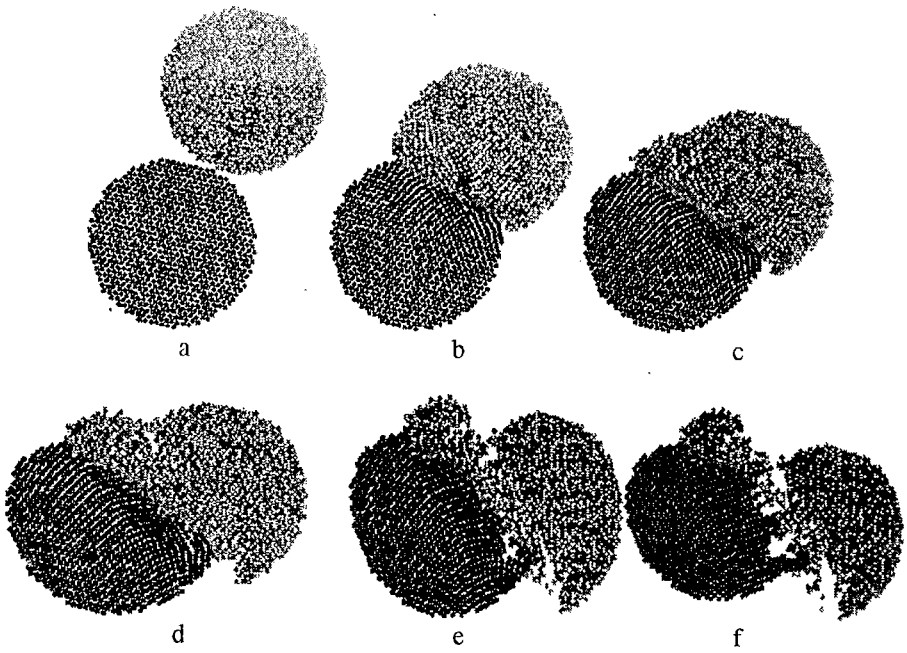

Fig. 3. Collision of aluminum and nickel particles. Structures at different time moments.

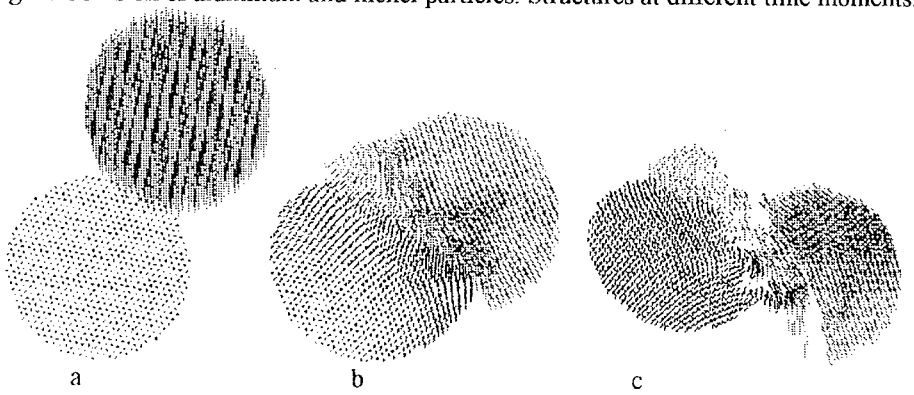

Fig. 4. Collision of aluminum and nickel particles. Velocities of automata.

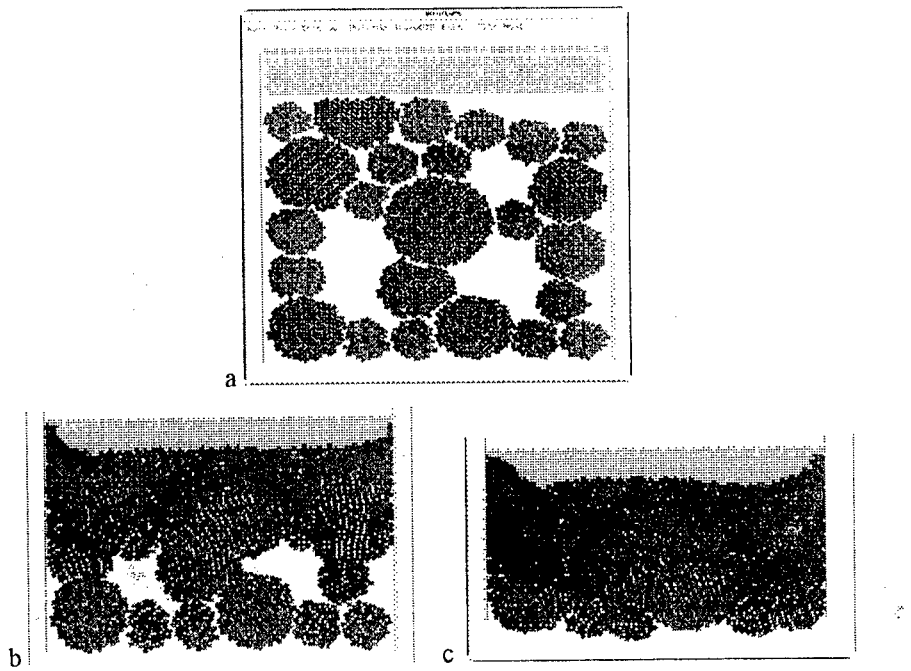

Fig. 5. Results of modeling of shock compaction of powder mixture. a – the structure window of **MCA-Analyzer** with initial structure; b,c – computed structure at t=25 μs and t=35 μs respectively.

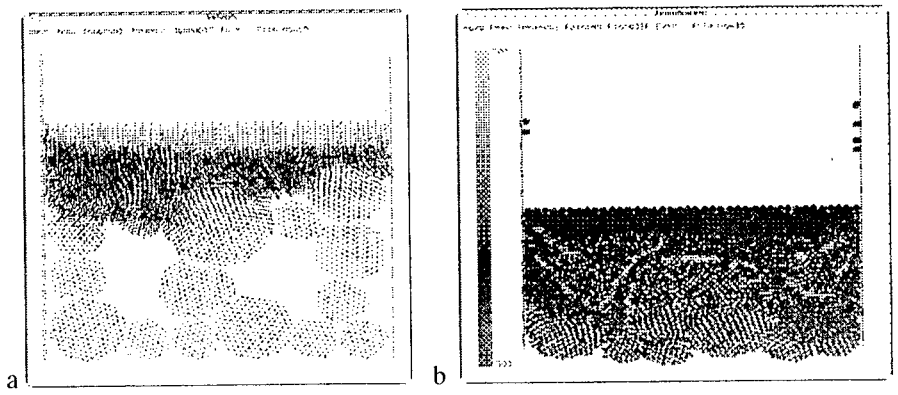

Fig. 6. Results of modeling of shock compaction of powder mixture. a – field of velocities (t=5 μs); b – field of temperatures (t=35 μs).

4. Fracture Processes Under Compression

- Sintered powder materials (PM)

Consider the sintering PM material based on Al-Cu alloy under compression. Special experiments was provided using the INSTRON equipment and then corresponding simulation was carried out. The results of experiments are presented in Fig. 7. Initial simulated structure is presented in Fig. 8,a (size of the sample is 1.7x0.9 cm). Velocity of loading plate is 10 cm/sec. Evolution of the simulated sample structure is shown in Fig. 8,a – c. As is evident from presented data the simulation results are in good agreement with those obtained experimentally.

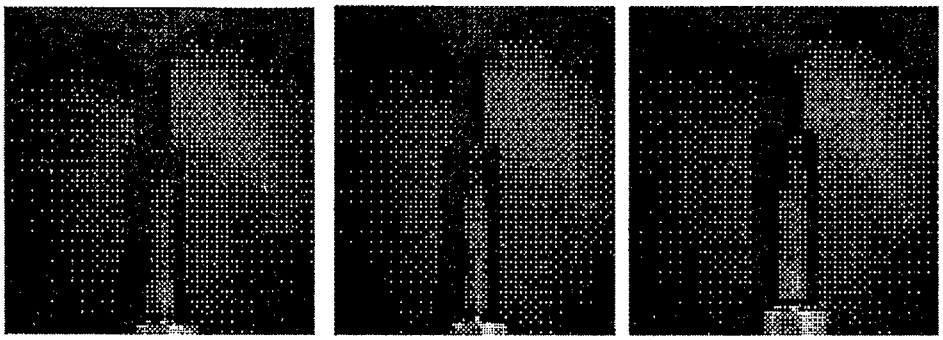

Fig. 7. Evolution of the sample (experimental results).

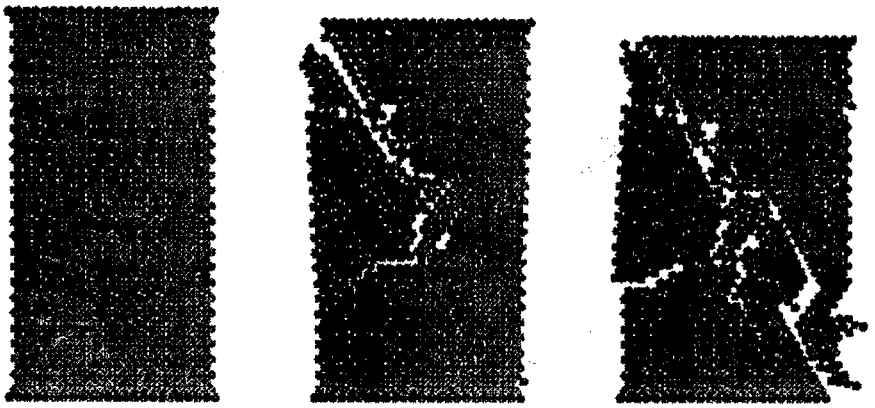

a) b) c)

Fig. 8. Evolution of the sample structure (results of simulation).

- *Ceramics*

Based on ZrO_2 ceramic sample of 0.6x0.4 cm in size was simulated. The load was applied by setting up the constant velocity to all the elements of the upper layer (piston). It was varied in the range of 50 ÷ 500 cm/sec. Porosity of the simulated material was effectively taken into account by introducing the ruptures of the links between some automata, that corresponds to micro-pores. Macro-pores were simulated by removing separate automata off the sample. The porosity of the simulated sample was varied in a wide range from 0 to 50 %. Analysis of the obtained results showed good enough agreement (up to 30%) with experimental data [2,3]. Due to advantages of the method it was possible to discover that the regions of short term local flow may be formed even in brittle ZrO_2 (Fig. 9,a). The size of this region is of about 0.08 cm. The life-time of this phenomena is of about $1.0*10^{-7}$ sec. After this time the region is smeared. Analysis of the links between the automata showed that regions of local flow correspond to formation of micro-damages (Fig. 9,b,c). The calculation showed that in many cases the main crack propagates along the path indicated by the local flow regions (Fig. 9,.d).

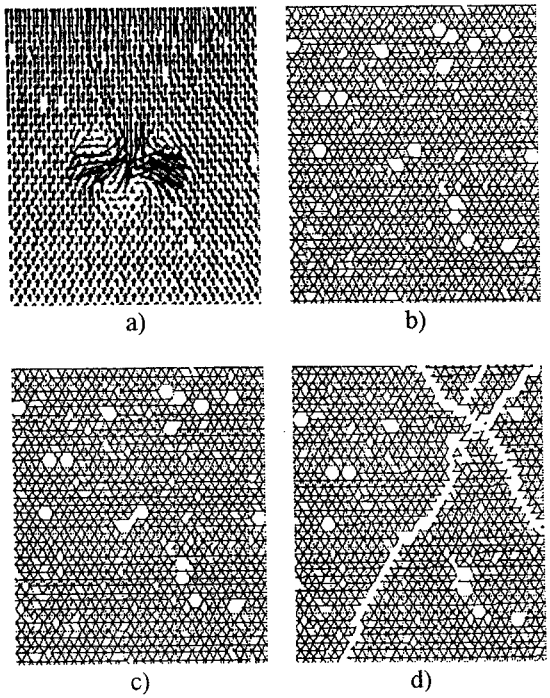

Fig. 9 Part of the sample in the region of local flow: automata velocity field (a). The grid represents the links of the automata: b) before micro-damage; c) after micro-damage; d) after fracture.

- Concrete

The strength as well as durability of concrete can be evaluated by compression test of concrete cylinders. The sizes of the standard cylinder are 6 inches in diameter and 12 inches in length. The typical experimental stress-strain data are shown in Fig 10. The results of MCA modeling of the compression tests of a cement paste, aggregate and concrete are also shown in Fig 10. The results presented in Fig. 10 have to be explained in detail. As the first step the compression testing of cement paste was simulated. The inter-automata interactions and properties of a single cement paste automaton was fitted to the experimental stress-strain data (Fig 10). The same procedure for the aggregate was used at the second step. Note, that the size of the both types of the automata was equal to $2.0*10^{-2}$ cm. At the last step the concrete sample was generated directly by the cement paste and the aggregate automata. The concrete had an aggregate content of about 52%. The comparison of experimental stress-strain relations of the concrete and those obtained by MCA modeling (Fig. 10) shows a good agreement.

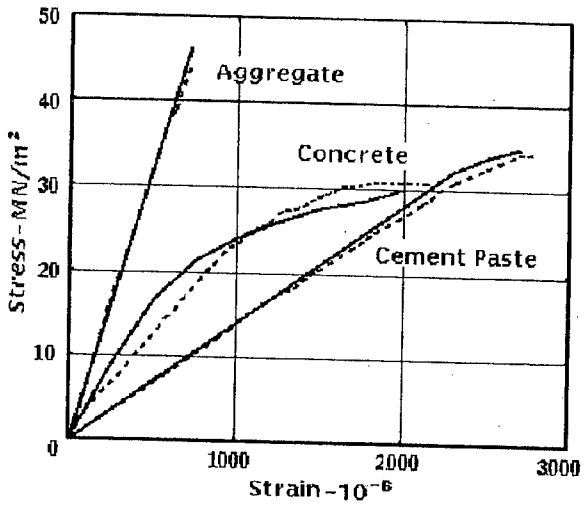

Fig. 10. Stress-strain relation for aggregate, cement paste and concrete: solid line – experimental results; dotted line – MCA simulation results.

Fig. 11 shows the calculated structure of the inter-automata linkages and one of the regular kind of concrete cylinder after compression test [4]. The similar type of the failed part is evident.

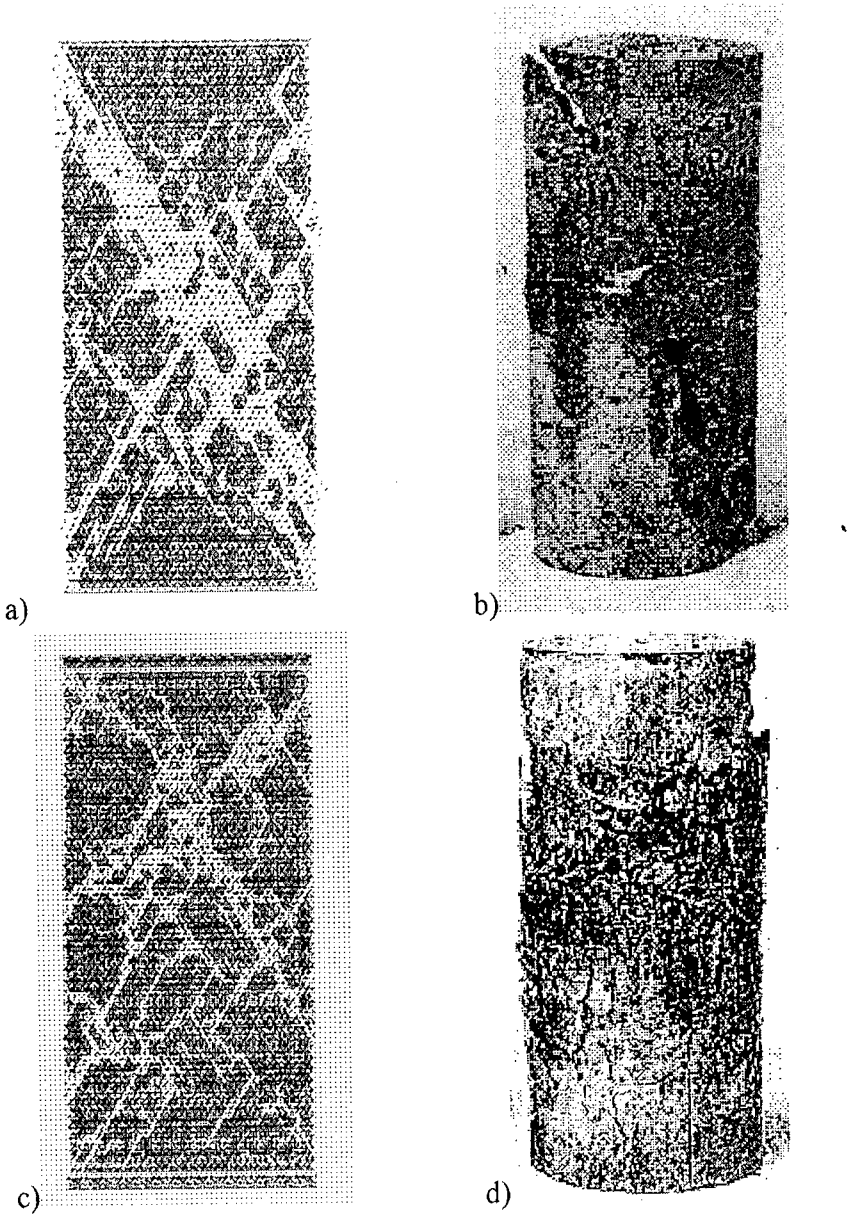

Fig. 11. Compression test results. High–strenght concrete: a) MCA simulation results; b) experimental results. Normal–strenght concrete: c) MCA simulation results; d) experimental results.

2.4. Structure Behavior

To demonstrate an ability of the developed approach to describe concrete and reinforced-concrete constructions computer simulation of behavior and fracture of the two-storied structure under shear-type deformation imitating crust movement during earthquake has been made. For this purpose two dimension frame structure was examined. Fig. 12 shows breadboard and measurement of this sample.

In the Fig. 12 one can see that the stationary stopper limits the movement of the upper floor of the structure. Bottom of the structure imitates the foundation lying on the earth and shifting with it at an earthquake.

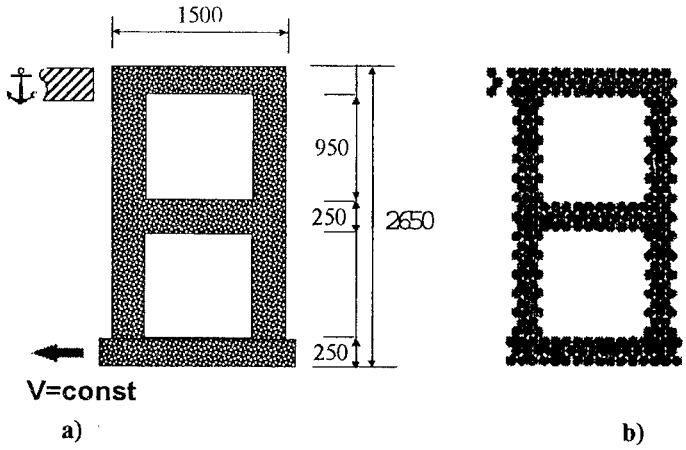

Fig. 12 a) breadboard structure; b) concrete structure.

A separate automaton of the structure was considered as the concrete one. So the mechanical properties of an automaton tied with the same of the test concrete cylinder. In this calculations the size of an automaton was equal to 1 cm. Specific characteristics of cellular automata and parameters of an inter-element interaction were measured up to with the parameters of the high-strength concrete [4].

Displacement of the crust was imitated by the leftward even movement of automata of the construction foundation. The velocity of the movement was equal to 1 m/sec. Damping the upper floor of the structure, the stationary stopper (Fig. 12) controlled the shear type of the structure deformation.

Fig. 13.a shows the prime stages of the fracture of the considered structure under the above mentioned loading conditions. It can be seen, that at the first stage the cracks are initiated and grow near the butt-joints of the middle floor with the walls of the structure. This is the result of the process, when the walls are bonded by the moving foundation squeeze "girder" and lend the wavy contortion to it.

Further damage of the structure proceeds near the butt-joints of the walls with the foundation of the structure. So, the structure tends to tilt as a whole. At the same time another crack is initiated and grows in the right wall near the butt-joint of the wall with the "girder". This is a result of the resistance to bending of the upper part of the right wall by the middle floor.

The developed **MCA Method** makes it possible to analyze the influence constructive modifications of the frame on response and fracture of the structure. To illustrate such abilities of the method in the present work various modifications of the initial structure (Fig. 12,b) were introduced.

Fig. 12,b shows the prime stages of fracture of the structure with the thickening middle floor (here and further loading scheme analogous to the showed one in the Fig. 12,a was used). One can see the fundamental change of the fracture pattern. The upper storey has been completely broken down, whereas the lower floor has been. Consequently the broken structure may be repaired, while the damaged base structure (Fig. 13,a) cannot be repaired.

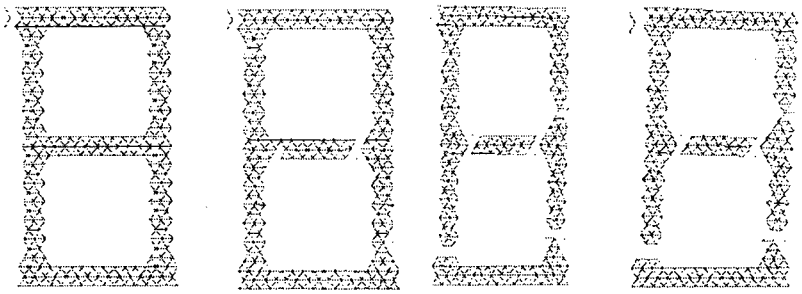

Initial structure

a)

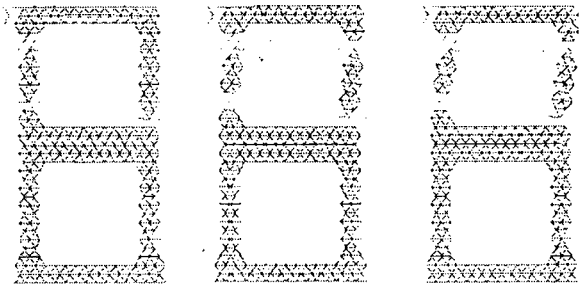

b)

Fig. 13. Structure of inter-element bonds at different stages of fracture: a) control structure; b) heavy bay structure.

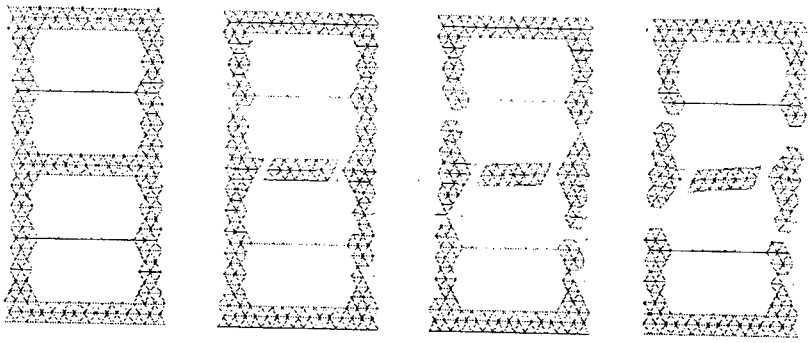

Initial structure
a)

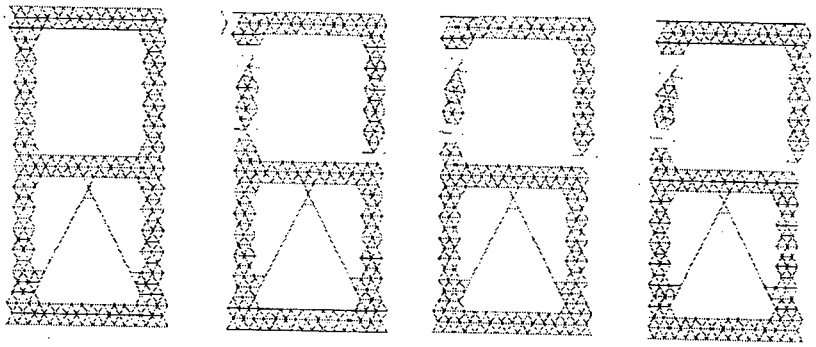

Initial structure
b)

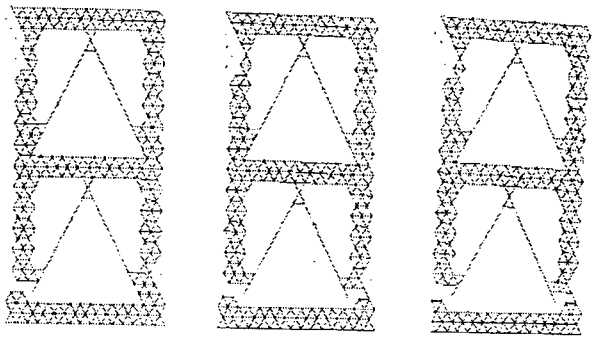

c)

Fig. 14 Different types of reinforcing of structure by steel trusses: a) horizontal trusses; b) bottom storey trusses; c) double storey trusses.

MCA Method allows also to research the influence on behavior and fracture of modified structures by various modes of strengthening of the base structure (Fig. 12,b). For example trussing of the walls at the both storeys of the structure by steel trusses (Fig. 14,a) causes the fracture of the walls and the middle floor being between trusses. If only the lower storey of the structure is trussed by steel trusses (Fig. 14,b), then only the upper storey is broken down. The fracture pattern in this case is of the same type as in the Fig. 13,b. Trussing the both storeys of the structure by steel trusses (Fig. 14,c) leads to the fracture localization only near the foundation of the structure. The walls and middle floor of the structure therewith are uncrippled.

The present work also demonstrates the ability of the **MCA Method** to analyze the influence on the features of the fracture of the structure by the type of material of strengthening members.

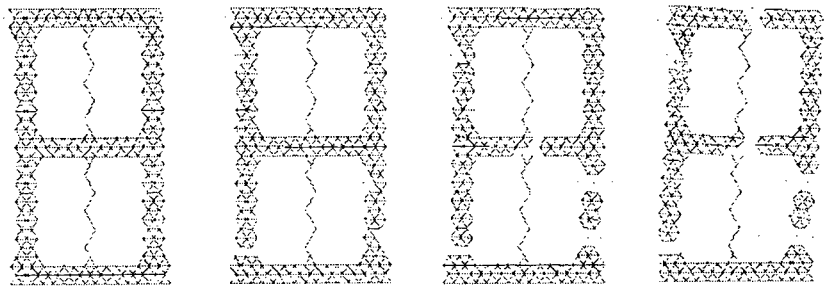

Initial structure a)

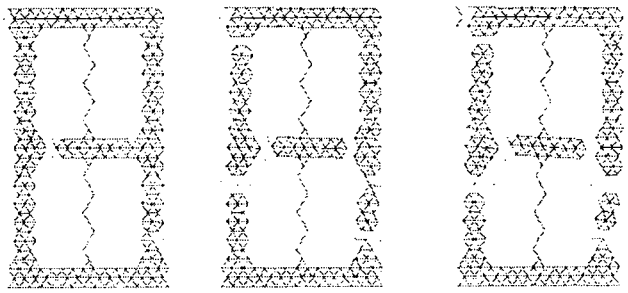

b)

Fig. 15. Different types of material of vertical shores: a) steel shores; b) shores like reinforced concrete.

A structure with steel (Fig. 15,a) and like reinforced-concrete (Fig. 15,b) vertical strengthening shores was modeled. It can be seen that the structure with the steel trusses first damaged in the lower part of the walls (near the foundation of the frame). Further the both floors of the structure "burst" in the butt-joints with the shores.

Another fracture pattern is seen in the Fig. 15.b. Here first the middle floor severs oneself from the walls of the structure, because the "yielding" trusses are not able to resist to wavy contortion of the "girder". Thereafter the walls start to crack. At this takes place, in contrast to the structure in the Fig. 15.a, the upper floor of the structure is remained intact.

The outlined examples demonstrate, that the **MCA Method** allows to simulate the behavior and fracture of all manner of the concrete and reinforced-concrete constructions under various types of external loading. The present approach provides the way to research the influence of constructive modifications on vitality of the construction as a whole and its separate members. It also allows to research the influence of the same modifications on the features of fracture process.

The advantages of **MCA Method** permit the use of this approach to optimize the structure of the analyzed construction according to specific requirements and the computer aided expertise of concrete constructions for natural catastrophes.

3. Final remark

At the conclusion it should be pointed out that because Movable Cellular Automata Method is based on the particle concept and includes all the advantages of classical cellular automata it is very easy to develop special aided software for specific problems of various types.

References

1. S.G.Psakhie, Y.Horie, S.Yu.Korostelev, A.Yu.Smolin, A.I.Dmitriev, E.V.Shilko, S.V.Alekseev. Russian Physics Journal V.38. (1995), P. 1157–1168.

2. N.L.Savchenko, T.Yu.Sablina, T.M.Poletika, A.S.Artish, S.N.Kulkov Powder met. (Russian), 1/2, (1994), P. 26–30.

3. N.L.Savchenko, T.Yu.Sablina, S.N.Kulkov: Izv. VUZov. Fizica.(Russian), 8, (1994), P. 89–95.

4. A.M.Neville. Properties of Concrete. John Wiley and Sons.- New York, 1973.- P.686.

Special report

PHYSICAL MESOMECHANICS OF MATERIALS AND ITS IMPACT ON SHOCK CHEMISTRY

Panin V.E., Makarov P.V., Smolin I.Y.
Institute of Strength Physics and Materials Science, SB RAS, Tomsk, Russia

Abstract. The fundamental difference of the physical mesomechanic approach from traditional description of deformation and fracture of materials consists in an explicit form consideration of internal structure heterogeneities of materials on the mesoscale level. Experiments and theory demonstrate that just these heterogeneities - grains boundaries, inclusions and etc. - cause essentially heterogeneous fields of stresses and deformations in mesovolumes of material under loading. Just mesolevel of consideration allows to clear up mechanisms of plastic deformation and fracture and to understand principles of physical and chemical transformations related to deformation. As appendix of the developed approach to shock chemistry it is considered: 1) processes of localization of deformation on the mesolevel and formation of the centers of reaction; 2) development of cumulative processes and formation of stable vortexes driven in shock wave front.

1. Basic principles

The concept and method of our approach are based on the ideas of physical mesomechanics [1,2]. The fundamental difference of the physical meso-mechanics approach from traditional description of deformation and fracture process in materials consists in the following:

a) A material is considered as hierarchically organized system of structural levels of different scales: micro, meso and macro.

b) Heterogeneities of internal structure of materials on the meso-scale level are considered in the explicit form.

On *macroscopic* level - the level of the averaged description in the model contributions from micro- and mesolevels to shear strength are taken into account. So a macropartical is the representative mesovolume.

On *microscopic* level heterogeneities of defect structure are considered by using of defect distribution function and dislocation kinetics for plastic strain rate is suggested. So deformation of a material on microlevel is described in terms of continuum theory of defects. Taking into account processes of nucleation and multiplication of defects in the elastic precursors and fronts of strong and weak shock waves kinetic constitutive equations are constructed for dislocation continuum.

The approach allows to follow the microstructure evolution. Dependencies of factors of viscosity of shock loaded metals are investigated. Evolution of shear strength in metals (its temporary decreasing in shock wave front and recovery behind it) is described as process of localization of deformation in shear planes of microscopic scale (microbands). It is caused by their local heating up and subsequent cooling down.

On the *mesoscopic* level heterogeneities of internal mesostructure are considered in explicit form. Experiments [3] and theory [4,5] demonstrate that grains boundaries, inclusions and etc. cause essentially heterogeneous stress and deformation fields in meso-volumes of material under loading. It results in development of shear bands formation and other types of deformation localization. Just mesolevel of consideration allows to clear up mechanisms of plastic deformation and fracture and to understand principles of physical and chemical transformations related to deformation. Just in volumes of mesoscale level in materials under loading areas of localized deformation are formed depending on initial heterogeneities and conditions of loading, self-organizing processes develop. Rotary plasticity is developed and material is found hardly fragmented and hashed.

But on the macroscale level of averaged description the information connected with fluctuations and localized deformation on the mesolevel is completely lost. Though just fluctuations determine further development of related to each other processes of chemical and physical transformations and deformation and fracture.

2. Results of calculations

A map of a polycrystalline Al mesovolume is shown in fig. 1. The results of numerical modeling of shock wave propagation in this mesovolume are shown in fig. 2-4. On mesolevel the front of a shock wave forms mesoscopic shear bands which cover from unit grains up to several grains (fig. 3). The process of formation of fragments is finished in waves of unloading. Opportunity of development of microcumulative processes and formation of microvortexes appears. Fg. 6 shows derivation of velocities from average values in the rows of computational grid perpendicular to the direction of shock wave propagation. Stresses corresponding to this derivations of velocities $\sigma = \rho c \Delta u = 0.1 \div 0.3\,\mathrm{GPa}$. These microvortexes can move in front of a shock wave under certain conditions. It should be mentioned that strain localization patterns under quasi-static loading in the same mesovolume is qualitively different and one of them is shown in fig. 7.

Conclusions

Localization of deformation is caused by structural elements of meso scale levels. They are the grains in the offered example. Therefore the length of the meso shear bands is in order of grain size. Shear bands are formed in the direction of main shear stresses. In some cases joints of these shear bands form bands of localized deformation of greater scale.

The rotational mode of deformation is developed. In the presented example rotation of individual grains form the elementary rotational cells. Rotations of grains cause shear bands generation near-by grain boundaries and grain joints.

So a new approach for description of shock induced chemical processing determined by heterogeneities of internal structure on the micro and meso levels is

presented. It includes numerical mmodeling of the meso shear bands formation in metals under shock wave loading and its impact on shock induced chemical processing.

References

1. V.E.Panin (ed.). *Structural levels of plastic deformation and fracture*, Nauka Publishing. Novosibirsk (1990) (in Russian)
2. V.E.Panin (ed.). *Physical Mesomechanics and Computer-Aided Design of Materials*, Vol. 1.2, Nauka Publishing. Novosibirsk (1995) (in Russian). English edition: V.E.Panin (ed.), *Physical Mesomechanics of Heterogeneous Media and Computer-Aided Design of Materials*, Cambridge International Science Publishing, Cambridge (1997) (to be printed).
3. V.E.Panin, Physical Mesomechanicsf plastic deformation and experimental results obtained by optical methods, *Journal of the Japan Society of Applied Physics* 9 (1995) 888-894
4. P.V.Makarov, Microdynamic theory of plasticity, *Russian Physics Journal* October (1992) 334-346
5. V.E.Panin, P.V.Makarov, M.M.Nemirovich-Danchenko, V.N.Demidov, I.Y.Smolin, O.I.Cherepanov, Methodology of computer-aided design of materials with specified strength characteristics. In V.E.Panin (ed.), *Physical Mesomechanics and Computer-Aided Design of Materials*, Vol. 2 Nauka Publishing, Novosibirsk (1995) pp. 3-76 (in Russian)

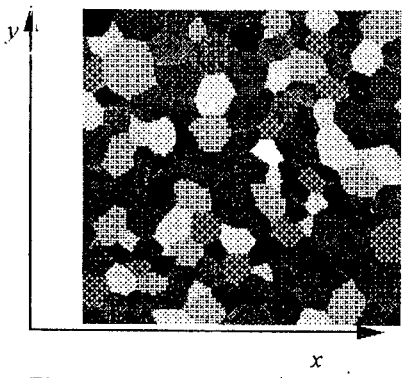

Fig. 1. A map of mesovulume of polycrystalline Al.

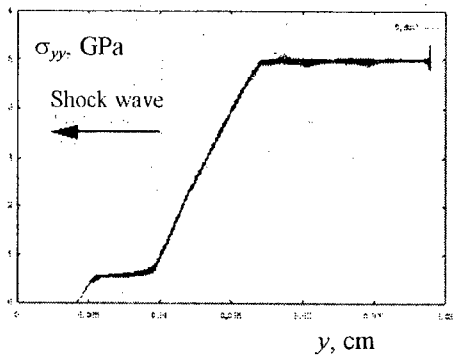

Fig. 2 Distribution of stresses σ_{yy} in the mesovolume along the lines parallel to the direction of shock wave propagation.

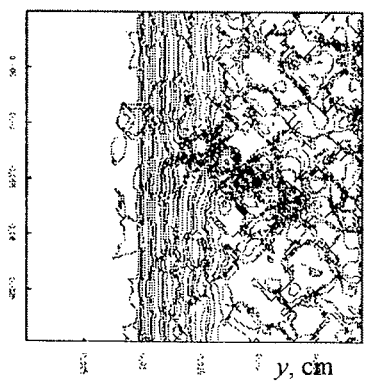

Fig. 3. Contour map of plastic deformation and meso shear bands formation in the mesovolume of material under shock wave loading.

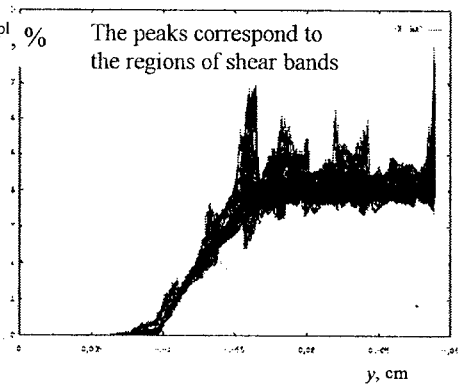

Fig. 4. Distribution of plastic deformation in the mesovolume along the lines parallel to the direction of shock wave propagation.

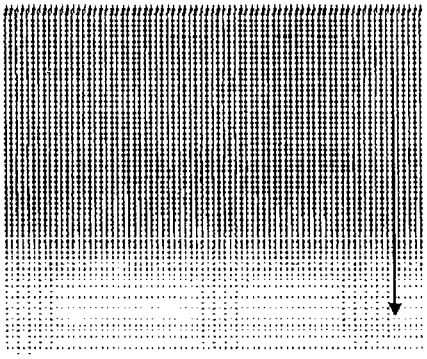

Fig. 5. Velocity field in the mesovolume under shock wave loading.

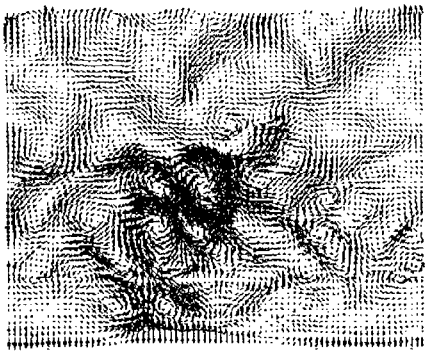

Fig. 6. Derivation of velocities from average values in the rows of computational grid.

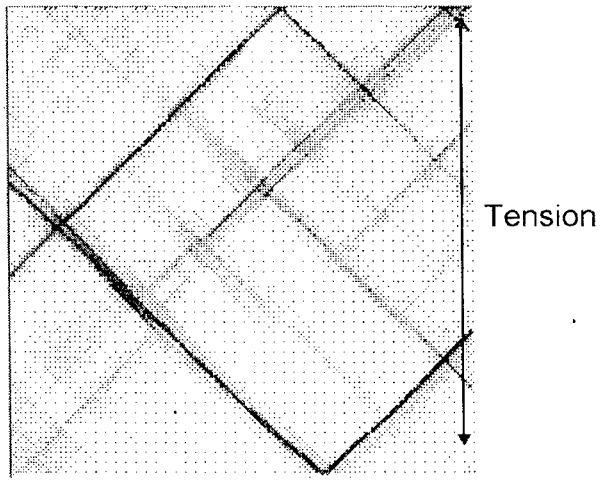

Fig. 7. A pattern of strain localization under quasistatic tension in the same mesovolume. Darker zones correspond to larger plastic deformation.

Special report:

INVESTIGATIONS AT MULTI-USER ORIENTED TsNIIMASH LARGE-SCALE BALLISTIC FACILITY

P.V.Kryukov

(CSRI of Mechanical Engineering Problem . Moscow, Russia)

• OBJECTIVES OF THE PROJECT AND THE CURRENT STATE OF THE ART

The objective of the project is to provide to various interested organizations and individual scientists a free access to the TsNIIMASH large-scale ballistic facility and support them in conducting their own research at it. The facility has unique characteristics and for many years was not available for both foreign and domestic civilian investigators being solely used for development of strategic weapons. It is planned to use donations of international scientific foundations operating at the Russian territory and money allocated from the Russian National Budget to prepare and conduct ballistic experiments within the project, i.e. to provide the facility to the international community of investigators free of charge.

The TsNIIMASH large-scale ballistic facility is the largest and the most complicated test- bench in the world amongst its kind. Each experiment has a capacity to simultaneously load various samples with different content which opens an opportunity to exploit the facility in multi-user oriented mode and invite a great number of research organizations and prominent individuals from many countries. Unique sets of launch velocities and loading parameters (pressure, loading cycle duration, shear, and temperature) can be achieved at the facility; no other facility or method can provide comparable sets of loading values.

A solid body, when compressed to high pressures at the presence of certain activating factors, such as temperature and shear, can experience a vast spectrum of phase and other transformations. This provides an investigator opportunities to research:

* Processes in numerous solid phase reactions that form meta-stable polycrystalline states with either amorphous or nano-phase structures which can possess diverse valuable properties (superconductivity at high critical parameters; unique magnetic, mechanical or catalytic characteristics);
* Formation of compacts of powders of various materials, including diamond powders at densities close to the x-ray density;
* Processes involving different polymorphous phase transformations, e.g. in carbon, boron nitride, etc.

In the framework of the project investigations it is foreseen that advanced materials with unique physical and chemical properties will be synthesized and subsequently applied in various industries on a large scale.

The following additional directions of aeroballistic experiments were selected for the TsNIIMASH facility:

* Investigation of destruction dynamics of massive body colliding with a compact

impactor;
* Investigation of combustion process in a fuel injected into a hypersonic air flow;
* Investigation of scram acceleration of a hypersonic projectile moving in the bore filled with an oxygen/hydrogen mix;
* Investigation of various methods of gasdynamic acceleration of projectiles to velocities over 10 km/s.

- **INVESTIGATIONS ON SYNTHESIS OF NEW MATERIALS**

It is proposed within the project to conduct dynamic experiments at the TsNIIMASH large-scale ballistic facility and perform loading ampules containing various samples. These ampules with the samples are positioned upon the target which is then installed at the end of the ballistic bore of the facility. The dynamic loading of the samples is planned to attain as a result of a high-speed impact of a 30-kg steel disc (impactor), having diameter 0.5 m and 20 mm thick, at a velocity 2.5 km/s.

In case that the ballistic bore is air evacuated, the impactor strikes the target yielding the maximum pressure around 60 Gpa during 8 ms. If the bore is preliminary filled with gaseous hydrogen then the shock is dampened; hydrogen also reduces the pressure slope, makes it smoother as well as helps homogenous pressure distribution upon the target area. Variation of initial pressure of the hydrogen inside the ballistic bore and the impactor's velocity provides control of loading conditions in the vast range of loading pulse length and maximum pressure values. At longer loading pulse and the pressure higher than the yield limit of the target material, the target is being plastically deformed under radial unloading waves. Hence, to preserve the central partof the target 0.3 m in diameter from destruction, the loading pulse length should be not greater than 40 ms. Due to the sound unloading waves in the dampened impact the profile of the pressure in the bulk of the samples is fairly homogenous thus practically excluding their shock-wave heating. A long 30 ms pressure slope, which is formed when the impactor moves along the ballistic bore, helps get rid of cavities in powder materials at a moderate speed without their collapse. As the hydrogen adiabatically expands and pushes the impactor in the reverse direction, back from the target, the samples in ampules are being unloaded. The layer of the dampening gas prevents formation of tensile stresses during samples' unloading which otherwise could have led to mechanical damage of the samples. The second loading cycle, which otherwise could have been caused by the second impact of the disc impactor, as well as contact of the samples with the high temperature gas jets are prevented because a compressed air is injected in the gap between the recoiling impactor and the target.

Parameters Attained on Experemental Balistic Facility

• Ballistic bore caliber	0.5 m
• Ballistic bore length	60 m
• Full length of the facility	200 m
• Detonating mix formula	$2H_2+O_2$
• Pressure beyond the Detonation Front	up to 300 atm
• Energy yield at mix combustion	up to 1.2 GJ
• Mass of Discus Projectile/Striker	9 kg
• Max.Terminal Velocity of Discus Projectile	up to 3500 m/s
• Max.Kinetic Energy of Discus Projectile	up to 55 MJ
• Discus Angular Rate	250 rps
• Discus Rotation Axis/Bore Axis Misaligment	better than 30''
• Maximum Magnetizition of Discus Material	1.4 Tesla

High Speed Throwing: Experimental Results (V=2 km/s)

Discus projectile/striker

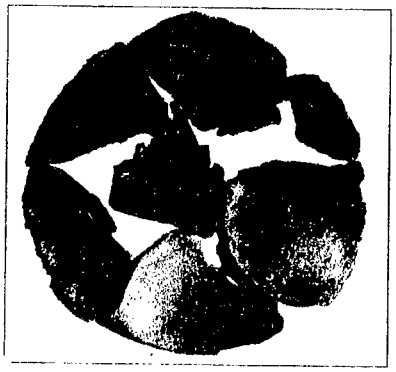

Cast iron target

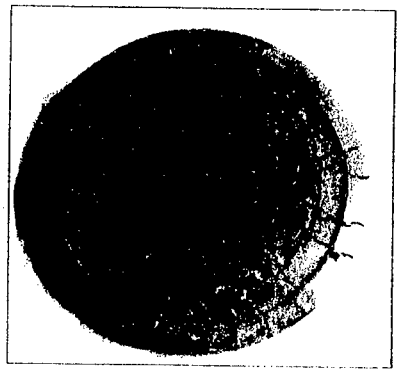

Experimental Ballistic Facility Design

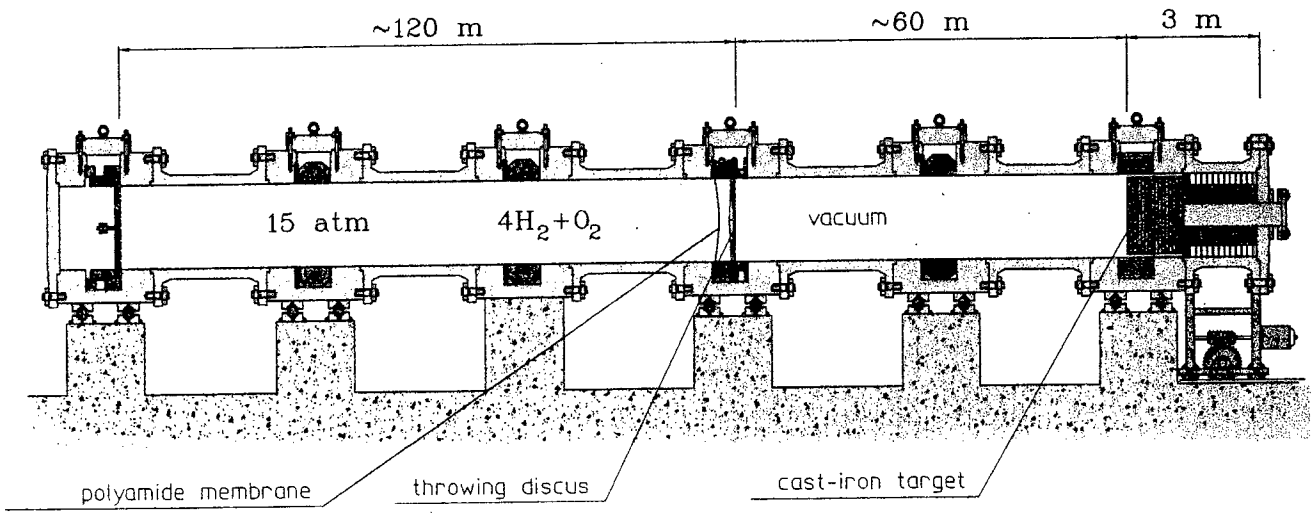

Special report

CALCULATION OF THE SHOCK HUGONIOT FOR METALS AND ALLOYS.

V.M.Kuznetsov, G.E.Rudenskii, R.I.Kadyrov, P.P.Kaminskii
Institute of Strength Physics and Material Science, SB RAS.

1. Introduction

The problem of shock Hugoniot calculation still remains to be a topical one in spite of the considerable progress achieved in the field of theoretical investigations into solids' properties under conditions of shock-wave loading. The reason behind this lies first with a procedure for calculation of adiabatic curves where Debye-Mie Gruneisen approach is used, and second, there is an absence of the reliable enough models for binding forces in solids that may be applied not only to pure metals but to their alloys as well. There are various methods for calculating the thermodynamic properties in case of pure metals such as pseudopotential method [1], effective medium method [2], and embedded-atom method [3], nevertheless, such a problem has not yet been solved in case of transient metals. This may be due to the specificity of their atoms' electron structure and taking it into account correctly requires more complex models of the atomic interaction to be employed.

In the present paper the binding forces model is proposed for metals and alloys. This model is based on the formalism of electron density functional and allows to take into account many-body interaction effects. The model parameters are determined from the consistency between the theoretical and experimental properties of pure metals. No extra parameters are introduced in relation to alloys. A distinctive feature of the developed method is its relative simplicity of calculation, the absence of externally dependent parameters what allows one to employ thus obtained potentials in studying the kinetics of processes applying the molecular dynamics simulation.

The developed method has been applied in this work for calculation of shock Hugoniot in Ni, Al metals as well as in NiAl (B2-structure) and Ni_3Al ($L1_2$-structure) alloys. The calculation of the shock Hugoniot both on pure metals and alloys has been conducted with the use of the quasiharmonic approximation without resort to the Debye-Mie Gruneisen model.

A calculation procedure has been proposed to obtain the result that can be applied to investigate the phase transitions in alloys and to develop a plan of shock-wave experiment.

2. Electron density functional method

MEDF procedure is based on the theory of electron density functional where the full energy of a solid body is represented by functional $E[\rho]$ of the electron density $\rho(\mathbf{r})$. The exact form of $E[\rho]$ expression is not known in case of solids.

To construct a model electron density functional, the configurational expansion has been applied to the many-electron function in terms of one-electron determinants which basis functions were selected using the Wannier functions' representation. This gives us an opportunity to introduce (in terms of one-electron approximation) non-integer

filling numbers for the electron shells of atoms as well as to take into account sp-hybridization effects in transition metals. Such an approach enables us to divide all the electrons in the system into core ones (internal atom shells and valence d-electrons in case of the transition metals) and nearly free ones what allows us to write well-founded enough expressions for subsystems' energy. A criterion for dividing the electrons into two subsystems is a degree of localization of the considered electron shells in relation to the atom nucleus. In this work, for instance, the number of free electrons in Al has been taken equal to 3 (configuration $3s^2 3p^1$) and 1.4 for Ni (configuration $3d^{8.6} 4s^{1.4}$) in accordance with the results of quantum mechanics calculation.

On such subdivision of electrons into two subsystems, full energy of a solid body may be written in the following form:

$$E = E_v[\rho_v] + E_c[\rho_c] + E_3[\rho_v, \rho_c] , \qquad (1)$$

where first component represents energy of free electrons, second component is energy of core electrons and third component relates to the interaction between the above mentioned subsystems.

Nearly free electrons.

As it has been done according to the pseudopotential norm-conserving method [1] let us move from the real density of nearly free electrons that suffers intense oscillations in the vicinity of atom nucleus due to it being orthogonal to core electrons to pseudo-wave functions that only fluently decrease there. Due to passing to the pseudo-electrons that possess corresponding distribution of their density $\rho_v(\vec{r})$ we now can write their full energy using the nearly uniform electron gas approximation [4], namely:

$$E_v[\rho_v] = E_v^q[\rho_v] + T_v[\rho_v] + \Delta T_v[\rho_v] + E_v^{ex}[\rho_v] + E_v^{cor}[\rho_v] \quad (2)$$

Here E_v^q, T_v and E_v^{ex} are successively Coulomb, kinetic and exchange components of the valence subsystem energy; ΔT_v is the Kirzhnitz's correction [5] for nonuniformity of the electron density, and E_v^{cor} is the correlation energy in the form obtained by Gombas [6] as a result of extrapolation of electron gas correlation energy in case of high and low density.

To approximate the density of valence pseudo-electrons in MEDF one may use the approximation of superimposed spherically symmetric atom functions of density ρ_v^α:

$$\rho_v(\vec{r}) = \sum_{j,\alpha} C_j^\alpha \rho_v^\alpha(\vec{r} - \vec{R}_j), \qquad \int \rho_v^\alpha(\vec{r}) dV = n_v^\alpha , \qquad (3)$$

where n_v^α is a number of free electrons in atom of the type α.

The second order smallness expansion of nearly free electrons' energy components (2) as a function the free electrons' mean density allows us to present E_v as follows:

$$E_v[\rho_v] = E_o(\tilde{\rho}_v) + \tfrac{1}{2}\sum_{\alpha\beta}\sum_{i,j} C_i^\alpha C_j^\beta V_{\alpha\beta}^v(\tilde{\rho}_v, \vec{R}_{ij}), \qquad (4)$$

- where energy E_o as well as appearing in (4) effective pair potential are dependent on the mean density of valence electrons (on crystal's volume). The value of C_i^α equals to 1 or 0 depending upon whether an i-lattice point is taken by the atom of the type α or not.

Core electrons.

The energy of core-core interaction is given using the Kim-Gordon approximation [7] as a sum of effective pair short-range potentials $V_{\alpha\beta}(R_{ij})$, which include (like it is done with the tight-binding method) Coulomb, kinetic, exchange and correlation components:

$$E_c[\rho_c] = \tfrac{1}{2}\sum_{\alpha\beta}\sum_{i,j} C_i^\alpha C_j^\beta V_{\alpha\beta}^c(\vec{R}_{ij}). \qquad (5)$$

The energy of isolated cores is taken as an initial point in full energy calculation. The E_C contribution to the binding energy is zero in case that densities of core electron of neighboring atoms are not overlapped.

Pseudopotential.

The energy of core-valence interaction in case of alloy take the form:

$$E_3 = \sum_{j,\alpha} C_j^\alpha \int d\vec{r} W_\alpha\left(|\vec{r} - \vec{R}_j|, \rho_v\right)\rho_v(\vec{r}). \qquad (6)$$

Here W_α is a local norm-conserving interaction pseudopotential for atoms of the type α. It has an effect on free electron density ρ_v moving to **r**. Let us note that the pseudopotential is explicitly dependent on free electron density ρ_v, whereas the density dependence of the core electrons is a pure parametrical one because of we have used frozen cores approximation.

The full variation problem in case of system of particles is in finding such type of ρ_v using which minimizes energy E under given external conditions. This is equivalent to the solution of the problem $\delta E=0$. To avoid difficulties stemming from the necessity to find the form ρ_v for each new atomic configuration, the W_α pseudopotential is constructed in such a manner that a full energy minimum condition for any type of configuration $\{\vec{R}_j\}$ would be true for one and the same fixed type of nearly free electron density function ρ_v^α (3).

Being the result of expansion of the core-valence interaction up to second order of smallness and in the vicinity of $\tilde{\rho}_v^\alpha$ (equilibrium mean nearly free electrons' density of the metal of α type) full energy may be written in the form:

$$E = E_o[\tilde{\rho}_v] + \frac{1}{2}\sum_{\alpha\beta}\sum_{i,j} C_i^\alpha C_j^\beta V_{\alpha\beta}(\tilde{\rho}_v, R_{ij}) +$$

$$\frac{1}{6}\sum_{\alpha\beta\gamma}\cdot\sum_{ijk} C_i^\alpha C_j^\beta C_k^\gamma V_{\alpha\beta\gamma}(R_{ij}, R_{ik}), \qquad (7)$$

where the second term includes in itself pair energy components of both core and valence subsystems together with their interactions and the last term is a three-particle addition to the energy of the core-valence interaction.

To determine pseudopotential's parameters we resorted to the following known from the experiments properties of pure metals: equilibrium volume, bulk modulus, shear modulus C_{44}, vacancy formation energy, pressure at 20% of compression and tension at zero isotherm being approximated with the use of the universal equation of state [8].

To minimize the full energy, the nearly free electron density function ρ_v is constructed, according to (3), as a superposition of the atomic density functions of alloy components being approximated by Slater's functions. The Slater's functions' parameters were selected in such a manner that to provide the best coincidence with tabulated by Herman and Skillman [9] electron density distribution for separate atoms.

Alloys.

The full energy of an alloy is dependent not only on its atomic volume but also on its crystal structure parameters. Because of this, to determine basic state thermodynamic characteristics of NiAl and Ni_3Al alloys there was carried out a procedure for energy minimization over the atomic volume and crystal structure parameters.

The basic state of Ni_3Al is $L1_2$ structure type with the atomic volume v_0=76.12 a.u. A competitive phase is f.c.c. $D0_{22}$ structure type. Moreover, we considered also its f.c.c. lattice — base structural modification $D0_3$. The calculations of made by us for Ni_3Al formation enthalpy of each considered structural modification showed that $L1_2$ phase is stable at the equilibrium volume v_0=76.38 a.u.

Basic state of NiAl alloy is realized as B2 structure type with v_0=82.28 a.u. The calculation of NiAl formation enthalpy in case of competitive structure types b.c.c. $B3_2$ and f.c.c. $L1_0$ have supported energy stableness of B2 phase with atomic volume of 82.26 a.u.

3. Elastic moduli and phonon spectra calculations.

To verify the applicability of MEDF for description of thermodynamic properties of the considered metal and alloys, phonon spectra and Fuks's second order elastic moduli (the so-called static moduli) were calculated for Ni, Al, NiAl и Ni_3Al. The calculation results for the bulk modulus B and shear moduli C_{44} and C' (at T=0 and P=0) are given below in Table 1 together with the corresponding values obtained from experiments.

Table.1. Elastic moduli of Ni, Al, NiAl and Ni_3Al. Experimentally obtained values were borrowed from [10]. All values are given in GPa.

	B	Bexp	C_{44}	C_{44}exp	C'	C'exp
Al	79	79	56	31	21	26
Ni	187	188	118	132	30	55
NiAl	156	166	101	112	23	35
Ni_3Al	187	175	108	129	30	40

The reduced value of C' modulus in all considered systems is due to using approximation of spherically symmetrical atomic functions of density for core and valence electrons.

Since contribution from the thermal oscillations was taken into account in calculating shock Hugoniot by a quasiharmonic model where the wave vector **k** dependence of oscillations' frequency is used, we calculated the phonon dispersion dependencies $\omega_j(\mathbf{k})$ for all considered above metals and alloys. The phonon spectra calculation results for NiAl and Ni_3Al are illustrated in Fig.1 in comparison with experimental data.

In case of pure metals the deviation between theoretical and experimentally obtained dispersion curves does not exceed 10%.

4. Calculation of equation of state and shock Hugoniot.

The Hugoniot equation takes the following form in case of that the substance is at rest in front of the shock wave:

$$P_H(v,T) = 2(E_H(v,T) - E_o) / (v_o - v), \qquad (8)$$

where P_H is a Hugoniot pressure:

$$P_H = \partial F / \partial v . \qquad (9)$$

Here v_o is equilibrium volume of an elementary cell, E_o is a substance' energy before the shock wave front, E_H and F are correspondingly energy and free energy of the substance beyond the shock wave front calculated per one atom. In case of quasiharmonic approximation

$$F(v,T) = E_z(v) + \nu_p \frac{\hbar}{2}\int d\omega \cdot \omega \cdot g_n(\omega) + \nu_p k_B T \int d\omega \cdot g_n(\omega) \cdot \ln\left(1 - e^{-\frac{\hbar\omega}{k_B T}}\right)$$

$$E(v,T) = E_z(v) + \nu_p \frac{\hbar}{2}\int d\omega \cdot \omega \cdot g_n(\omega) + \nu_p \hbar \int d\omega \cdot \frac{\omega \cdot g_n(\omega)}{e^{\frac{\hbar\omega}{k_B T}} - 1}, \qquad (10)$$

$g_n(\omega)$ is a frequency distribution density being normalized to unit:

$$g_n(\omega) = \frac{1}{V_{\vec{k}}} \sum_{j=1}^{\nu_p} \int d\vec{k} \cdot \delta(\omega - \omega_j(\vec{k})), \qquad (11)$$

ν_p is a number of phonon modes (3 for metals, 6 for NiAl of the B2 structure and 12 for Ni_3Al of the $L1_2$ structure); V_k is a volume of a reciprocal lattice.

Mie-Gruneisen approximation is common to be used for calculation of P_H, namely, the contribution from temperature-dependent part of F to the pressure is determined by the expression $P_t=(\gamma E_t)/v$, whereas different dependencies such as for example Landau-Slater, Zubarev-Vaschenko and Dougdale-McDonald formulas are used to define the volume dependence of the Gruneisen parameter. Apart from Mie -Gruneisen approximation, Debye's approximation $E_t(v,T)=3k_BTD(\theta/T)$ may be applied to calculate temperature dependence of energy $E_t(v,T)$. There is a number of various dependencies to approximate volume dependence of the Debye temperature $\theta(v)$, one of them is an approximation based on representation of γ via Debye frequency ω_d: $\gamma=\partial\ln\omega_d/\partial\ln v$ from where one can derive the dependence $\omega_d(v)$ under condition that the dependence $\gamma(v)$ and equilibrium value of $\omega_d(v_O)$ are known.

Al these thermodynamic models have a row of the following drawbacks which become even more substantial when models are applied to calculation of alloy properties.

1) Using the Debye model, it is unavoidable to know the volume dependence of ω_d. The choice of the dependence form being well-ground and reasonable enough still remains to be to a great extent arbitrary. Furthermore, to use the model it is necessary to know the value of the Debye frequency ω_0 at $v=v_0$ (or $\gamma_0=\gamma(v_0)$ for some models). Although its value was reliably established from indirect experiments for pure metals including Ni and Al, there are no not only such data in case of alloys but even no reliable evaluation criteria exist.

2) Substitution of the phonon spectra $g_n(\omega)$ with Debye density distribution function $g_d(\omega)$ looks like very rough approximation for being applied in case of alloys because there are isolated from acoustic levels peaks of oscillations' optical modes.

3) Applying Mie-Gruneisen approximation also results in necessity to use arbitrary approximations for the volume dependence of γ and in some cases it is required to know value of γ_0 which has never been determined for alloys.

In connection with the aforesaid we have made a decision to refuse from employing Debye-Mie-Gruneisen approximations and conducted the calculations of equations of state on metals and alloys according to purely quasiharmonic model.

Calculation procedure was as follows:

— $g_n(\omega)$ function was calculated (linear tetrahedron numerical integration method [14] following by ZB) at different values of volume v taken from within the interval $[0.5v_0, v_0]$;

— the equation (8) was numerically resolved (by modified Newton method) in relation to T at each value of volume v, in so doing pressure P_H was calculated by numerical differentiating of free energy over the volume. Energy E in itself as well as free energy F were calculated according to expressions (10) (integration by method of trapeze).

It is worth to note that this procedure has some methodological details relating to the necessity for self-consistent choice of a calculation accuracy: a) accuracy of $g_n(\omega)$ function which is defined simultaneously by the number of division tetrahedrons ZB and

step of ω; b) accuracy of pressure P_H which is a function of step of v; c) accuracy of Hugoniot equation solution (8) which is influenced by the step of T. When the choice of these value is done in a non-self-consistent manner, there could be observed such $P_H(v)$ behavior (oscillating, spasmodic) that has no physical meaning.

The results on calculating shock Hugoniot in Ni, Al, NiAl and Ni_3Al are shown in Fig.2 and Fig.3. Comparing them to experimental data for pure metals one may see a substantial divergence at higher compression values ($x<0.65$). This may be related to the frozen core approximation since Kim-Gordon approximation [7] fails in attempt to describe such high compression. As one would expect, the results of the Hugoniot temperature calculation for pure Al and Ni are in good agreement with half-empirical evaluations of [15-16] shown in Fig.2.

It is well known that the electron conductivity contribution to energy and pressure become a prominent one at high temperatures. Free energy of the thermal electrons may be evaluated with the use of the half-empirical formula [14]: $F_e = -\frac{1}{2}\beta_o T^2 \cdot x^{\gamma_e}$, where β_0 is an electron analogue of Gruneisen parameter. For $T\to\infty$ γ_e tends to 2/3. Fortunately, electron contribution to the pressure and temperature at shock Hugoniot is substantial only at high compression values ($x<0.65$).

To enable a comparison with used in [17] expressions for $\gamma(v)$, we have calculated mean Gruneisen parameter $\gamma=(P_tV)/E_t$ at the every point belonging to a shock Hugoniot. As it may be seen from Fig.2. these results are well agree to each other within the compression value field $x>0.65$.

We have not come across the experimental data for principal Hugoniot observed on NiAl and Ni_3Al alloys. The results of our calculations (Fig.3.) demonstrate more complicate dependence $P_H(v)$ as compared to what is possible to obtain through use of well-know rule for averaging the Hugoniot pressure of pure metals [13]. Unusual behavior of the Gruneisen parameter in alloys may be related to the specific character of their phonon spectra. As could be shown, the Gruneisen parameter $\gamma_{max}=\partial\ln\omega_{max}/\partial\ln v$ calculated from the maximum frequency ω_{max} of phonon spectrum would be closer to γ_{Al} and would have a similar linear character. Analogously calculated but with the use of minimal frequency (but not zero) Gruneisen parameter γ_{min} would demonstrate intense oscillations that would be similar to those shown in Fig.2 as average γ for alloys. The same could be said about small deflection of Ni $\gamma(v)$ dependence. The result would be close to the exact value of γ if one would make calculations taking into account a medium frequency of a spectrum. These regularities will result in appearing almost linear segment at pressure P_H curve for alloys within the range of $x\sim0.6$—0.65 since the volume dependence for optical (maximal) differs from that of for acoustic (minimal) frequencies.

5. Conclusion

The carried out calculations of shock adiabatic curves on NiAl and Ni_3Al revealed the unusual behavior of the Gruneisen parameter which may be related to the specificity of volume dependence of crystal lattice atom oscillation frequency.

A direct logical extension of this work is an investigation into structural phase transitions under shock loading, calculation of isotropy curves in unloading of alloys.

The possibilities of MEDF are not limited only by metallic bond systems: the interaction potentials obtained within the frames of MEDF can be applied for calculations of thermodynamic properties in ceramic materials.

References

1. D.R.Hamman, M.Schluter, C.Chiang. Phys.Rev.Lett. — 1979 — v.43,№20 — p.1494-1497.
2. Jacobsen K.W., Norskov J.K., Puska M.J. Phys.Rev.B. — 1987 — v.35,№14 — p.7423-7442.
3. Foiles S.M., Baskes M.I., Daw M.S. Phys.Rev.B. — 1986 — v.33,№12 — p.7983-7991.
4. March N.H., Jones W. Theoretical solid state physics. — Dover Publ.Inc., New York — 1985 — v.1 — 680p.
5. Kirzhnitz D.A. JETP — 1957 — v.32,№ 1 — p.115-123.
6. Gombas P. Pseudopotentiale springier.— Werlag.,Vien.,New York.— 1967 — p.136.
7. R.J.Gordon, Y.S.Kim J.Chem.Phys. — 1972 — v.56,№ 6(2) — p.3122-3133.
8. Vinet P., Rose J. H., Ferrante J., Smith J. R. J.Phys.Condens. Matter.— 1989 — v.1,№1— p.1941-1963.
9. Herman F., Skillman S. Atomic structure calculation.— New Jersey: Prentic-Hall Inc. — 1963 — p.421.
10. S.Rubini, P.Ballone Phys.Rev.B. — 1993 — v.48,№ 1 — p.99-111.
11. Mark Mostoller, R. M. Nicklow, D. M. Zehner. Phys.Rev.B. — 1989 — v.40,№ 5 — p.2856-2872.
12. Stassis, F.X. Kayser, C.K. Loong, D. Arch. Phys.Rev.B. — 1981 — v.24,№ 6 — p.3048-3053.
13. Condensed matter properties under high pressures and temperatures., Ed. by R.F.Trunin. — Arzamas:VNIIEF — 1992 — p.187-197.
14. Hama J., Watanabe M., Kato T. J.Phys.: Cond.Matter. — 1990 — v.2,№ 36 — p.7445-7452.
15. L.V.Altshuler, A.A.Bakanova, R.F.Trunin. JETP — 1962 — v.42,№.1 — p.91-104.
16. L.V.Altshuler, S.B.Kormer, A.A.Bakanova, R.F.Trunin. JETP — 1960 — v.38,№.3 — p.790-798.
17. L.V.Altshuler, S.E.Brusnikin, E.A.Kuzmenkov. PMTF — 1987 — №1 — p.134-146.

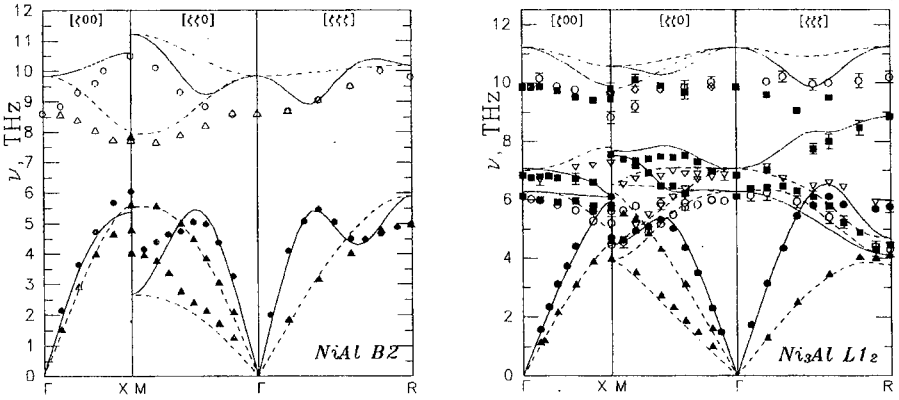

Fig.1 Calculated phonon dispersion curves of $NiAl$ ($B2$) and Ni_3Al ($L1_2$) (solid lines – longitudinal, dashed lines – transverse modes). Experimental data (points) from [11] – for $NiAl$ and [12] – for Ni_3Al.

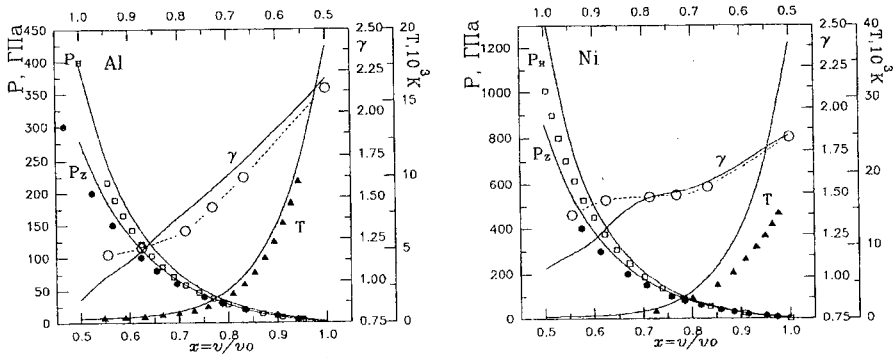

Fig.2 Calculated shock Hugoniot of Ni and Al (P_H – principal Hugoniot, P_z – zero isotherm). Experimental data (points) from [17]. Hugoniot temperature T calculations (triangles) from [15] – for Ni and [16] – for Al.

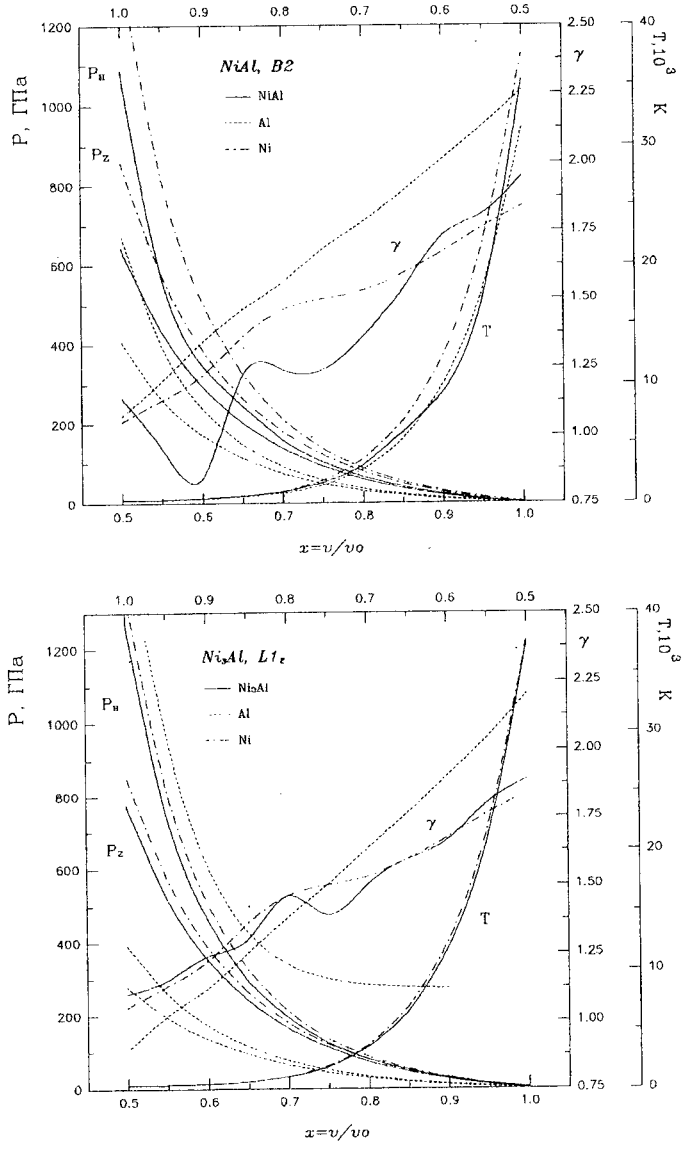

Fig.3 Calculated shock Hugoniot of $NiAl$ and Ni_3Al (P_H – principal Hugoniot, P_z – zero isotherm). Dashed lines – our results for Al, dot and dash – for Ni.